ROTATION OF BACTERIAL FLAGELLA AT HIGH FREQUENCY

Thesis by

Graeme Lowe

In Partial Fulfillment of the Requirements

for the Degree of

Doctor of Philosophy

California Institute of Technology

Pasadena, California

1987

(Submitted December 19, 1986)

Acknowledgements.

I would first and foremost like to express my gratitude to my advisor, Howard Berg, who made this thesis possible. I have learnt much from Howard's scientific insight and technical ingenuity. His support and enthusiastic encouragement have guided me through many difficult times, and his kindness and sense of humor have made it a pleasure to work in his lab. I also wish to thank all of my co-workers in the laboratory who have willingly offered their help and advice through the years. Thanks to Pat Conley, Steve Block and Jeff Segall for their technical assistance during my transition to experimental biology, to Bob Smyth for his programming expertise, to Markus Meister for many illuminating discussions about physics, and to both Markus and Dave Blair for their helpful comments on the manuscript. I am grateful to Jerry Pine, Henry Lester, David Goodstein and Mike Cross for serving on my thesis committee. It is a pleasure to acknowledge the kindness and hospitality of many friends who have made my graduate life more enjoyable. Thanks to those with whom I have shared many interesting experiences in field biology: Jim and Ellen Strauss, Jeff Mayne, Blaine Hebert, Chuck Kristensen, and Steve and Laurie Kutcher. Special thanks go to Galen and Betsy McCray, in whose home I have always been welcome, and, of course, to my family for their continued love and support from afar. Finally, I gratefully acknowledge financial assistance from Caltech via several Teaching Assistantships, Graduate Research Assistantships and Special Tuition Awards, and from a Pfeiffer Foundation Fellowship and an Anthony Fellowship.

Abstract.

Flagellated bacteria propel themselves through their fluid environment by rotating one or more helical filaments which are driven at their base by a reversible motor powered by a protonmotive force. In some species many filaments join together to form a single flagellar bundle during swimming. Past work has characterized the functional properties of the motor at low speed and high torque from studies of cells tethered by a single filament. This thesis describes work in which properties of the motor at high speed and low torque were investigated by studying free swimming cells.

A method was developed for measuring the rotation rates of filaments in bundles of swimming cells. Images of cell bodies were projected onto the photocathode of a photomultiplier tube whose sensitivity is spatially inhomogeneous, and the power spectral density of the output was computed using the Fast Fourier Transform. Averages of many spectra revealed a peak at high frequency due to the vibration of the cell body by the rotating filaments. This method was analysed in detail by mechanical simulations and computer models. Techniques were also developed for following the rotation of single motors by attaching markers to sheared flagella. Most experiments were done with a motile strain of Streptococcus. At 22°C, filaments of this organism rotate at ca. 100 Hz relative to the cell body. Higher frequencies were seen in Escherichia coli at the same temperature, ca. 180 Hz.

The relation between torque and speed of the flagellar motor at fixed protonmotive force was determined by varying the viscosity of the

medium. Torque was found to drop linearly with increasing speed over the upper half of the speed range. A comparison with the torque generated by tethered cells suggests that linearity may hold over the entire speed range. This behavior is consistent with a scheme whereby the free energy available per proton is dissipated in a series of small steps.

The bundle frequency of glycolysing Streptococcus was found to increase linearly with temperature, by a factor of 7 from 10°C to 42°C, corresponding to an increase in torque by a factor of 3. The protonmotive force did not vary by more than 10% from 16°C to 32°C. Conditions were found under which cells swam when artificially energized by a comination of transmembrane pH gradient and potassium diffusion potential. These cells exhibited a large deuterium isotope effect, their speed dropping by 30 - 50% in D_2O. Thus, proton transfer reactions appear to be limiting the rate of motor rotation in swimming cells.

TABLE OF CONTENTS

Acknowledgements ii

Abstract iii

Table of Contents v

Chapter 1. Introduction 1

Chapter 2 Development of Experimental Methods 14

§2.1 Introduction 15

§2.2 Observation of high frequency rotation using markers 16

§2.3 Experimental methods - rotating markers 21

§2.3.1 Polystyrene latex bead markers 21

§2.3.2 Titanium dioxide markers 26

§2.4 Data acquisition 28

§2.5 Bundle frequency measurements on cell populations 34

§2.6 Data analysis for spectra of swimming cells 55

Chapter.3 The effect of viscosity on flagellar rotation 72

§3.1 Introduction 73

§3.2 Methods 75

§3.2.1 Viscous solutions 75

§3.2.2 Preparation of cells used in bundle frequency measurements 77

§3.2.3 Preparation of cells used in tracking experiments ... 78

§3.2.4 Methylcellulose experiments 79

§3.3 Results 82

§3.4 Discussion 90

Chapter 4. The effect of temperature on the flagellar motor 96

§4.1 Introduction 97

§4.2 Methods 99

§4.2.1 Temperature control 99

§4.2.2 Preparation of cells used in bundle frequency measurements 100

§4.2.3 Preparation of cells for tracking experiments 102

§4.3 Results 103

§4.4 Measurements on E. coli 106

§4.5 Discussion 110

Chapter 5. Rapid rotation of flagellar bundles in swimming bacteria. (Nature, 1987. In press) 119

Chapter.6 Artificially-energized swimming cells 140

§6.1 Introduction 141

§6.2 Methods for artificial energization 144

§6.3 Temperature experiments 147

§6.4 Isotope substitution experiments 154

Chapter.7 Summary and Outlook 159

§7.1 Summary and discussion 160

§7.2 Outlook 165

Appendix. Buffers and reagents 173

References 175

CHAPTER 1

INTRODUCTION

How do things move? Attempts to answer this question in the inanimate world have driven the evolution of the science of physics. It is only natural that those of us interested in both physics and biology should pose the same question for living objects. Our current understanding of the laws which determine the motion of nonbiological objects is fairly complete, at least for relatively simple homogeneous systems at the atomic and molecular level and above. Given a system in a defined initial state, we can make definite predictions about its state at later times based on its equations of motion. Although governed by the same physical laws which describe the behavior of inanimate objects, living organisms are highly complex and a presciption for predicting their detailed time evolution would seem to be beyond our present grasp. However, the real interest in biological systems lies in the question of how they are designed to solve the problems of survival and transmission of genetic information. The capacity to carry out these tasks is greatly enhanced by being able to control the environment by moving from one place to another. It is therefore not surprising that even the simplest of organisms have evolved mechanisms of motility. Generating movement requires the expenditure of energy. By studying how this occurs, we can hope to gain some insight into how energy transduction systems in general might function at the molecular level. How do physical laws constrain their design? Do the devices found in nature represent optimal solutions to certain engineering problems? It seems logical to begin to tackle these issues by examining the motile mechanisms of the simplest of unicellular organisms - the bacteria.

Forms of bacterial motility fall into two categories: non-flagellar and flagellar. The mechanisms of locomotion utilized by members of the

first group are unknown. In the second group, locomotion depends on a rotary engine, the flagellar motor, which drives a shaft (the rod) emerging from the cell wall of the organism. A long rigid helical filament is linked to this shaft via a flexible attachment called the hook. The assembly consisting of a filament, a hook and an engine (or basal body) is termed a flagellum. Rotation of the helix generates a thrust which drives the cell body through its fluid environment. Some bacteria (known as peritrichously flagellated) possess several flagella emerging from the cell wall at random locations. Escherichia coli, Salmonella, and Streptococcus belong to this class. When these cells swim, their filaments bend at the hook and align to form a helical bundle (Fig. 1.1). The hook of each flagellum acts as a universal joint which allows the motor to transmit to the filament a torque which is not parallel to the shaft. In this way the bundle is driven by a net torque approximately equal in magnitude to the sum of the magnitudes of the individual torques. The bundle has a left-handed helicity, so when the net torque points away from the cell body (a state known as counterclockwise rotation), wave propagation proceeds distally and cells swim in a smooth linear fashion (called a run). When the motors reverse their sense of rotation and turn clockwise, the bundle breaks apart and cells undergo an erratic motion called tumbling, which randomly reorients the cell body but does not give rise to much translational movement. The path of a cell is a three dimensional random walk in which the time spent in a run and the time spent in a tumble are both random variables obeying exponential distributions. By modulating the mean times of these distributions in response to chemoreceptor inputs, bacteria can bias their motion up or down gradients of chemicals, a

process known as chemotaxis. Bacterial chemotaxis has been reviewed by Macnab (1978), Parkinson (1981), and Hazelbauer and Harayama (1983). For a review of bacterial motility, see Macnab (1979), and Macnab and Aizawa (1984).

Bacterial motility was first observed over 300 years ago by Leeuwenhoek using a simple hand-ground lens. The first detailed observations of the motion of flagella had to await the development of microscope condensers for dark field illumination. Using this method Reichert (1909) visualized both bundles and single filaments in a variety of bacteria. He observed the rotation of the cell body in response to forces generated by the motion of the helix, although he assumed that the latter propagated helical waves rather than undergoing true rotation relative to the body. Reichert also postulated the existence of a gyratory motion of the body caused by forces perpendicular to the helix. Metzner (1920) combined dark field microscopy with stroboscopic illumination to measure the rates of flagellar rotation in relatively large bacteria, Spirillum volutans and S. undula, both elongate helical cells about 30 μm in length, with bundles comprised of about 25 filaments arising from each end of the cell. Bundles rotated at about 40 Hz and the cell body counter-rotated at 12 - 14 Hz. In Chromatium okenii, a bacterium with a 10 μm long cell body and a bundle of about 40 filaments arising from one end, the bundle rotation frequency was 40 - 60 Hz, and the body rotated at 2 - 8 Hz. More recent measurements of flagellar rotation frequencies have relied on cinemicrography. Swan (1980) measured bundle frequencies for S. volutans ranging from 30 Hz to 171 Hz for the trailing bundle, and 19 Hz to 75 Hz for the leading bundle. Shimada et al. (1976) examined the

much smaller (ca. 2 μm long) organism Salmonella abortus-equi in highly viscous media and found bundle frequencies in the range 10 Hz - 20 Hz. The bundles of such small bacteria scatter much less light, and therefore the maximum frequencies this method can detect are limited by the film speed and the short exposure times per frame.

The flagellar filament is a thin (<20 nm diameter) hollow cylindrical tube built from monomers of a protein called flagellin with a molecular weight of approximately 40,000 (Iino, 1969). Flagellin units are transported in presumably unfolded form through the hollow interior to the tip of the filament where they add to its length by crystallization (Iino, 1974). This structure seems extremely simple when compared to that of the eukaryotic flagellum which propagates helical waves by generating force along its entire length. Hence one might suspect that in bacterial flagella, force is generated in the basal region and that the filaments actually rotate relative to the cell body. Using the evidence available at the time, Berg and Anderson (1973) argued convincingly in favor of this hypothesis. It provided a simple explanation for the observation that pairs of cells of a poly-hook mutant (which lacks filaments but has abnormally long hooks) counter-rotated when cross-linked with a bivalent anti-hook antibody (Silverman and Simon, 1972). When these mutants were attached to glass by their polyhooks, again using antibody, the cell body was seen to rotate (Silverman and Simon, 1974). Rotation can be directly visualized in a mutant with straight filaments by attachment of polystyrene latex beads (Berg, 1975a).

The flagellar motor has proven to be difficult to study by conventional biochemical and biophysical techniques. Structural studies

have been hampered by its small size and location. Transmembrane proteins are difficult to crystallize for X-ray diffraction studies, and electron micrographs of isolated basal bodies have not been very revealing. Stacks of rings are visible surrounding the central rod, two in gram-positive cells and four in gram-negative cells, which possess an outer membrane (Fig. 1.2). It is believed that torque is generated by interactions between the inner two rings - the S-ring or stator, attached to the cell wall, and the M-ring or rotor, attached to the rod (Berg, 1974). Analysis of electron micrographs of the M-ring have revealed a sixteen-fold rotational symmetry in E. coli (DePamphilis and Adler, 1971). Freeze fracture studies of the membrane of the polarly flagellated bacterium Aquaspirillum serpens show 14 to 16 particles arrayed around the periphery of annular depressions (Coulton and Murray, 1978).

Most of the recent studies of the functional properties of the flagellar motor have used either E. coli or a gram positive species of Streptococcus. The latter organism was chosen because it lacks endogenous energy reserves and can be easily starved. Manson et al. (1977) used this to show that the motor is driven by a proton flux down a transmembrane gradient of the proton electrochemical potential (also known as the protonmotive force) defined as:

$$\Delta p \equiv \Delta\mu_{H^+}/e = \Delta\psi - 2.3(kT/e)\Delta pH \qquad (1.1)$$

where $\Delta\mu_{H^+}$ is the difference in proton electrochemical potential between the interior and exterior of the cell, $\Delta\psi$ is the difference in electrical potential, ΔpH is the difference in pH, k is the Boltzmann constant, T the absolute temperature, and e the electronic charge. Motility was observed in cells energized by either a transmembrane pH

gradient or a membrane potential. Addition of N,N'-dicyclohexylcarbodiimide (DCCD), a potent inhibitor of the transmembrane ATPase (Harold et al., 1969), did not abolish this motility. This ruled out the possibilty that the protonmotive force was causing motility indirectly by driving ATP synthesis. Other cations such as Na^+, Ca^{2+}, and Mg^{2+} were not required for motility. The protonmotive force is utilized widely in biological systems both as an energy source for molecular processes such as ATP synthesis or active transport, and in regulatory roles (Taylor, 1983). In E. coli it is generated under aerobic conditions by an electron transport chain in which proton efflux is coupled to electron transfer. In Streptococcus, which is anaerobic, glycolysis produces ATP whose hydrolysis is coupled to proton efflux by the ATPase (Kagawa, 1984).

Much has been learnt about the properties of the motor using tethered cells. A flagellar filament is attached to glass and the output of the motor can be monitored directly by following the rotation of the cell body. In both tethered and swimming cells, analysis of the forces is considerably simplified by the fact the the Reynolds number is very small (ca. 10^{-5}). Inertia is negligible, and thus at any time the force and moment acting on any element of the cell due to the motors is completely balanced by the force and moment due to viscous drag.

Manson et al. (1980) demonstrated that the angular velocity of tethered cells increases linearly with the protonmotive force up to about 100 mV. There appeared to be a threshold of less than 20 mV, which is smaller than the protonmotive force associated with the thermal energy (kT/e = 25 mV). They also found that the angular velocity was inversely proportional to the viscosity of the medium, implying that the

torque generated by the motor is independent of speed, up to speeds of around 10 Hz. A similar result was found for E. coli (Berg and Turner, 1979). Khan and Berg (1983) found that the torque in tethered Streptococcus was independent of temperature and did not change when deuterons were substituted for protons.

Tethered cells are well suited for studying the fine structure of motor rotation. De-energized cells do not exhibit free rotational Brownian motion, implying the presence of barriers to rotation. These barriers disappear when a threshold Δp is exceeded, and a spinning cell undergoes unconstrained rotational diffusion (Khan et al., 1985). By repeatedly energizing and de-energizing cells and observing their initial and final angular positions, the barriers were found to have a five- or six-fold symmetry (Khan et al.,1985, Meister, 1987). The torque generated at finite Δp and zero speed, termed the stall torque, has been measured by stopping tethered cells with a fluid flow (Meister, 1987). The stall torque was found to be equal to the torque in spinning cells under all conditions tested. Block and Berg (1983) have demonstrated the existence of discrete force-generating units in the motor. They inserted a plasmid carrying motB, a gene required for motility, into cells of a mutant lacking this gene. When these cells were tethered and transcription of motB was activated, discrete steps in angular velocity were observed.

At very light external loads (and therefore very small external torque) the motor was found to rotate an order of magnitude faster than in tethered cells (Berg et al., 1982). A hook mutant of E. coli lacking filaments was tethered to glass and cell bodies were imaged onto the edge of a pinhole. When the transmitted light was detected by a

photomultiplier, high frequency signals could be seen (mean ± SD for 20 cells 104 ± 29 Hz). These were assumed to result from the vibration of the body by the spinning hook. I shall hereafter refer to the speed in the limit of zero external torque as the idle speed.

This thesis describes my efforts to increase our knowledge about the properties of the motor in the regime of light loads and high rotation speeds. I worked mainly with Streptococcus. Some experiments were done with E. coli, in order to make contact with Howard's earlier measurements on hooks. Chapter Two documents a novel technique for detecting high frequency motions of swimming microorganisms. In Chapter Three, this technique is used to determine the torque-speed diagram of the motor. In Chapter Four, the temperature dependence of the idle speed of the motor is deduced from measurements on swimming cells. Chapter Five outlines the results and implications of this work. Chapter Six describes the methods developed for artificial energization of swimming Streptococcus and their application to the study of the effects of temperature and isotope substitution on the flagellar motor. Chapter Seven contains a summary and some speculations about future experiments. Throughout the text I have used abbreviated notations for certain buffers and reagents. These have been listed in the appendix.

Figure 1.1 A swimming cell of Streptococcus V4051

Cultures of this gram-positive, peritrichously flagellated organism consist of mixtures of motile chains containing variable numbers of spheres (cocci). Diplococci composed of two spheres (as shown) predominate at late exponential phase. The drawing shows a swimming cell with 4 filaments rotating in a bundle. The shape of the cell body was sketched from electron micrographs (Manson et al., 1980, Higgins and Shockman, 1976). The dimensions of the filaments are similar to those obtained from micrographs of stained preparations (Meister, 1987) in which the mean diameter of the helix was 0.7 μm. The mean wavelength was 3.2 μm.

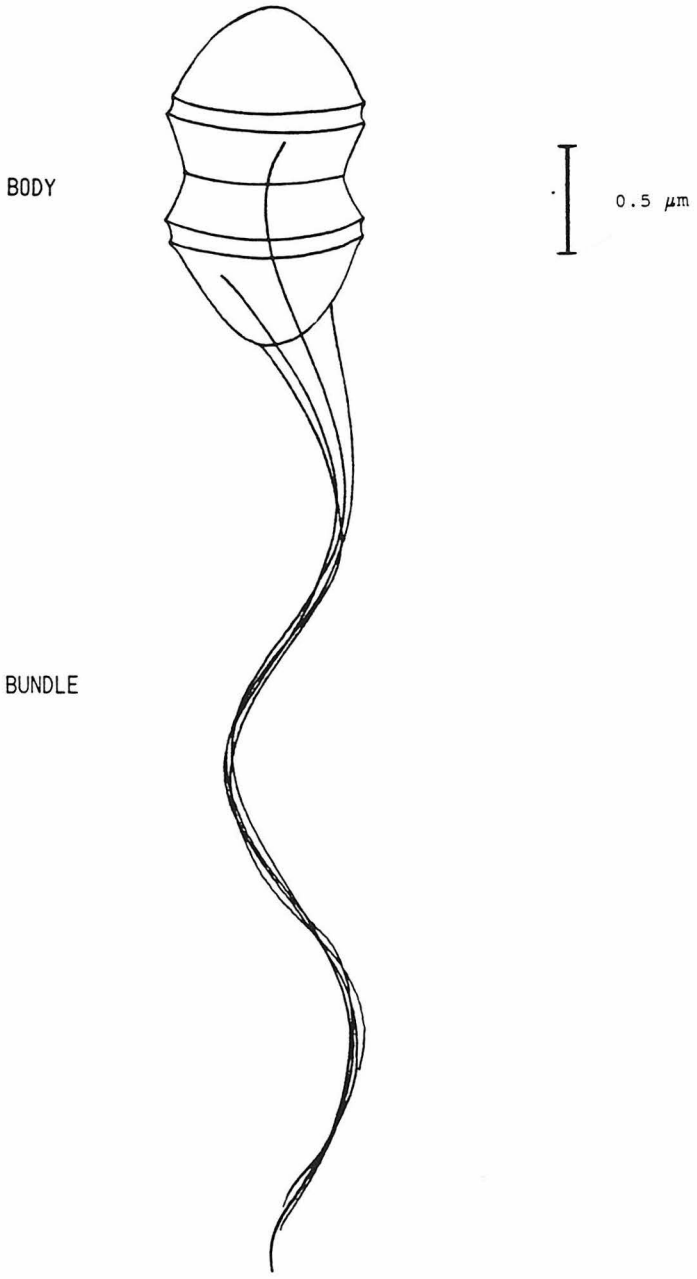

Figure 1.1

Figure 1.2 The structure of the basal body of a bacterial flagellum

A. A three-dimensional model of the basal body of a gram-negative bacterium. The outer pair of rings may allow the rod to pass through the outer membrane. The L-ring is associated with the outer membrane and the P-ring with the peptidoglycan layer or cell wall. The inner pair of rings may be involved in torque generation. Measurements are in nm. (Adapted from DePamphilis and Adler, 1971).

B. Cross section of a model of the basal body of a gram positive bacterium. The M-ring is attached to the rod and the S-ring is attached to the cell wall. Torque is generated by interactions between these two rings. (From Berg, 1975a).

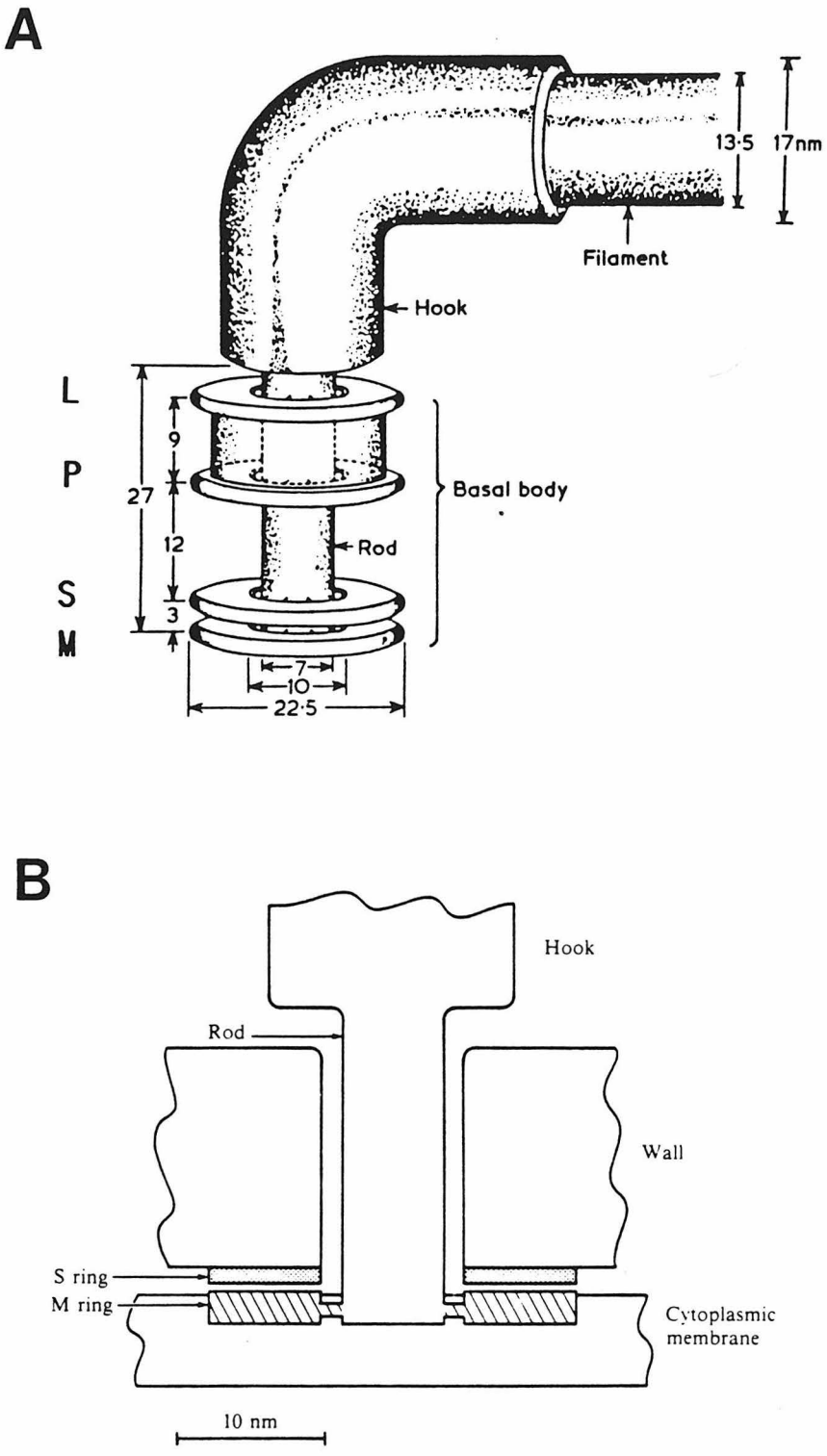
A
13·5
17nm
Filament
Hook
L
P
S
M
9
27
12
3
Basal body
Rod
7
10
22·5
B
Hook
Rod
Wall
S ring
M ring
Cytoplasmic membrane
10 nm

Figure 1.2

CHAPTER 2

DEVELOPMENT OF EXPERIMENTAL METHODS

§2.1. INTRODUCTION.

The purpose of this chapter is to document, in historical order, the development of two rather different approaches to the study of high speed motor rotation. The first involves sticking a small particle to a flagellum and watching the motor spin it at high speed. The second involves detecting the small amplitude gyrational motion of a swimming cell body being shaken by a flagellar bundle rotating at high speed. While the first method only allows one to observe a single motor at a time, the second method looks at the average behaviour of many cells. For most experiments, the second method turns out to be far superior in terms of both reliability and ease of implementation. It also has the aesthetic appeal that one is watching a natural event and does not require the experimenter to subject living bacteria to cruel and unusual punishment. However, for some problems it is still useful to know how to look at single motors, so I describe the protocols for this in detail for future reference. Both methods rely on the extraction of kinematic information from moving microscope images, and it was this common link which allowed me to make the transition from one to the other using the techniques of digital spectral analysis.

§2.2. OBSERVATION OF HIGH-FREQUENCY ROTATION USING ATTACHED MARKERS.

The feasibility of studying the properties of a single flagellar motor driving an external load with a frictional drag coefficient smaller than that of a tethered cell by several orders of magnitude was demonstrated by Berg et al, 1982, using a hag$^-$ strain of Escherichia coli (MS912). This mutant lacks flagellar filaments but is capable of forming intact hooks driven by functional motors. If these hooks are not straight, their rotation may result in a rotating force which acts in a direction perpendicular to the axis of the rod, and which vibrates the cell body at the frequency of rotation. This vibration was detected by focusing the edge of the image of a cell body onto a pinhole and using a photomultiplier to measure changes in the intensity of the transmitted light. The photomultiplier output was monitored on a strip chart recorder, and a small periodic signal was discerned as the cell passed over the pinhole. Attachment of a polystyrene latex sphere (bead) of diameter 0.6μm to the surface of the hook would be expected to significantly enhance the amplitude of this signal, since the vibration amplitude of the body increases as the square of the radius, r, of the object being rotated by the motor (assuming that the ratio of r to the distance between the axis of rotation and the symmetry axis is approximately constant). Equating the force exerted on the cell body via the tether to the drag force on the object gives the amplitude of the body oscillation as: $A \simeq r^2/R$, where R is the mean diameter of the cell body. Thus the addition of a bead would improve the signal by a factor of order $(0.6\mu m/20nm)^2 \simeq 10^3$. In fact, the pinhole system was used to observe the vibration of the markers directly. Their amplitude would be greater than that of the shaking cell body by a factor of about R/r.

However, the signal obtained by observing the image with the photomultiplier would also be reduced by a factor proportional to the ratio of image intensities, and in the case of phase contrast microscopy this ratio would be equal, in first order, to r/R, so that the signals obtained from markers and from cell bodies would be of comparable amplitude.

Instead of using E. coli, I decided to study the flagellar motors of the motile Streptococcus strain V4051, since this organism lacks an endogenous energy supply and can thus be starved and energized with an artificial protonmotive force. The properties of the motor of Streptococcus have been studied extensively in the heavy load regime utilizing tethered cells. Since anti-hook antibody (prepared from mutants) was not available for this bacterium, it was necessary to examine wild-type cells by removing the filaments by shearing and attaching polystyrene latex spheres to the remaining stubs. The motion of these beads could then be examined with the pinhole apparatus which had been used to study E. coli. In the latter case it had already been found that 0.6μm diameter beads rotate at about the same speed as free hooks, indicating that the motor was operating at constant speed, independent of external load (Berg et al., 1982). Thus it was reasonable to expect that such markers could also be used to study the motors of Streptococcus in a similar operating domain. A technique was developed in which cell bodies were attached to a glass coverslip and, as before, the rotation of markers was directly observed with a pinhole.

A number of technical problems had to be surmounted to make this method work with Streptococcus. Attempts to obtain spinning beads by attaching them to cells whose filaments had been shortened by repeated

passage (64 times) between two syringes connected by polyethylene tubing (I.D. 0.58mm) - this was the standard method used in tethering cells - were unsuccessful. The filaments sheared in this way were not short enough to prevent attached beads from making contact with, and adhering to, the surface of the coverslip on which the cells were stuck. Much effort was spent searching for a way to treat the glass surface so that it would bind to the surface of cell bodies but not beads. For example, a protocol was devised in which glutaraldehyde was covalently linked to the surface of a coverslip using a silanizing reagent (3-aminopropyltriethoxy-silane). After cell bodies were attached to this activated surface, an attempt was made to render the remaining exposed surface unreactive using compounds containing an amine functional group. No treatment could be found which produced a surface incapable of also binding polystyrene latex beads. The difficulty was finally overcome by shearing the cells with a Waring blendor, which reduced the mean filament length sufficiently to allow a non-zero probability that an attached bead would fail to make contact with the glass surface. Cell bodies could be attached to the coverslip by treating it with either poly-D-lysine or the dye Alcian Blue 8GX, after cleaning with hot fuming nitric acid. These molecules presumably mediate, by virtue of their positive charge, ionic interactions between the negatively charged acid cleaned glass and bacterial cell wall. It was found that beads would spontaneously attach to flagellar filaments in aqueous solution, but that the buffers of high ionic strength required to maintain the physiological viability of the cells also caused the beads to clump at high densities. The simplest way to obtain a high yield of cells with attached beads involved incubating cells and beads together in a low

ionic strength buffer, washing out the excess beads, and restoring the cells to a high salt environment containing the divalent cation Mg^{2+}, which might conceivably reverse damage occurring at low ionic strength. Using these methods (summarized in §2.3), latex beads of diameters 0.357μm and 0.557μm were successfully attached to filaments and observed to rotate at high speeds ranging from 20 Hz, for large clumps of several beads, to 140 Hz, for single small beads.

As the brightness of the phase contrast image of a particle is approximately proportional to the difference between the optical path length across its diameter and that across the volume of displaced fluid, the smaller beads were more difficult both to locate by eye and to detect with the photomultiplier tube. In order to decrease the rotational drag coefficient of the markers without an attendant loss in image contrast, smaller, more refractile, particles were sought. This led to the use of 0.1-0.2 μm diameter titanium dioxide (rutile) particles with a refractive index of 2.75, almost twice that of the beads (1.59), yielding a 5.5 times greater difference between the particle index and that of water. It was found that when flagellar filaments were coated with antifilament antibody, they would bind strongly to the acid cleaned surface of the rutile particles. Under dark-field illumination, attached particles were easily found and provided a significant enhancement in signal-to-noise ratio over the latex beads.

Although a number of experiments were done using the above techniques, progress was impeded by several drawbacks inherent in this approach. Firstly, only a small fraction of the total number of possible marker - cell - substrate configurations were suitable for experiments.

The markers on most cells were simply glued to the coverslip, and for those that were free to rotate, large variations in tethering geometry meant that only a few consistently spun in the high frequency range. Secondly, in experiments requiring flow to exchange buffers, markers were often dislodged by hydrodynamic drag. Even when the drag force was insufficient to separate particles from their filament tethers, uncontrolled changes in their orientation relative to the cell body and flagellum could not be ruled out. Thus, a flow of buffer would sometimes result in a shift in the rotation frequency, and at other times cause the particle to become stuck to the glass.

§2.3. EXPERIMENTAL METHODS - ROTATING MARKERS.

§2.3.1. Polystyrene latex bead markers.

Polystyrene latex spheres (diameters 0.357 μm and 0.557 μm) were obtained from Dow Chemical Co. as a suspension of particles in a dilute detergent solution. The suspensions used in my experiments had been stored for many years in imperfectly sealed plastic vials so their concentrations were unknown and varied between lots, in some cases reaching 100 % solids (i.e. completely dried out). This material was diluted or resuspended into buffer B (pH 7.5), to give stock suspensions of concentration $(1.3 \pm 0.4) \times 10^{12}$ cm^{-3} (as determined by a Petroff-Hausser bacterial counter), which were stored at 4°C with 0.1 % w/v sodium azide to inhibit the growth of bacterial contaminants. Before each experiment, a 200 μl aliquot of the stock was pelleted (in an Eppendorf microfuge) and resuspended by vortexing (200 μl volumes) into a buffer to be used for incubation with cells (specified below). This wash was repeated two more times and the final resuspension volume of 100 μl was dispersed with a sonicator (Heat Systems Ultrasonics Inc. Model W-225R equipped with standard 419 tapered microtip) set at power 7.0, cycle 50%, 10 cycles. Pellets tended to be compact and vortexing for many minutes at high speed was usually required to resuspend them.

Circular coverslips (12 mm diameter) were cleaned using the following standard protocol. About 30 slips were placed in a 50 ml glass jar and swirled for several minutes in 20 ml of acetone to remove any hydrophobic material. The acetone was decanted off and the rinsing procedure repeated three times with 95 % ethanol. The rinsing was then repeated ten times in glass-distilled water so as to completely remove

any organic solvent. After the final decant, 10 ml of fuming nitric acid was added and the container was covered with a loose lid, to prevent escape of NO_2, and incubated at 70°C in a water bath for 1 h. At the end of this period, acid was removed by pipette and the slips rinsed into distilled water and stored in the same container covered with parafilm at room temperature. Stored in this way, they remained usable for several weeks.

For attachment of cells to glass, acid cleaned coverslips were soaked in a 0.4 mg/ml solution of poly-D-lysine (molecular weight 151,700, U.S. Biochemical) in distilled water for 5 min, removed and rinsed by swirling for 5 - 10 s in distilled water and then air dried. Grease (Apiezon L) was applied in a 3 mm wide ring on the rim of the coverslip using a syringe, and a drop of cell suspension (60 μl) was applied inside the ring. The slip was covered to prevent evaporation and cells were allowed to sediment onto the surface under gravity for 30 min. An alternative treatment involved soaking the cleaned slips in a 1% w/v solution of the dye Alcian Blue 8GX (No A-5263, C.I. 74240, Ingrain Blue 1, Sigma Chemical Co.) for the same time, rinsing as above in distilled water, and air drying. Both of these treatments yielded cells firmly stuck to the glass, with no detectable Brownian motion. Another method was to simply sediment a cell suspension in buffer containing 0.1 M glucose onto an acid cleaned surface. Through some unknown mechanism, the glucose caused cell bodies to attach loosely to the surface, with visible Brownian motion. When the medium was exhanged for one containing 0.1 M Mg^{2+}, cells became more tightly attached and Brownian motion was reduced. The glucose also had the desired effect of inhibiting the attachment of beads onto the acid cleaned glass.

In initial experiments, cells of the wild-type strain V4051 were used, but later work was done with the smooth-swimming mutant SM197, in order to eliminate reversals of rotation sense while studying markers. Cells were grown at 35°C with swirling in KTY medium (Harold & Papineau, 1972, see Appendix), and all subsequent manipulations were done at 22°C. A working stock was stored at -20°C in KTY with 20% v/v glycerol, and a fresh saturated culture was grown from this each week and maintained at 4°C. Experimental cultures were grown by diluting 1 volume of this culture into 100 volumes of fresh KTY medium and growing for 3.5 h to mid-exponential phase (density about 2×10^8 - 4×10^8 cells / ml).

The following protocol yielded preparations containing spinning beads. A 5 ml experimental culture was grown as above and pelleted in a 15 ml glass corex tube using the SS34 rotor of an RC2-B Sorvall centrifuge at 7,500 rpm (6780 x g). The cells were resuspended in 5 ml of buffer T (pH 7.5) + 10 mM D-glucose by vortexing. This wash procedure was repeated twice and cells were resuspended to a final volume of 10 ml, placed in a Waring Blendor (Model 7010G) and sheared on the high speed setting for 60 sec. To reduce heating of the suspension, the blendor was used at 4°C. Cells were then pelleted as before and resuspended in 5 ml of buffer B (pH 7.5) + 10 mM KCl + 0.1 M glucose (hereafter referred to as Buffer B1), for bead incubation. They were pelleted again, resuspended to 200 μl of Buffer B1, transferred to a microfuge tube, pelleted in an Eppendorf microfuge, and resuspended in the 100 μl of bead suspension prepared as above in buffer B1 by vortexing at low (1 - 3) speed. Cells were incubated at room temperature (22°C) for 40 min on a rotating rack. This prevented sedimentation while beads found flagellar stubs by diffusion. Beads attached spontaneously

upon contact with the surfaces of flagellar filaments. After incubation, the suspension was transferred back to a corex tube, 5 ml of buffer B1 was added, and the cells were pelleted at low speed (2,500 rpm, 755 g) for 1 min. The supernatant containing most of the beads was decanted off, and the cells were resuspended in 2 ml of buffer B1 by slow manual swirling. Cells from this suspension were tethered to a treated coverslip, as described above, and the slip was attached to a stainless steel flow chamber (as described in Berg & Block, 1984). Buffer B1 was flowed through to remove unattached debris, and then the medium was replaced with Buffer T (pH 7.5) + 0.1 M glucose + 10 mM $MgCl_2$. At this point, the view under the microscope of the surface of the coverslip usually conjured up images of a battlefield, with a dense covering of immobilised cells and beads scattered in a two-dimensional Poisson distribution. Typically, about 20 % of the cells were associated with beads, and of these only about 20 % displayed any kind of motion - usually Brownian motion. Usually at least half an hour of searching was required to turn up more than half a dozen spinning markers, and most of these were large and bright enough to be clumps of several beads rather than single beads. Although the rotary motion of large clumps was easy to pick out against a predominantly static backgound of stuck cells, smaller clumps and single spinning markers could only be recognized by a slightly blurred appearance and occasional wobbling motions. Still others gave no clue as to their rotary nature until examined directly with the pinhole. The physiological viability of the cells was directly affected by the total time they had spent in buffers of low ionic strength, so efforts were made to keep this period shorter than about 80 min.

In experiments where cells were attached to acid-cleaned slips with glucose, they were harvested from the KTY growth medium, washed and blended as above (in the same buffer), resuspended to a final volume of 1.5 ml and tethered on an acid cleaned slip (30 μl per slip). The buffer was then changed using an open flow arrangement in which old buffer was removed from one end of the droplet and new buffer introduced at the opposite end using 5 μl pipettes (Clay Adams No.4614, Accu-fill 90 Micropet) attached to 1 ml syringes (B-D Glasspak) via polyethylene tubing. In this way the medium was changed to buffer B1, and then to a bead suspension in buffer B1, prepared as described above except that the concentration was lower (10^{10} cm^{-3} over the cells). A standard closed flow chamber could not be used here as the beads would have coated the bottom window (which cannot be acid cleaned easily), making optical microscopy very difficult. Beads were left to settle for an hour, and then washed off by a further flow of buffer B1 containing 0.1 M glucose. The coverslip was attached to a flow chamber and the medium replaced by buffer B + 0.1 M glucose + 0.1 M $MgCl_2$ + 0.1 M KCl. Preparations obtained by this method presented a similar appearance to those obtained with treated slips, except that cells were less tightly attached, exhibiting more Brownian motion as well as an increased chance of falling off during flows. On the other hand, there were fewer beads stuck to the coverslip. This method also had the advantage that the period of exposure to a medium of low ionic strength could be reduced, since tethering was accomplished in a buffer of high ionic strength.

§2.3.2. Titanium dioxide markers.

A suspension of 0.1-0.2 μm diameter rutile particles (Polysciences, Cat.#7795) was made by vortexing 70 mg of particles into 0.5 ml of buffer B (pH 6.5) and dispersed with a sonicator (instrument and settings as for the latex beads). This suspension was added to 5 ml of fuming nitric acid in a 15 ml glass corex tube at 70°C in a water bath and incubated for an hour, with stirring every 10 minutes. The suspension was then allowed to cool to room temperature and, after addition of 5 ml of distilled water, covered with a plastic cap to contain corrosive fumes, washed 3 times in distilled water by centrifugation (6780 X g, 1 min) resuspended into 6 ml of distilled water and dispersed by sonication as before (20 cycles). Before each experiment, a 100 μl aliquot of this stock was washed into buffer B1 (pH 6.5) and resuspended to 70 μl by sonication.

The protocol for preparing cells for an experiment was similar to that used in the experiments with beads involving attachment to pretreated coverslips, with the following modifications: (1) The pH of buffer B1 was readjusted to 6.5 to reduce clumping of the particles, (2) after washing and blending, cells were resuspended in 100 μl of buffer B1 (pH 6.5), and 1.6 μl of rabbit antifilament antibody (R1 V4051 F1a IgG 1:10 in 0.1 M KPO_4, J.Izant 3/10/77) was mixed in by vortexing. Cells were incubated with the antibody at 22°C for 5 min, and then pelleted and resuspended twice in 5 ml of buffer B1 (pH 6.5) in corex tubes (6780 X g, 1 min), pelleted again, resuspended to 200 μl, and transferred to a microfuge tube. A final spin in an Eppendorf microfuge gave a pellet which was then resuspended by vortexing in the 70 μl rutile suspension. Subsequent washing and tethering steps were the same

as for the latex beads. During incubation on the rotating rack, a lot of clumped debris fell out and adhered to the walls of the microfuge tube. The cell suspension was recovered without sucking off any of this precipitate. Resuspension of the final pellet of cells with attached particles was limited to the upper layers of the pellet, again to exclude clumps at the bottom. The visual search for spinning particles was made easier by viewing these preparations under dark-field illumination, which improved the contrast of images of rutile particles while reducing the intensity of images of cell bodies, which appeared as opalescent envelopes.

§2.4. DATA AQUISITION.

In all experiments a photomultiplier tube (RCA 4886) was used to measure the intensity of light transmitted through the pinhole. The microscope (Nikon Optiphot or Nikon S-Ke) was mounted on a stable platform (a granite table, Standridge Granite Corp., or an air suspended vibration isolation table, Serva Bench 21654-1, Barry Controls, respectively) to reduce the effects of floor vibration. Coverslips with cells and markers were examined at room temperature (22°C) and searched by eye until a marker was found attached to a cell. The image of the marker was positioned over the pinhole by listening to the output of an audio circuit whose frequency fell as the photomultiplier current increased. The photomultiplier current was converted to a positive voltage whose DC component was removed by summation with a negative supply. The resulting output was amplified and passed through a two-pole low pass filter (3 dB cutoff at 72 Hz) and a single-pole high pass filter (3 dB cutoff at 0.16 Hz or 1.6 Hz). An oscilloscope (Tektronix 465B) displayed the filtered signals, and they were recorded with a strip chart recorder (Gould 220).

The signal obtained from a rotating latex bead marker is shown in Fig. 2.1A. Here, the signal-to-noise ratio is large enough for the mean frequency during an interval to be measured directly from the record by counting the number of oscillations in that interval. For the data shown, the mean frequency is 98.4 Hz. Fig. 2.1B shows the record corresponding to a marker with a much smaller vibration amplitude. Although periodic high frequency oscillations are clearly discernible on top of the low frequency signal generated by the particle passing

repeatedly over the pinhole (compare Fig. 2.1C., obtained from a de-energized tethered cell undergoing Brownian motion), it is more difficult to estimate their frequency due to the difficulty in telling them from noise. This problem becomes worse as the signal-to-noise ratio decreases. In order to analyse noisy signals objectively, the data were examined in the frequency domain, initially with a digital spectrum analyser (Hewlett-Packard, HP3582A) using the Fast Fourier Transform (FFT) algorithm. This instrument opened up the possibility of rapid, on-line data acquisition and analysis, allowing many particles to be tested for periodic signal content during a single experiment. Much weaker signals could be detected by averaging power spectra recorded over many consecutive time intervals. Software was written with the help of Bob Smyth to implement these functions on a PDP-11/34 computer to allow detailed data analysis. Filtered signals were digitized using an LPS-11S Laboratory Peripheral System (Digital Equipment Corporation). A 12-bit A/D converter sampled data at a maximum rate of 2048 points per second.

Fig. 2.2 shows the amplitude spectrum (the square root of the power spectrum) obtained from a vibrating titanium dioxide marker attached to a rotating filament. The shape of this curve can be understood qualitatively by considering three separate contributions. Firstly, there is a noise baseline generated by (1) shot noise from the photomultiplier (white over the observation bandwidth) and (2) by Brownian motion of the marker. The shape of this noise baseline is affected by the transfer function of the filters. Secondly, there is a low frequency peak at 22 Hz, and its first harmonic at 44 Hz, corresponding to slow precessional motion of the marker over the pinhole. Thirdly, the high frequency motion of the marker, spinning at

the rotation frequency of the motor, generates a peak at 104 Hz, and a harmonic at 220 Hz. The presence of the harmonics is a consequence of nonlinear transduction of the marker oscillation by the pinhole-photomultiplier combination. This nonlinearity mixes the high frequency and low frequency peaks of the spectrum, producing sidebands at 104 ± 22 Hz, and also broadens peaks by mixing them with the noise spectrum. Peaks may be broadened further by fluctuations in the rotational drag coefficient of the tethered particle.

Figure 2.1. Pinhole signals.

Signals from rotating markers attached to flagella of Streptococcus were transduced by a pinhole and photomultiplier. Attachment protocols and filter settings are given in the text.

A. The signal from a 0.56 μm diameter polystyrene latex bead attached to a sheared flagellar stub of a diplococcus of strain V4051 stuck to a polylysine coated glass surface. The low frequency modulations correspond to a slow large amplitude periodic motion of the bead and the high frequency signal to its vibration at the motor frequency. The cell was in Buffer T (pH 7.5) with 1mM $MgCl_2$ and 0.01 M glucose.

B. The signal from a second vibrating bead isolated from the same preparation as in A, above. This bead exhibits a faster low frequency oscillation which, in combination with random noise, obscures the high frequency signal.

C. The signal generated by the body of a de-energized tethered cell executing bounded rotational Brownian motion over the edge of the pinhole.

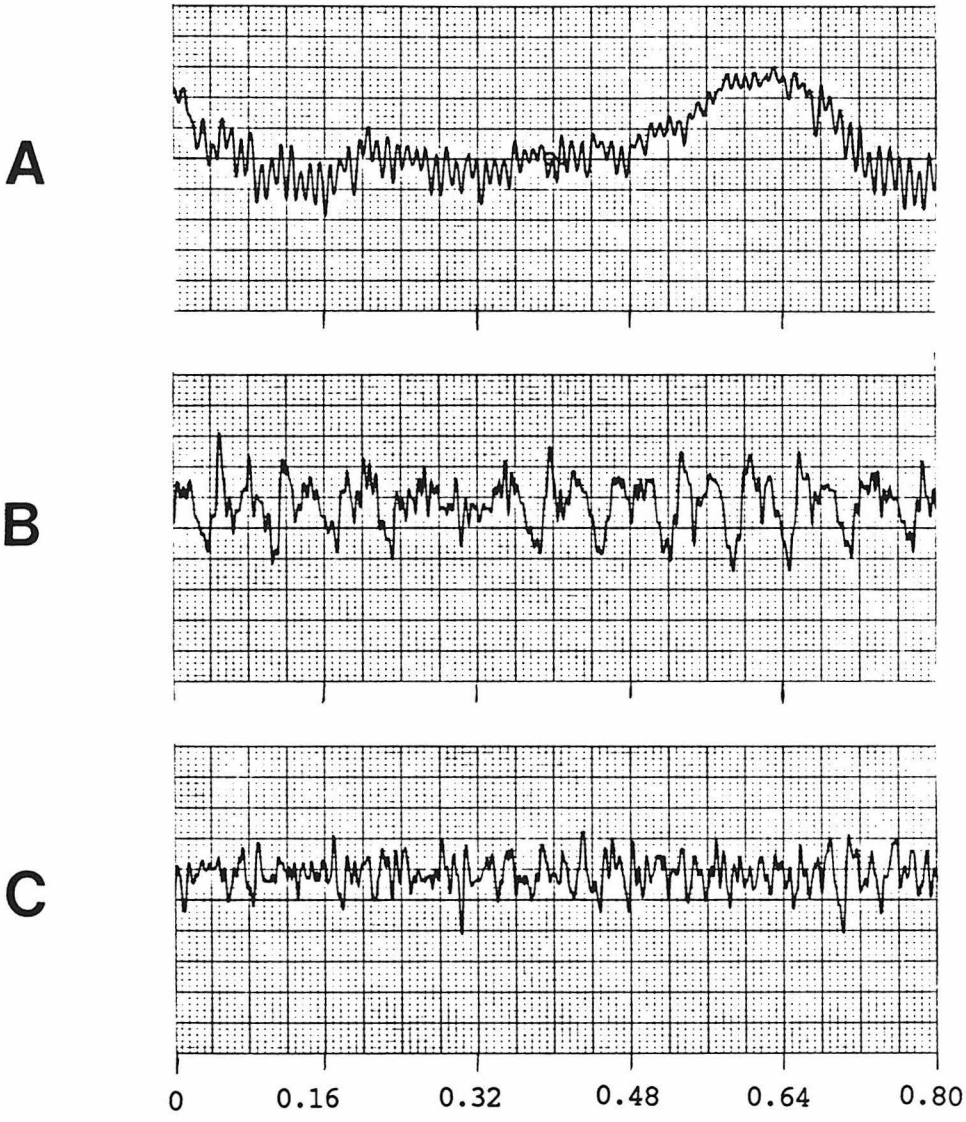

Figure 2.1

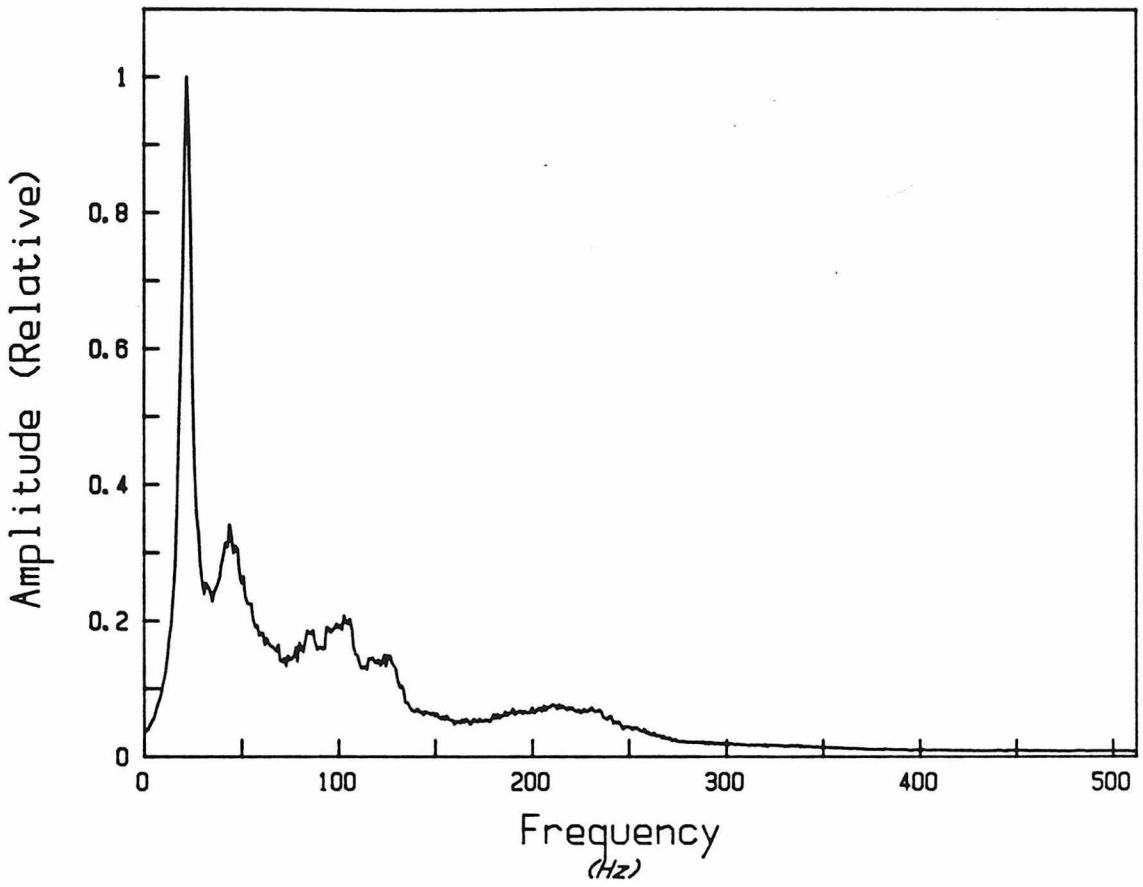

Figure 2.2. Amplitude spectrum from a titanium dioxide particle.

The particle was attached to a sheared flagellar stub of a cell of Streptococcus SM197. Cells were prepared as described in the text (§2.3.3). The filtered pinhole-photomultipier signal was sampled at 1024 Hz, and spectra for 227 blocks of data, each of 1 s duration, were averaged.

§2.5. BUNDLE-FREQUENCY MEASUREMENTS ON CELL POPULATIONS.

Although the above techniques made possible the study of flagellar motors at high speeds and low external loads, experiments were tedious and their outcome uncertain. Moreover, many measurements would have been required to average over random variations in parameters for different motors, cells, and cultures. At the end of the summer, in 1984, Howard returned from a visit to the Istituto di Biofisica, Pisa, Italy, where Cesare Ascoli and Carlo Frediani had been studying the motion of flagellated algae by observing the light scattered by populations of swimming cells under oblique illumination. He suggested that I try this method on Streptococcus using the system I had set up to look at markers. Only slight modifications were required for this - the pinhole was removed to allow the photomultiplier to receive light from a wider field of cells, a preparation of swimming cells was substituted for cells stuck to glass, and the light source was masked off to provide asymmetric illumination through a dark field condenser. The idea was to detect the variation in the intensity of light scattered into a fixed solid angle by a cell body as the angle between the axis of symmetry of the body and the incident beam changed while the cell was swimming. This variation would be expected to be small, since the cell body of Streptococcus is only a few microns long, not much larger than the wavelength of visible light. The flagellated algae are at least an order of magnitude larger. After computing the average of several hundred power spectra, each obtained from the Fourier transform of a one second data block, a broad peak could be seen centered at 95 Hz (Fig. 2.3). Since suspensions of non-motile cells failed to produce such a peak, its

presence was attributed to periodic motion of the cell body at the frequency of rotation of the flagellar filaments. Since many cells had swum over the field of detection during the measurement period, its broad shape was assumed to reflect the distribution of frequencies over the cell population. At low frequency, the shape of the spectrum was dominated by a wide, asymmetric peak with a maximum at 10 Hz, which was also absent for non-motile cells. This peak was assumed to be generated by the low frequency, large amplitude rolling motion of the cell body rotating in a sense opposite to that of the flagellar bundle. One important observation was not consistent with the hypothesis that these periodic signals were due to orientation-dependent light scattering - when the mask was removed from the light source leaving an axially symmetric illumination geometry, the peaks did not disappear, but increased in height!

Tests were performed to elucidate the true mechanism of detection. Spectra remained unchanged when dark field illumination was replaced by phase contrast, showing that the detailed structure of the image was unimportant. Subsequent tests and experiments were conducted using phase contrast optics. Comparing Fig. 2.3 with Fig. 2.2, it can be seen that the swimming cell spectrum has features in common with that of a single particle vibrating over a pinhole, suggesting that the entire photocathode may be acting like a pinhole. If the peaks in Fig. 2.2 are smeared by a distribution over a population of cells then the low frequency harmonics would create a broad asymmetric peak and the high frequency peak would blend into its sidebands. Since the pinhole system is primarily sensitive to lateral motions of the particles, it was decided to test if this was also the case for the whole photocathode

surface. The image of an isolated dust speck (about the same size as a cell body) on a coverslip was scanned across the photocathode while remaining in focus, using the stage of the tracking microscope (Berg, 1978). A function generator was used to drive the X or Y inputs of the stage with a triangular wave of frequency 0.05 Hz, and the output was recorded on a strip chart recorder (Fig. 2.4). The large variations in the output amplitude indicate that the quantum efficiency of the photocathode is not uniform over its surface, but varies sharply with position. This response pattern was not an artefact of the microscope optics - when the photocathode was rotated through 90°, the pattern also rotated through the same angle. Under the conditions used to obtain the spectrum of Fig. 2.3, the average length of a cell body (about 3 μm) was about one third the width of each bump in the response pattern (the total width of the photocathode was about 39 μm, referred to the focal plane).

The next step was to attempt to reproduce the shape of the spectrum of swimming cells by moving images of dead cells over the photocathode. Cells of Streptococcus were de-energized with FCCP and attached loosely (via the glucose tethering procedure described in Sec.2.3.2) to the surface of a small circular coverslip, which was in turn attached to the top of a tantalum tracking chamber. In order to mimic the oscillatory motion of cell bodies, the tracking stage was driven with a sinusoidal Y-axis input at a frequency of 10 Hz, and two different amplitudes were tested (0.6 μm and 3.5 μm peak-to-peak). Spectra obtained at various amplitudes and focal plane locations are shown in Fig. 2.6. A sharp peak occurred at the input frequency (10 Hz) and at integer multiples of this frequency, indicating a non-linear response to the motion. The

amplitudes of the harmonics decreased at smaller input amplitudes, and the ratio of the signal amplitude (peak height in excess of the noise baseline in the amplitude spectrum) to that of the noise baseline (at the same frequency) decreased as the cells were moved vertically out of focus, with an approximate fourfold reduction at distances of 10 μm and 20 μm from the focal plane for the 0.6 μm and 3.5 μm input, respectively, and a shallower fall-off at greater distances. In the 150 μm deep tunnel slide used to make these measurements, a large signal would be expected from cells moving in the zone 10 - 20 μm above and below the focal plane, and a smaller signal from cells in the remaining volume. However, the latter out-of-focus cells would be expected to make a significant contribution to the overall signal owing to their greater numbers.

The effect of increasing the input amplitude for cells vibrating along the Y-axis in the focal plane was also investigated. The height of the fundamental peak in the amplitude spectrum increased, saturating at large inputs (2 - 3.5 μm), and the height of the first harmonic increased relative to that of the fundamental. Thus, the transduction of motion in the focal plane into photomultiplier current becomes increasingly non-linear at large amplitudes.

Since the phase contrast optical system converts vertical motions of cell bodies into changes in the light intensity distribution of their images in the X-Y plane, the effect of vertical motions (along the Z-axis) was also tested using a sinusoidal input. It was found that the relative importance of Z-axis oscillations depended on the amplitude of the input. Thus, for large input amplitudes (3.5 μm p-p), the Z-axis signal was comparable to the Y-axis signal (about 80% of the latter in

amplitude) at the focal plane. On the other hand, for small input amplitudes (0.6 μm p-p) this ratio dropped to about 10%. The mean amplitude corresponding to swimming cells is probably somewhere between these two extremes. As the cell field was shifted away from the plane of focus, the amplitude of the Z-axis signal fell more sharply than did that of the Y-axis signal. At a distance of 20 μm, it was an order of magnitude smaller than its value at the focal plane. These observations indicate that most of the signal originates from horizontal Y-axis motions, with vertical Z-axis motions making only a minor contribution.

As the images of swimming cells traverse the photocathode they generate pulses with independent arrival times and widths equal to the transit times, creating a shot effect. The shape of each pulse will correspond to a particular section of the photomultiplier response function, for example one of the curves in Fig. 2.4. In order to investigate the contribution of this shot noise to the shape of the power spectrum, the field of tethered cells was subjected to uniform translation along the X-axis at a speeds of 13.3 μm/s and 26.6 μm/s, while the Y-axis drive received either a sinusoidal input of frequency 10 Hz and amplitude 3.5 μm (p-p), or no input. As can be seen in Fig. 2.7B, the shot noise had the effect of broadening the peak and its harmonics, the resulting widths being approximately equal to the width of the shot noise spectrum at low frequency i.e. of order 1/T, T being the mean time spent by a swimming cell as it passes over the detector.

The high frequency peak in the observed spectrum could not be simulated in these tests since the resonant frequencies of the transducers driving the tracking stage were in the same frequency range (80 and 110 Hz). However, the interaction between two signals, one at

higher frequency (30 Hz, along the Y-axis) and one at lower frequency (5 Hz, along the X-axis), was tested (Fig. 2.7D). The peak at higher frequency was seen to be broadened due to a series of sidebands. There was also a first harmonic at 60 Hz, again with sidebands. Since no high frequency harmonics were seen in the swimming cell spectra, the peak-peak amplitude of the high frequency oscillations of swimming cells must be less than that of the input used for the test - in this case 1 μm.

The tracking stage simulations were capable of reproducing many of the qualitative features seen in power spectra obtained from actual experiments, in spite of the fact that only three of the six degrees of freedom available to a motile cell could be controlled. Apparently the transformation, by the optical system, of orientational movements of the cell body into variations of light intensity distribution in the X-Y plane of the photocathode does not introduce significant distortions into the spectral information beyond those already inherent in the complex structure of the phase-contrast image and the non-linearity of the detector. Indeed, when the noise spectrum obtained for a suspension of de-energized cells undergoing coupled translational and rotational Brownian motion was compared with that for a suspension of 1.3 μm diameter polystyrene latex spheres at the same light level (for which only the translational motion could be detected), no differences were found.

A series of experiments was performed on suspensions of motile cells to test the "lateral motion" hypothesis of signal detection. First, the importance of various noise sources was examined by comparing spectra obtained from cultures of swimming bacteria with those from de-energized cultures. Data were collected, using a stainless steel flow

chamber of depth 400 μm (Berg & Block 1984), for (1) a culture of fully energized cells (the smooth swimming Streptococcus strain SM197), (2) the same culture de-energized by the addition of FCCP, (3) the de-energized cells flowing at a speed of 14.4 μm/s, and (4) an image containing no cells, at the same light level (c.f. Fig. 5.1). The difference between spectra (1) and (2) is due to the movements of the swimming cells, and that between (2) and (4) due to the Brownian motion of the cell bodies. The profile of spectrum (4) follows that of the bandpass filter applied to the photomultiplier output since the unfiltered output in this case corresponds to shot noise consisting of pulses of a few nanoseconds wide, generated by single photoelectrons emitted from the cathode. Over the observation bandwidth (1 - 256 Hz) this noise is indistinguishable from white noise. This detector noise allows one to define a signal-to-noise ratio, R_m, for the modulations in light intensity created by cell body motions:

$$R_m(f) = \frac{\text{(Amplitude of peak) - (Amplitude of detector noise)}}{\text{Amplitude of detector noise}}$$

evaluated at the frequency f. The power spectrum of Brownian motion, obtained by subtracting the power in (4) from that in (2), was found to be inversely proportional to the square of the frequency (Fig. 2.9). This $1/f^2$ dependence is true for any detector response function at frequencies much greater than D/L^2, where D is the diffusion coefficient of the cell body and L is the length scale over which the response changes its slope. The data in (3) provides a measure of the shot noise generated by cell images moving on and off the detector. The rate of flow is approximately equal to the mean swimming speed of the

cells measured by slow playback of video recordings made on the same culture (mean ± standard error, 15.7 ± 1.1 μm/s). Also shown in Fig. 5.1 is the shot noise spectrum resulting from a flow rate of 20.5 μm/s, which provides an upper bound for the shot noise expected for cells moving at their mean swimming speed. Although the shot effect may introduce some distortion at low frequency (where it is suppressed by the high pass filter), its main contribution is probably the broadening of peaks in the spectrum, as seen in the tracking stage tests.

Changing the magnification of the image by changing the eyepiece, or by using an optovar, showed that increasing the magnification (from the standard 40X objective, 20X eyepiece, 1X optovar combination) reduced the signal-to-noise ratio, R_m, at both low and high frequency peaks (by about 20% when the magnification was doubled). This effect could be understood by noting that at higher magnification and constant culture density, fewer cells cross the detector per unit time. On the other hand, at much lower magnification, the R_m was also reduced - apparently the benefit of having a greater number of cell images over the detector was offset by the reduction in their vibration amplitudes. In such experiments, the voltage applied to the photomultiplier tube was readjusted to compensate, if necessary, for changes in the mean output voltage induced by changes in the mean absolute light intensity reaching the detector. When the focal plane was shifted away from the middle of the chamber (depth about 150 μm) to a position near (within about 20 μm of) the ceiling or floor, the signal/noise ratio was found to decrease by about 20%. This behaviour is consistent with the Z-axis profile observed in the tracking stage tests. Although a significant fraction of the large amplitude signals to one side of the focal plane have been

excluded, there is still a major contribution from the large volume of cells which are out of focus. When the focal plane was shifted even further, to the other side of the coverslip constituting the floor of the chamber (i.e. 150 μm outside the chamber boundary), the signal/noise ratio fell to about 30% of its value at the middle of the chamber. This result also lends support to the notion that cells far out of focus generate a significant part of the signal. The total effect of contributions from cells away from the focal plane was quantified by eliminating them completely in a preparation consisting of cells swimming in a narrow gap, about 20 μm wide, between two glass coverslips (with the mean number of cells in focus being unchanged). A 50% reduction in signal/noise was noted.

Various barriers were placed in front of the photocathode to test their effect on the shape of the spectrum. The signal/noise ratio was reduced by about 20% for an opaque barrier with a large pinhole (diameter about 4 mm, or 10 μm in the focal plane), by about 30% for a sheet of weighing paper and by about 80% for a sheet of wax paper. The latter two barriers act as partial diffusers, removing detailed image structure so that cells in or near the focal plane are unable to contribute to the signal. The fact that a signal can still be detected in such cases can be understood by considering the entire photocathode to act as a single large pinhole which is sensitive to modulations in intensity produced by the motions of cells very distant from the focal plane.

An attempt was made to increase the signal-to-noise ratio by increasing the spatial derivatives of detector sensitivity in the X-Y plane using a mask with a pattern of filled and blank pixels. Each pixel

was a square of side 1.39 μm in the focal plane (or a 1/2 X or 1/4 X reduction thereof), and was filled at random (Julesz, 1971, Fig. 2.2.8-8) to avoid introducing a peak in the spectrum corresponding to the spatial frequency of a periodic lattice. The result was a reduction in the signal to noise ratio - apparently, any gain achieved by the edges of the mask was more than offset by the loss in detector area over regions of high spatial derivative on the photocathode itself. A linear graded filter (whose transmission is a linear function of distance along the X-axis) and a conical filter (whose transmission is a linear function of distance from a fixed point in the center of the image plane) were used in an attempt to make the detector response function more linear. Again there was a decrease in the signal-to-noise ratio, and no change in the shape of the spectrum.

In conclusion, all of the tests done on the detector system give results which are consistent with the idea that the lateral motion of images produces the observed signals. Further support for this mechanism comes from computer simulations described in the next section. The conditions under which bundle frequency measurements were first conducted were in fact very close to being ideal. The "standard" apparatus and experimental conditions for such measurements are described in detail in the legend of Fig. 5.1.

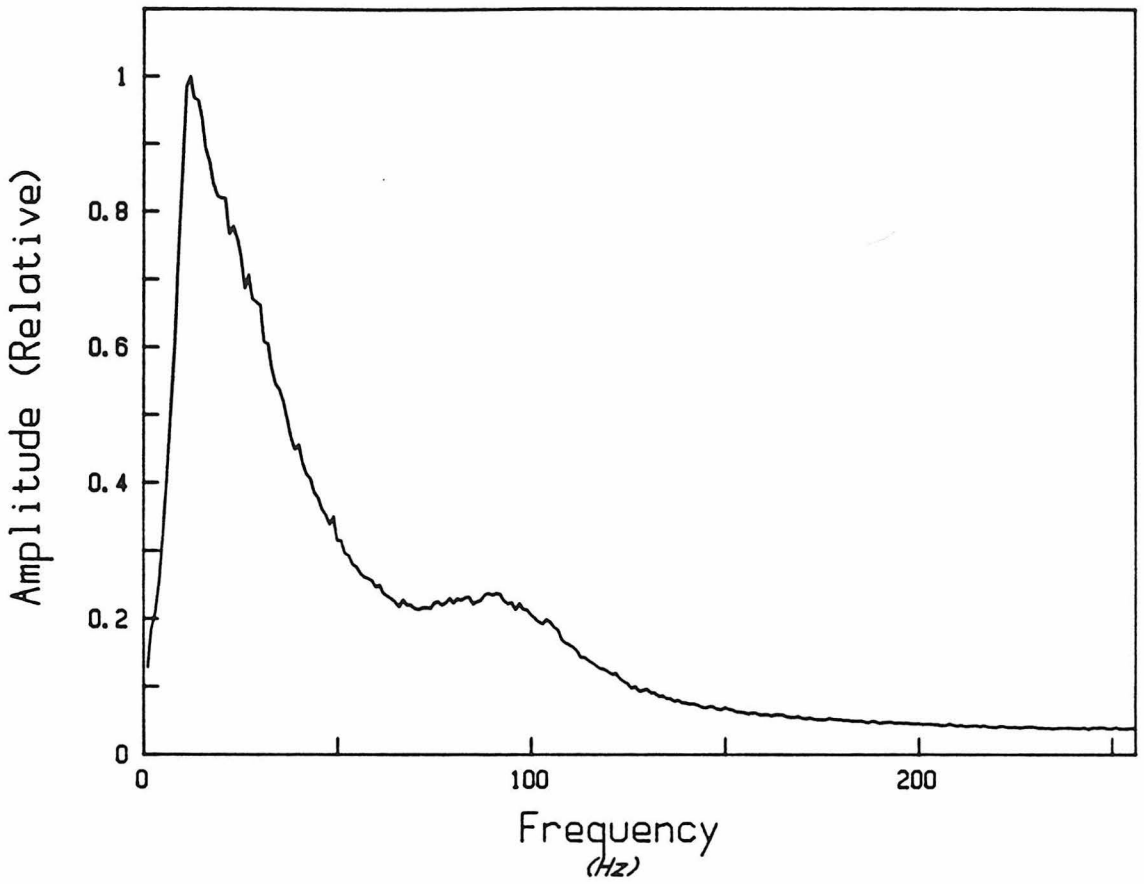

Figure 2.3. Amplitude spectrum of swimming Streptococcus SM197.

A suspension of cells was observed in KTY medium without a pinhole, under dark field illumination in an acid cleaned glass flow chamber (depth 150 μm). The focal plane was located near the top of the chamber. Other conditions and apparatus were as described in Chapter 5, except that both low pass and high pass filters had 3dB cutoff points at 72 Hz. The photomultiplier output was sampled at a rate of 512 Hz and spectra for 800 data blocks, each of 1 s duration, were averaged.

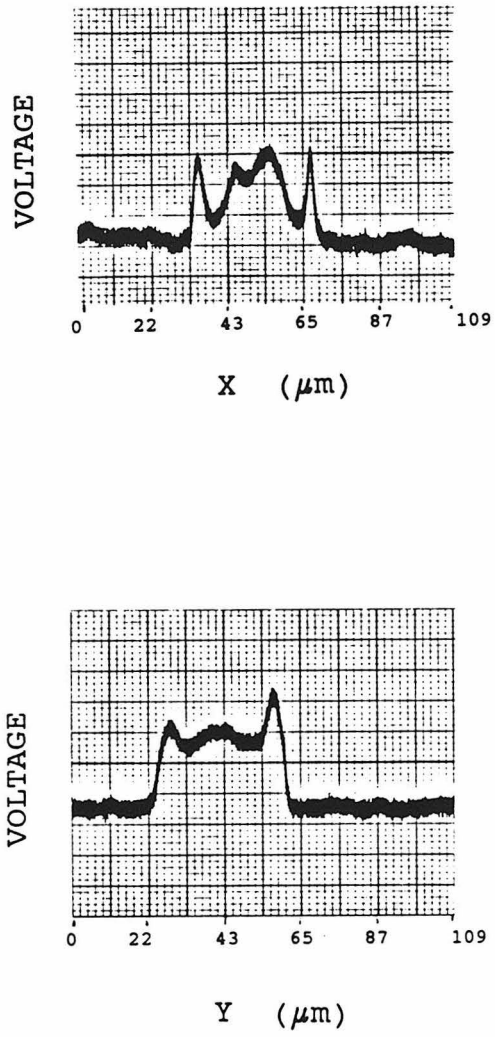

Figure 2.4. Photocathode response function.

The curves show the variation in photomultiplier output obtained by scanning the inverse phase contrast image of a small dust speck (that appeared as a bright object on a moderately bright background) over the surface of the photocathode in two orthogonal directions. The apparent diameter of the particle was about 3 μm, similar in size and intensity to the image of a cell body of Streptococcus. The output was amplified after subtraction of a constant voltage (as described in Chapter 5), but no bandpass filter was used.

Figure 2.5. Transfer functions for the bandpass filters.

A Hewlett-Packard HP3310A function generator was used to apply a sinusoidal input (0.163 V rms) at frequencies 20 + 5n Hz (n=0,1,..,49) and a Keithley 167 digital multimeter used to measure the RMS output voltage. A Tektronix 465B oscilloscope was used for measurements below 20 Hz. In earlier experiments, 3 dB cutoff frequencies of both filters were set at 72 Hz (A). In later experiments, the cutoff frequencies of the high pass filter was set at 72 Hz and that of the low pass filter at 200 Hz (B). In both cases filtering distorted and reduced the amplitude of the low frequency peak, but did not significantly alter the location of the high frequency peak. This was verified by dividing the filtered amplitude spectrum by the transfer functions and also by calculating spectra for the unfiltered photomultiplier output. Filtering permitted the selective amplification of high frequency components, circumventing the problem of quantization noise for small amplitude signals. It did not reduce the number of averages required to resolve the high frequency peak, since the relative error in the periodogram is approximately independent of frequency.

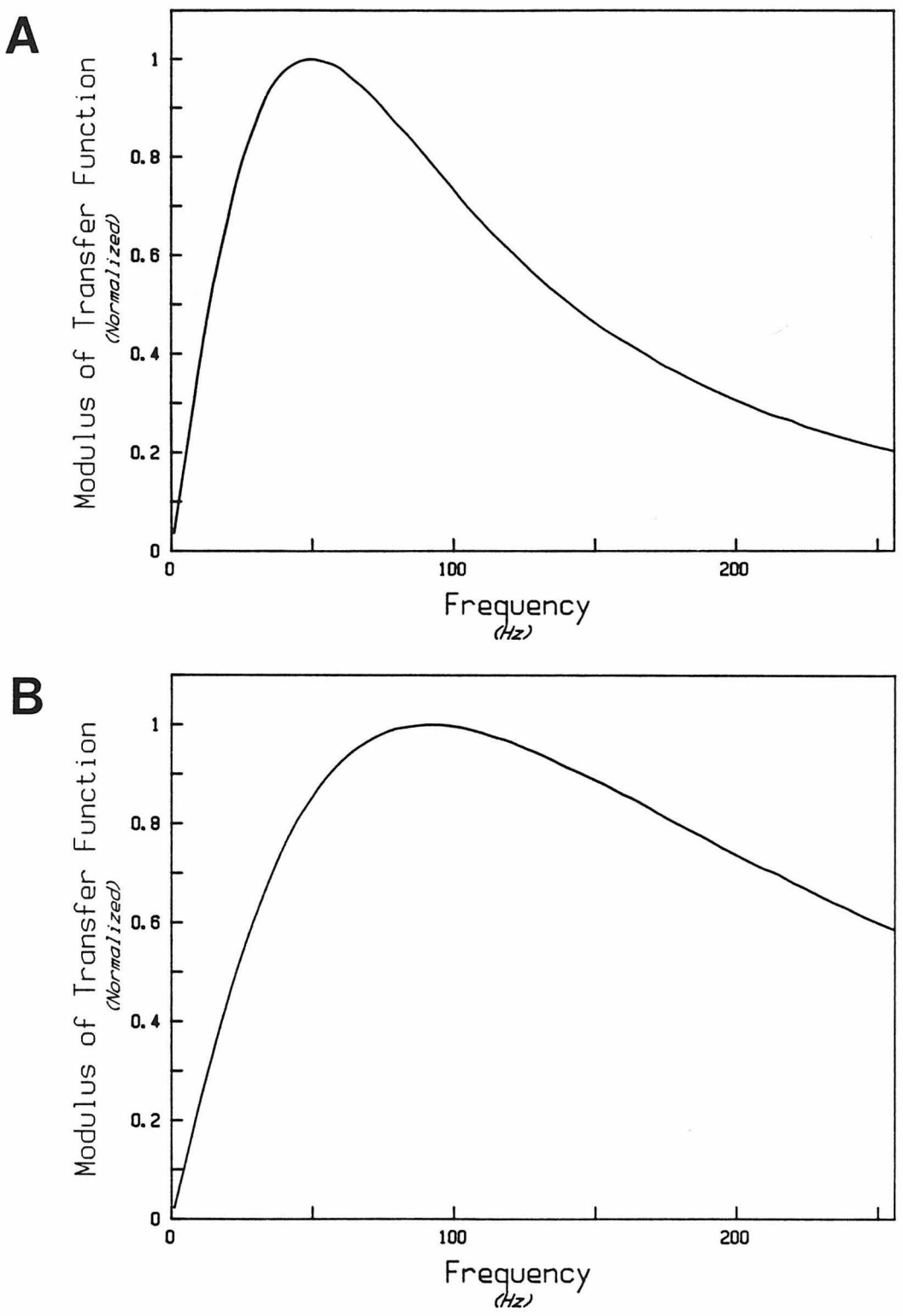
A
Modulus of Transfer Function
(Normalized)
1
0.8
0.6
0.4
0.2
0
0
100
200
Frequency
(Hz)
B
Modulus of Transfer Function
(Normalized)
1
0.8
0.6
0.4
0.2
0
0
100
200
Frequency
(Hz)

Figure 2.5

Figure 2.6. Tracking stage tests of the detector.

The plots illustrate the effect of position, amplitude and vibration axis on power spectra obtained by moving the images of de-energized cells over the photocathode using the tracking microscope stage. A suspension of cells of Streptococcus strain SM197 was exposed to 10 μg/ml FCCP and then loosely attached, in 10 mM glucose, to the surface of a 4 mm diameter circular coverslip, which was held onto the roof of a tantalum tracking chamber by Apiezon L grease. The 3 dB cutoffs for high and low pass filters were set at 72 Hz and 200 Hz respectively. Data were sampled at 256 Hz and spectra for 300 one second data blocks were averaged. The stage was not driven along the X-axis. All input frequencies were 10 Hz. All amplitudes refer to peak-to-peak (p-p) excursions.

A. Cells in focal plane, Y-axis drive amplitude 3.5 μm (p-p).

B. Cells in focal plane, Y-axis drive amplitude 0.6 μm (p-p).

C. Cells in focal plane, Z-axis drive amplitude 3.5 μm (p-p).

D. Cells 40 μm below focal plane, Y-axis drive amplitude 0.6 μm (p-p).

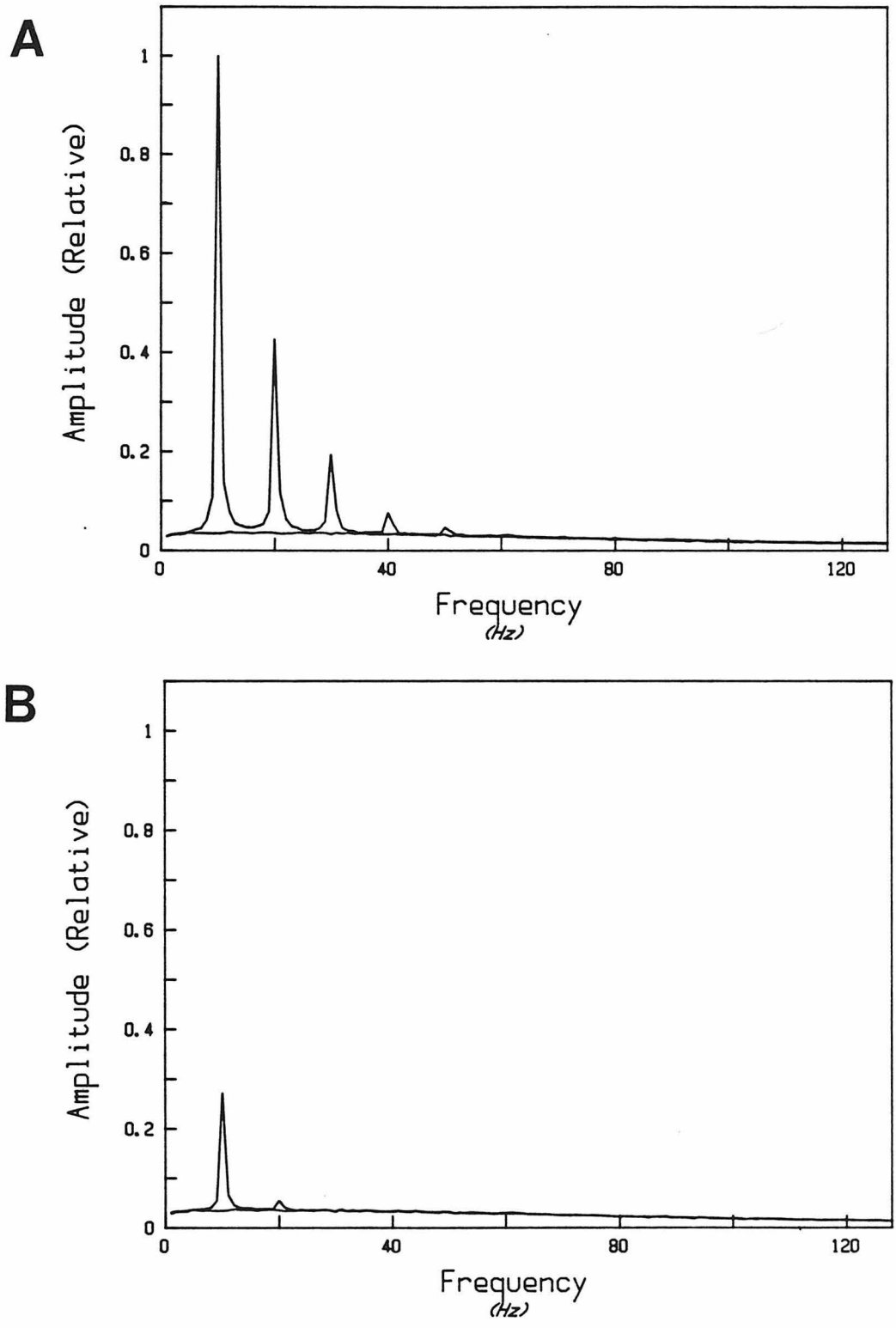

Figure 2.6 A,B. Amplitude

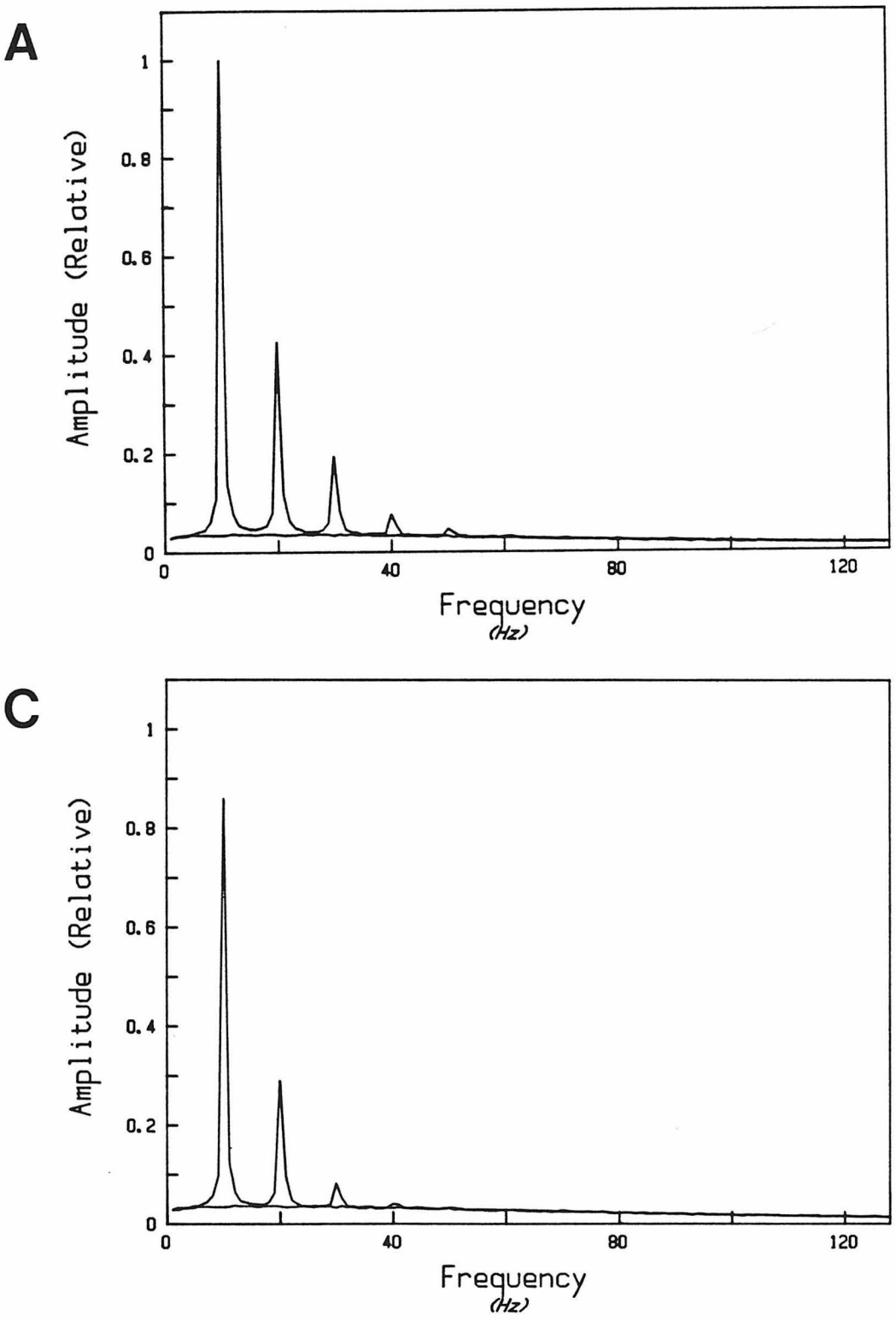

Figure 2.6 A,C. Vibration axis

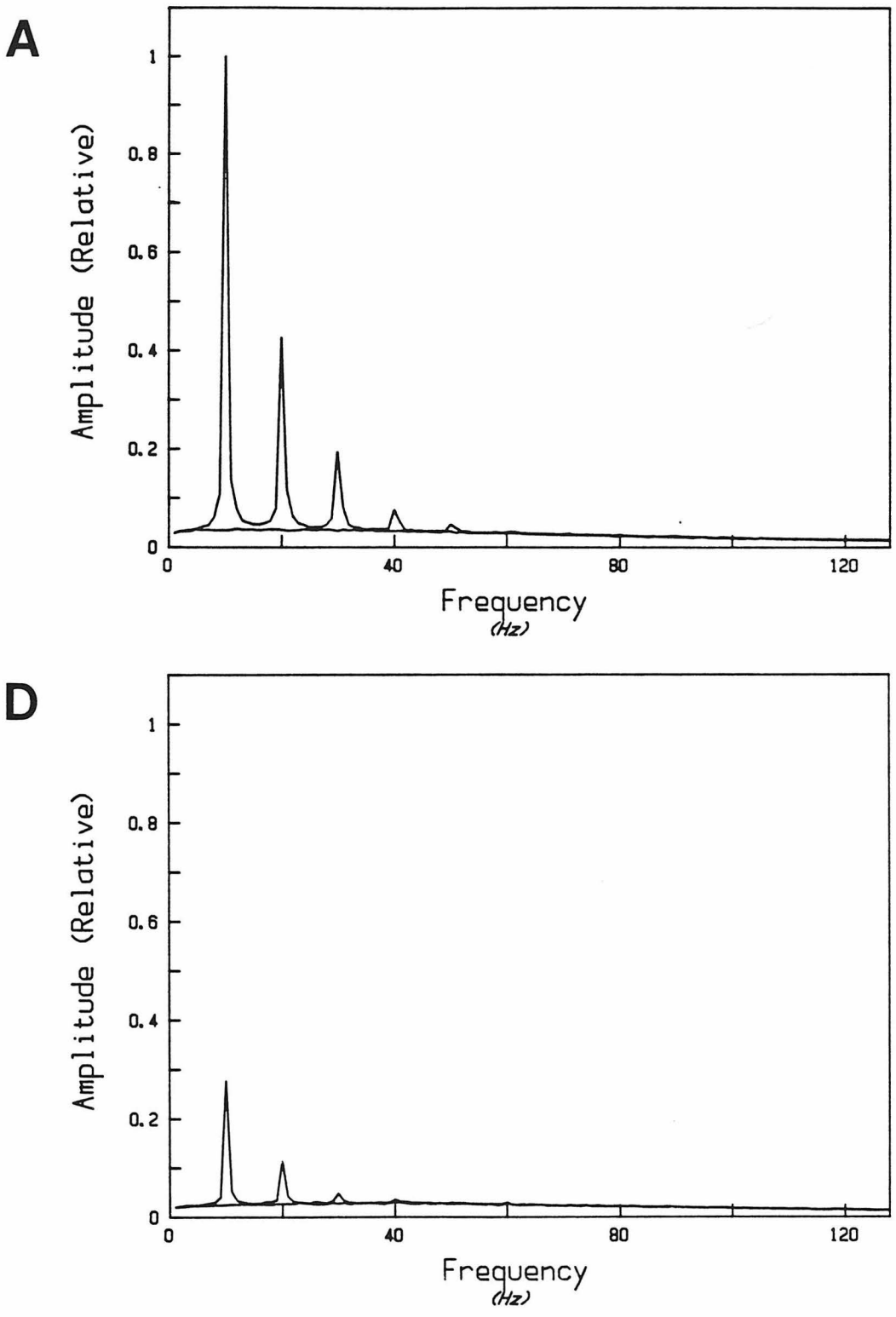

Figure 2.6 A,D. Position

Figure 2.7. Broadening effects in power spectra.

Spectra were obtained by moving the images of de-energized cells over the photocathode using the tracking microscope stage. Cells were prepared and data collected as in Fig 2.5. In all tests cells were located in the focal plane. Amplitudes refer to peak-to-peak (p-p) excursions. Amplitude spectra are plotted. A, B, and C illustrate the broadening effect of shot noise. D illustrates the broadening due to sidebands created by modulation of a high frequency signal by a low frequency signal.

A. Y-axis driven sinusoidally at 10 Hz, amplitude 3.5 μm (p-p).

B. Y-axis driven sinusoidally at 10 Hz, amplitude 3.5 μm (p-p),
X-axis driven by a triangular ramp at a uniform speed of 26.6 μm/s.

C. X-axis driven by a triangular ramp at a uniform speed of 26.6 μm/s.

D. X-axis driven sinusoidally at 5 Hz, amplitude of 3.0 μm (p-p),
Y-axis driven sinusoidally at 30 Hz, amplitude 1.0 μm (p-p).
The peak at 30 Hz has sidebands spaced 5 Hz apart.

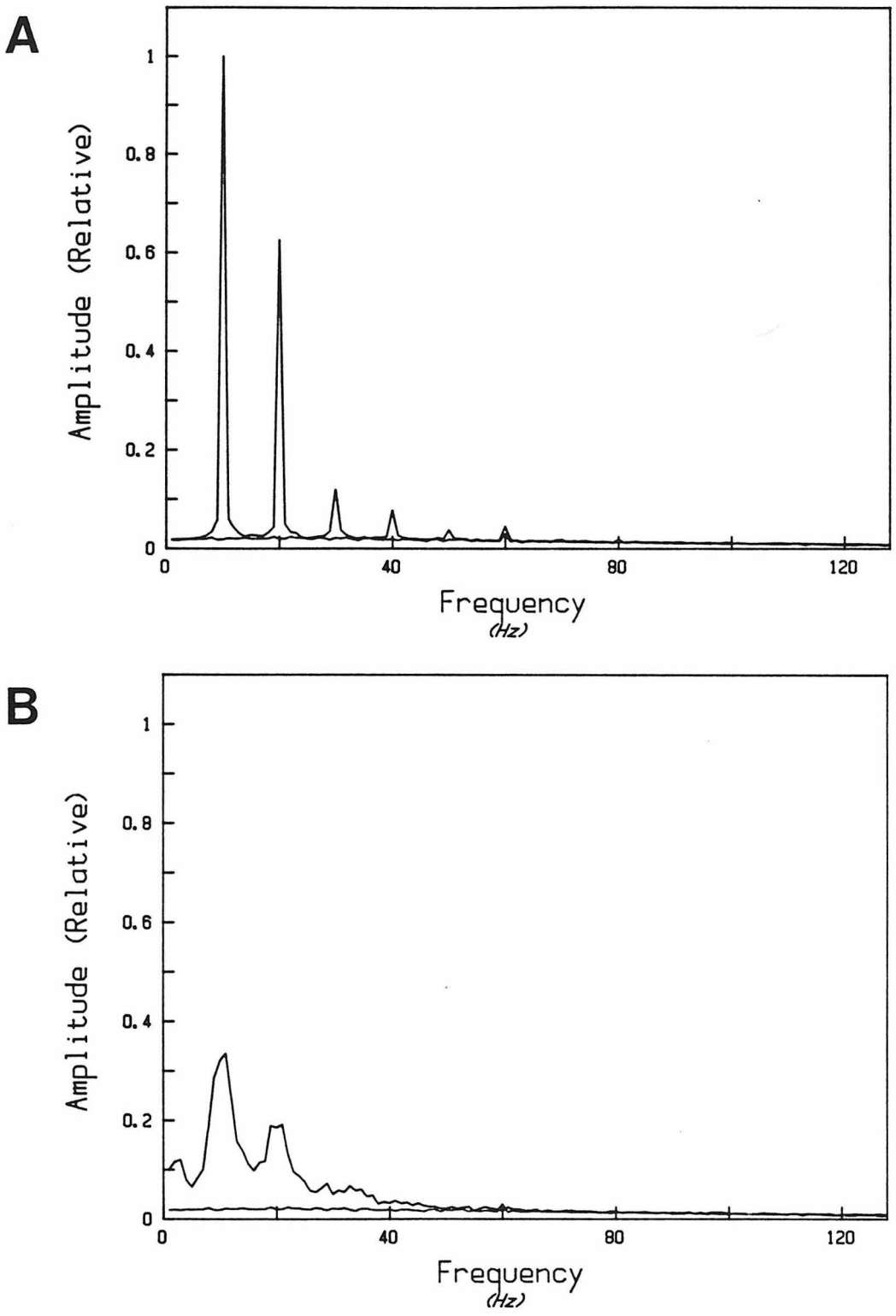
A
Amplitude (Relative)
1
0.8
0.6
0.4
0.2
0
0
40
80
120
Frequency
(Hz)
B
Amplitude (Relative)
1
0.8
0.6
0.4
0.2
0
0
40
80
120
Frequency
(Hz)

Figure 2.7

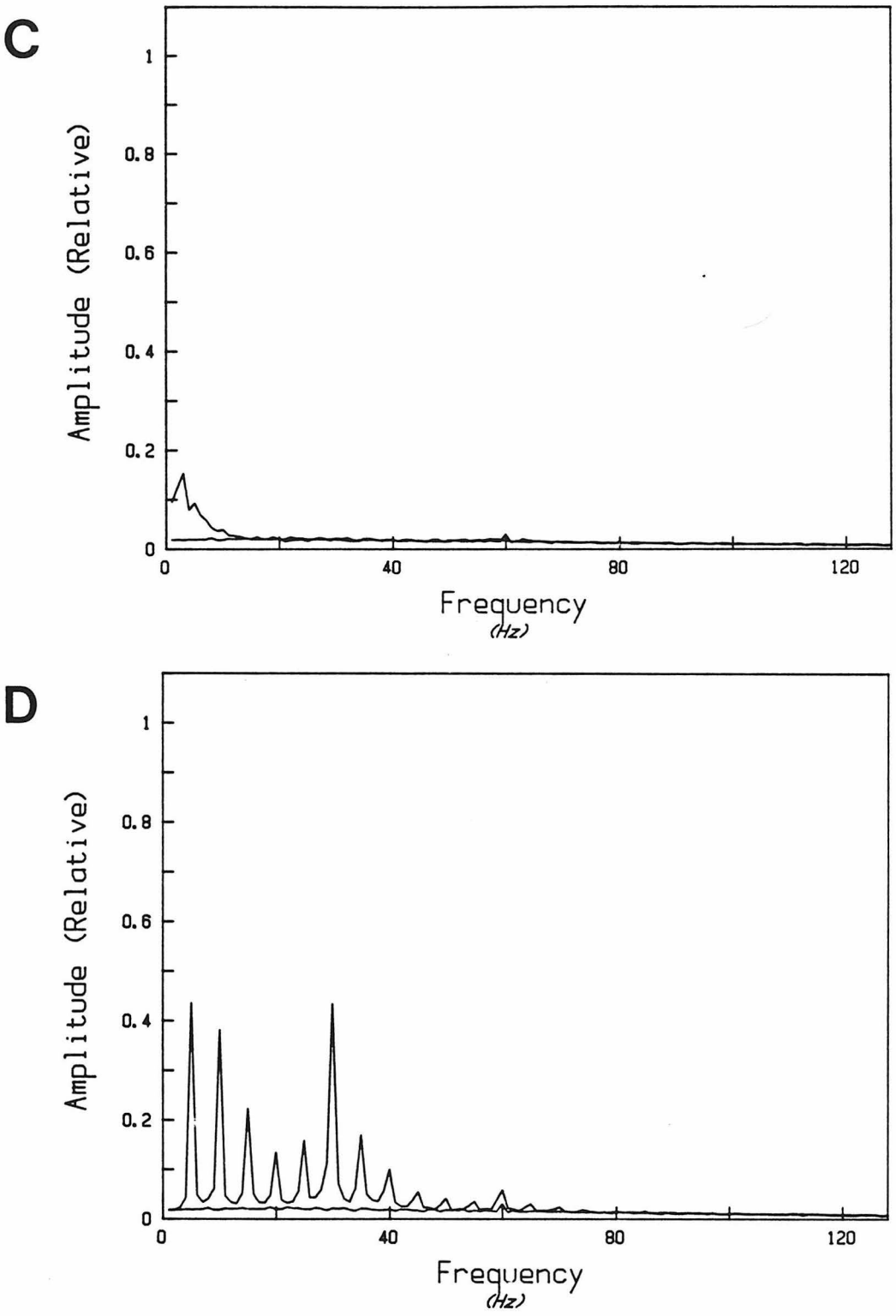
C
Amplitude (Relative)
1
0.8
0.6
0.4
0.2
0
0
40
80
120
Frequency
(Hz)
D
Amplitude (Relative)
1
0.8
0.6
0.4
0.2
0
0
40
80
120
Frequency
(Hz)

Figure 2.7

§2.6. DATA ANALYSIS FOR SPECTRA OF SWIMMING CELLS.

In principle, it should be possible to determine two useful parameters from the power spectrum obtained from a culture of swimming cells - the mean rotation frequency of flagellar bundles, $\langle f_f \rangle$, and the mean counter-rotation ("body roll") frequency of the cell bodies, $\langle f_b \rangle$, both averages over the cell population. The sum of these two frequencies is the average rotation frequency of flagellar motors relative to the cell body. Although Brownian noise, shot noise and detector non-linearity all cause distortions in the frequency domain, for a spectrum similar to that shown in Fig. 5.1 one might expect to be able to simply read off the bundle frequency from the position of the center of the high frequency peak, since this peak appears to be well separated from the tails of the low frequency peak and the noise spectra. Sidebands at frequencies $f_f \pm nf_b$, $n = 1,2,3,...$, would broaden the high frequency peak but preserve its symmetry. Thus, the symmetrical appearance of this peak about its maximum power frequency would reflect a symmetrical distribution of bundle frequencies over the cell population.

The situation is more complicated for the low frequency peak, whose shape is not only determined by the distribution of body roll frequencies, but is distorted by a series of higher harmonics, and by contributions from noise spectra. For the cell culture of Fig. 5.1, observations on single cells by slow playback of video recordings gave a body roll frequency of 6.7 ± 0.55 Hz (mean ± S.E.M.), although the peak maximum is at 8 Hz.

In order to gain an idea of how much the high frequency peak would be distorted by overlap with the low frequency peak, a computer program

was written to simulate the motion of a swimming cell over a non-linear detector. Let $\Phi(X,Y)$ be the quantum efficiency at a position (X,Y) on the photocathode and $F(X,Y;z,\theta)$ be the intensity distribution in the (X,Y) plane for the image of a cell body centered at X=0,Y=0, at a distance z above the focal plane and with its axis of cylindrical symmetry pointing along the vector defined by the spherical polar coordinates $(\theta,\phi=0)$. Then the photocurrent for a cell at an arbitrary location $\vec{x} = (x,y,z,\theta,\phi)$ is given by:

$$J = \iint_{\text{Detector}} F(R_\phi(X-x,Y-y);z,\theta)\Phi(X,Y)\,dX\,dY \qquad (2.1)$$

where R_ϕ is a rotation through an angle ϕ,

$$R_\phi(x,y) = (x\cos\phi + y\sin\phi \ , \ -x\sin\phi + y\cos\phi).$$

The current as a function of time can be calculated from this by substituting the equation of motion, $\vec{x} = \vec{x}(t)$, for a swimming cell. This exact model would require much effort in (1) elucidating the kernel F, which characterizes the optical properties of the microscope and cell body, (2) solving the complex hydrodynamic problem of the swimming bacterium, and (3) measuring the response function of the detector. It was therefore decided to simplify the model, while still retaining the main qualitative feature of nonlinearity, by restricting trajectories to the (X,Y) plane, replacing F with a delta function, and assuming a simple, single humped form for Φ.

The cell was modelled as a point moving at constant velocity, v, along the X-axis, while oscillating along the Y-axis (at the body roll and bundle frequencies), over a detector with a radial gaussian response

function. Thus the output current is given by:

$$I = \exp\left(- \left[X^2 + (Y + b)^2 \right] / 2\sigma^2 \right) \qquad (2.2)$$

where: $X = vt$

$Y = A\sin\Omega t + a\sin\omega t$

$\Omega = 2\pi f_b$ = body roll angular frequency

$\omega = 2\pi f_f$ = bundle angular frequency

σ = detector half-width

b = impact parameter (the distance of closest approach between cell body and center of detector).

The calculated output from this gaussian detector was Fourier transformed and multiplied by the transfer function measured for the bandpass filter applied to the experimental photomultiplier signal (Fig. 2.5). Initially v, A, a, f_b, and f_f were assumed to be fixed independent parameters. For simplicity, the parameters σ and b were given fixed values: σ = 1.5 μm, and b = 2 μm. Varying the detector width is equivalent to scaling the speed, v, the amplitudes, A and a, and the parameter b. Varying the parameter b changes the range of amplitudes over which nonlinearity becomes significant. For single input frequencies, the resulting power spectra qualitatively resembled those obtained previously in the tracking stage tests, although the relative amplitudes of the higher harmonics were different owing to the omission of the detailed shapes of the detector response and of the phase contrast images. The peaks were broadened when shot noise was increased by increasing the swimming speed, v. Increasing the amplitude, A, resulted in an increase in the amplitudes of the harmonics of f_b. These

synthetic power spectra were then averaged using a normal distribution for the bundle frequencies,

$$F_f(f_f) = \frac{1}{\sigma_f\sqrt{2\pi}} \exp(-(f_f-f_{fo})^2/2\sigma_f^2) \qquad (2.3)$$

with mean f_{fo}, and variance σ_f^2, summed from $f_{fo}-1.5\sigma_f$ to $f_{fo}+1.5\sigma_f$ in steps of $\sigma_f/20$, and a skew exponential distribution for the body roll frequencies:

$$F_b(f_b) = \frac{1}{f_{bo}^2} f_b \exp(-2f_b/f_{bo}) \qquad (2.4)$$

with mean f_{bo}, and variance $f_{bo}^2/2$, summed from 0 to $3.5\, f_{bo}$, in steps of $f_{bo}/20$. The choice of a skew distribution is justified below. Each cell is assumed to have fixed bundle and body roll frequencies, and $F(f)\delta f$ is the number of cells with frequency in the range $[f,f+\delta f]$. Two methods were used to obtain an average over these distributions. In the first case, the power spectrum was computed from the average signal:

$$\langle I\rangle = \sum_{i,j} F_f(f_f^i)F_b(f_b^j)I(f_f^i,f_b^j) \qquad (2.5)$$

where the index i labels the bundle frequency, and the index j labels the body roll frequency. In the second case the power spectrum of each term in the sum (2.5) was computed, and these spectra were then averaged. The experimental method actually involves a combination of averaging signals from many cells and averaging many power spectra. Many cells cross the detector simultaneously, producing an average signal which is sampled repeatedly over 1 second intervals. A power spectrum is computed from each sample and many such spectra are averaged. In both

cases, appropriate choice of model parameters allowed the computer generated spectra to closely mimic the experimental spectra. This does not imply that (2) and (3) are the actual distributions in populations of swimming cells. It merely confirms that the overall shape of the power spectrum is determined by the nonlinearity of the detector response function rather than by its detailed shape, and is also relatively insensitive to the detailed image structure and frequency distributions. When the body roll distribution was replaced by a normal distribution:

$$F_b(f_b) = \frac{1}{\sigma_b\sqrt{2\pi}} \exp(-(f_b-f_{bo})^2/2\sigma_b^2) \qquad (2.6)$$

with mean f_{bo}, and variance σ_b^2, summed from 0 to $3.0f_{bo}$ in steps of $f_{bo}/20$, the low frequency peak acquired bumps associated with harmonics at multiples of the frequency f_{bo}. These bumps were smoothed out considerably when the model was refined by allowing the swimming speed to vary with the body roll frequency:

$$v = r_1 f_b \qquad (2.7)$$

where r_1 depends only upon the geometry of the swimming cell. The value of r_1 was obtained from the mean values of v and f_b determined by playback of video recordings of swimming cells (r_1 = 2.3 μm for the cells of Fig. 5.1). In this way, higher frequency contributions to the peak were broadened by increased shot noise, leading to a skewing effect. Since the distribution of roll frequencies obtained from video recordings was not markedly asymmetric (Fig. 2.5), equation (2.4) cannot represent the true distribution; it is simply an approximate model of

the skewing effect. This effect smooths out the tail of the low frequency peak in the spectrum by bridging the gaps between higher harmonics.

Other experimental complexities may cause further smearing of the spectrum. For example, the computer models did not attempt to include contributions from out-of-focus cells. Moving a cell body out of the focal plane would have the following consequences: (1) Its image structure would change, thereby altering the relative amplitudes of the higher harmonics; (2) its image size would be magnified; this is equivalent to an increase in the parameters A and a (which would increase the harmonic amplitudes) and v (which would increase broadening due to shot noise); and (3) its image intensity would decrease. If cells were also allowed to have a velocity component along the Z-axis, these three factors would vary with time for each cell trajectory. Such features were not incorporated into the models because they would require a detailed study of the optical kernel, F, for the phase contrast images of cell bodies. However, it was found that harmonic bumps in the simulated spectrum could be smoothed out further by choosing large values for the amplitudes A and a, and for the swimming speed factor, r_1, thus partially incorporating the second effect of out of focus cells listed above. A more accurate model would include distributions of these parameters which depend on F. The idea that much of this smoothing might be due to out-of-focus contributions is supported by measurements made on suspensions of cells swimming in a very thin chamber about 10 μm in depth. In such a chamber, all cells remain in focus and spectra so obtained showed distinctly separated harmonic bumps, in agreement with the computer simulation results.

Apart from including intrinsic body roll and bundle frequency distributions, the models did not take into account biological variability in the cell culture. For an ensemble of cells with identically shaped bodies and bundles, a bundle frequency distribution might arise from a distribution of the motor torque, N, about a mean value. For example, the torque could be imagined to vary from motor to motor due to differences in the number of force generating units (Block & Berg, 1983), from bundle to bundle due to differences in the number of filaments, and from cell to cell due to differences in Δp. The bundle frequency is given by:

$$f_f = \frac{n}{2\pi G} N \qquad (2.8)$$

where G is a geometric factor approximately equal to the rotational drag coefficient of the flagellar bundle, and n is the number of filaments in the bundle. Thus any observed distribution in f_f will be determined by the distributions of the variables n, N and G. However, experiments described in Chapter.3 have shown that the bundle frequencies of swimming cells are approximately independent of changes in the value of G. Therefore the shape of the bundle frequency peak should primarily reflect the distribution of the product of the variables n and N, with some smearing and distortion due to convolution with the distribution of G. The omission of variability of bundle and body shapes should not have a major impact on the results of the computer models. I obtained the distribution of n for a sample of 355 cells using data derived by Markus from preparations of stained flagella (see his thesis) and found that it conformed reasonably well to a symmetric normal distribution (χ^2 = 1.06, 7 degrees of freedom). Thus, if n and N are assumed to be

independent, a symmetrical distribution of bundle frequencies (as seen in the power spectra) implies an approximately symmetrical distribution of motor torques, N. On the other hand, v and f_b are related to f_f by geometric factors which vary considerably between cell bodies of different shapes. For a given f_f, the thrust is fixed and the value of v is determined to first order by the translational drag coefficient of the cell body, and for a given torque, the value of f_b is determined to first order by the rotational drag coefficient of the cell body. Both of these drag coefficients vary considerably depending on the shape and angle of inclination of the swimming cell body relative to its axis of translation. In fact, frame by frame inspection of video recordings of swimming cells revealed that the instantaneous angle of inclination of a single cell was not fixed but fluctuated with time. It should be kept in mind that, in general, any correlation between bundle frequency and optical properties of cell bodies is a potential source of error. For example, cells with thick, bright cell walls might tend to have larger values of Δp, and hence have higher bundle frequencies, leading to a skewing of the bundle peak towards high frequencies. Obviously, many such correlations might be imagined. I have implicitly assumed the absence of such correlations in my analysis.

Brownian motion was included in the simulations by adding a two dimensional random walk to the equations (1) defining the position of the point in the X-Y plane, and allowing the cell body to undergo rotational diffusion. Paths were computed by integrating the following stochastic differential equations:

$$
\begin{aligned}
dX &= v\cos\theta dt - \sin\theta(A\Omega\cos\Omega t + a\omega\cos\omega t)dt + \cos\alpha dS \\
dY &= v\sin\theta dt + \cos\theta(A\Omega\cos\Omega t + a\omega\cos\omega t)dt + \sin\alpha dS \qquad (2.9) \\
d\theta &= dR
\end{aligned}
$$

where θ is the angle of the velocity vector $\vec{v}$ relative to the X-axis, α is uniformly distributed in $[0,2\pi]$, dS is the absolute value of a Gaussian random variable with mean zero and variance $4D_T dt$, and dR is the absolute value of a Gaussian random variable with mean zero and variance $2D_R dt$. D_T is the isotropic translational diffusion coefficient of the cell body, and D_R is its rotational diffusion coefficient about the minor axis. The values of these coefficients were taken as $D_T = 2 \times 10^{-9}$ cm^2/s and $D_R = 8 \times 10^{-2}$ radians^2/s, numbers which were obtained from the estimates of the drag coefficients calculated by Markus, who modelled cell bodies as cylinders (Meister, 1987). The effect of the Brownian noise was to add a baseline to the power spectrum and to slightly broaden the low frequency peak. There were no major distortions in the shapes of the peaks.

Various methods of estimating the mean bundle frequency from the power spectral data could be tested by using the computer model to compare the value of each estimator with the input frequency, f_{fo}. When the bundle frequency peak was well separated from the harmonic tail of the low frequency peak, a useful estimator was obtained as follows. A difference spectrum, S_2, was computed by subtracting the amplitude spectrum, S(A,a=0), containing only the body roll peak, from the amplitude spectrum, S(A,a), containing both the body roll peak and the bundle peak. The mean bundle frequency was then estimated using the formula:

$$f_1^* = \sum_{i=1}^{256} f_i S_2(f_i) \qquad (2.10)$$

where $f_i = i/256$ is the frequency corresponding to the i-th point in the discrete Fourier transform obtained from computing the values of the signal at the points $t_k = -0.5 + (k-1)/512$ s, k=1,...,512. The overlap was defined as the ratio of the area of intersection between the regions under the two spectra S(0,a) and S(A,0) to the area under the spectrum S(0,a). For overlap values up to about 30%, f_1^* underestimated the mean bundle frequency by less than 4%. When the overlap was 100% the error was much greater - typically in the range of 50%.

For data analysis, the following procedure was used. Power spectra were obtained from a culture of swimming cells and a smoothed spectrum was computed by averaging over many (N > 100) data blocks. Averaging N spectra reduces the variance, $\sigma_p^2(f)$, in the power spectral density by a factor of 1/N. A control (noise) spectrum was obtained from the same culture in which motility had been arrested by addition of a proton ionophore (FCCP or DNP), and this was smoothed using a cubic spline algorithm (Reinsch, 1967). A difference spectrum was computed by subtracting the noise spectrum from the spectrum for swimming cells, and this was also smoothed using the same routine. The smoothing parameter was chosen so as to remove fluctuations of order σ_p in the power. Test spectra obtained for very large N (>1000) verified that no detailed structure was being lost in such smoothing operations. Parameter values in the computer model with no Brownian noise were chosen by trial and error to generate a body roll spectrum which closely matched the smoothed difference spectrum at low frequencies. This simulated roll

spectrum was subtracted to give a spectrum, S_2, which was used to estimate the mean bundle frequency according to a modification of equation (2.10) in which the upper and lower summation limits were chosen to bracket the high frequency peak and exclude both high frequency noise and low frequency distortions due to model mismatch. The procedure was used for data obtained from metabolising swimming cells, whose bundle frequency peaks were narrow and well separated from the body roll peak. The shapes of these spectra were well reproduced by models having overlap values smaller than 30%.

Subtracting the noise spectrum removed the baseline introduced by photomultiplier shot noise and Brownian noise, although their broadening effects remained. How is this subtraction justified? Nonlinear coupling between Brownian and swimming motion is expected to be small around the high frequency peak where vibration amplitudes are much less than the distance over which the detector response, Φ, changes its slope. Also, modulation of the photomultiplier noise as cells move over the detector is expected to be small because a typical cell body induces a variation in the total photocurrent of only a few percent.

The control spectra with de-energized cells were obtained under conditions which approximated as closely as possible those under which swimming cells were observed. However, one might expect some difference in the Brownian motion contribution to the spectrum due the difference between the diffusion coefficients for cells with flagellar filaments aligned in a bundle and those for cells whose filaments are spread out in random directions. This error is probably small because the noise spectrum for de-energized cells looks identical to that for polystyrene latex beads, which are of similar size but which do not carry flagellar

filaments. Another source of error which is significant is the slow sedimentation of de-energized cells in the flow chamber during the course of data acquisition, resulting in a systematic reduction in the mean cell density at the focal plane. This problem was overcome by only collecting data on single preparations over times small compared to the sedimentation time (2 - 3 min) and accumulating data from several separate preparations.

Another estimator of f_{fo} tested was f_2^*, defined as the position of the local maximum of the bundle peak in the spectrum S_2. The values obtained in this case agreed to within a few percent with those obtained from f_1^*, which is consistent with the observation that the asymmetry introduced into the bundle peak by overlap is small. Amusingly enough, the values obtained by these rather elaborate procedures agreed to within a few percent with the frequencies taken directly off the raw data by eyeballing the location of the local maximum of the high frequency peak. The latter technique had been used to obtain bundle frequencies before the computer models were constructed. The models were useful in justifying the use of such methods and also helped to confirm the general ideas about how the detection process worked.

Figure 2.8. Swimming cell simulations.

Sample paths and power spectra were computed from models of swimming cells simulated as described in §2.6 (see text), except that rotational diffusion of the cell body axis was omitted. The detector response, Φ, was Gaussian with width 2σ = 3 μm. The impact parameter, b, was fixed at 2 μm. The body roll amplitude was set at 2.8 μm and the bundle induced gyrational amplitude at 0.112 μm.

A. Sample path for a cell swimming with speed 17.69 μ/s, body roll frequency 5.63 Hz, and bundle frequency 84 Hz, with initial velocity parallel to the Y-axis and initial oscillation parallel to the X-axis. The circle drawn has radius 2σ and defines the detector aperture.

B. Signal resulting from the sample path of A. (before the addition of photomultiplier white noise).

C. Filtered power spectrum computed from the signal shown in B. The filter transfer function corresponds to that measured for the experimental apparatus.

D. Amplitude spectrum obtained by averaging many spectra of paths like A., in which the bundle frequency was normally distributed with mean f_f = 90 Hz, standard deviation σ_f = 15 Hz, and the body roll frequency was normally distributed with mean f_b = 6.92 Hz, standard deviation σ_b = 3.23 Hz. The body roll frequencies were obtained by scaling the bundle frequencies by a factor, $1/r_2$ = 0.077, and then increasing the variance of the distribution by a factor of 2.8 to account for cell size variability. The swimming speed was correlated with the roll frequency according to Equation (2.7) of the text, with r_1 = 0.5 μm. Diffusion was incorporated as in Equations (2.9), and a white noise baseline was added (with an amplitude equal to 14% of the maximum detector response).

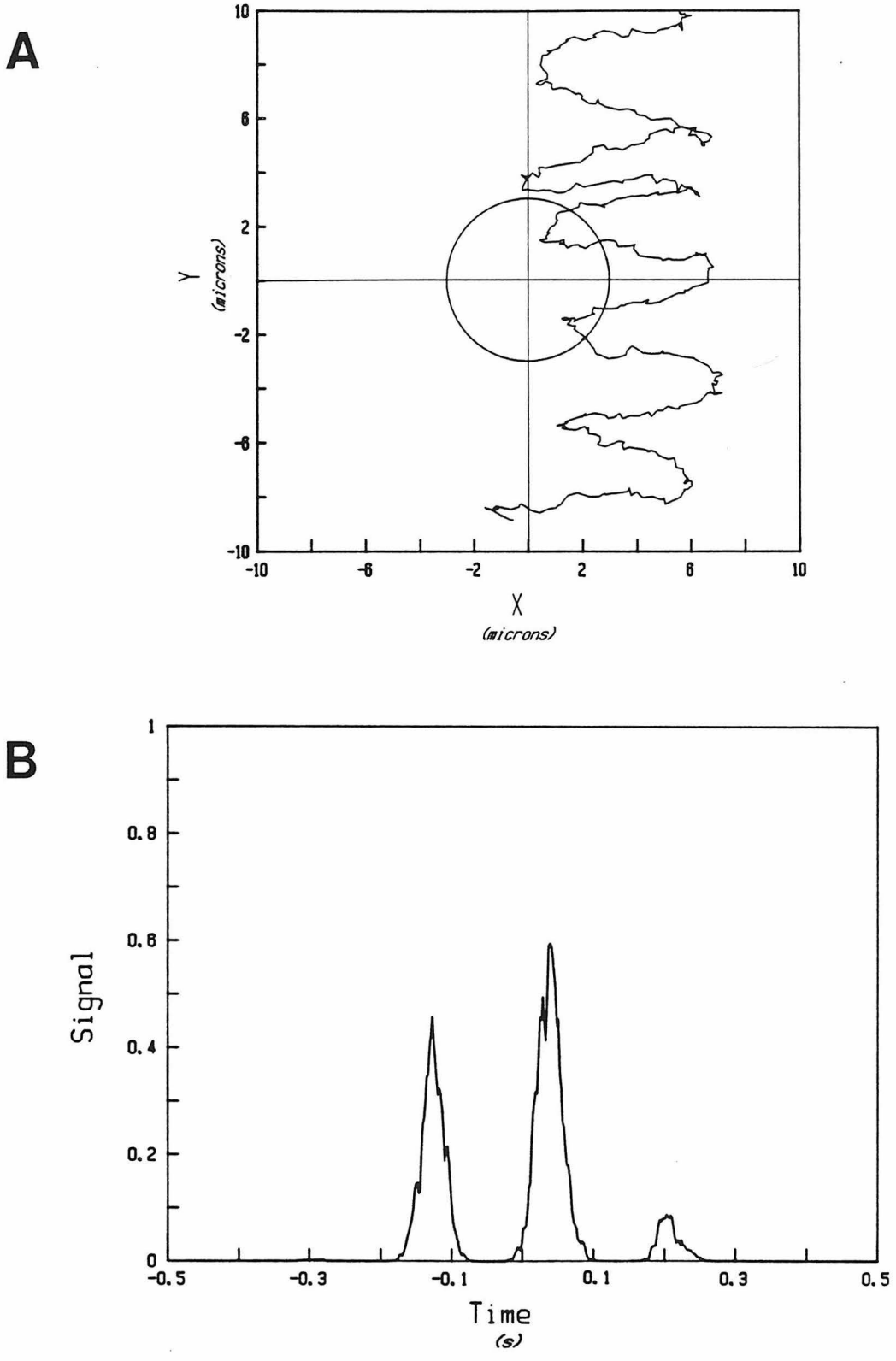
A
10
6
2
-2
-6
-10
Y
(microns)
-10
-6
-2
2
6
10
X
(microns)
B
1
0.8
0.6
0.4
0.2
0
Signal
-0.5
-0.3
-0.1
0.1
0.3
0.5
Time
(s)

Figure 2.8

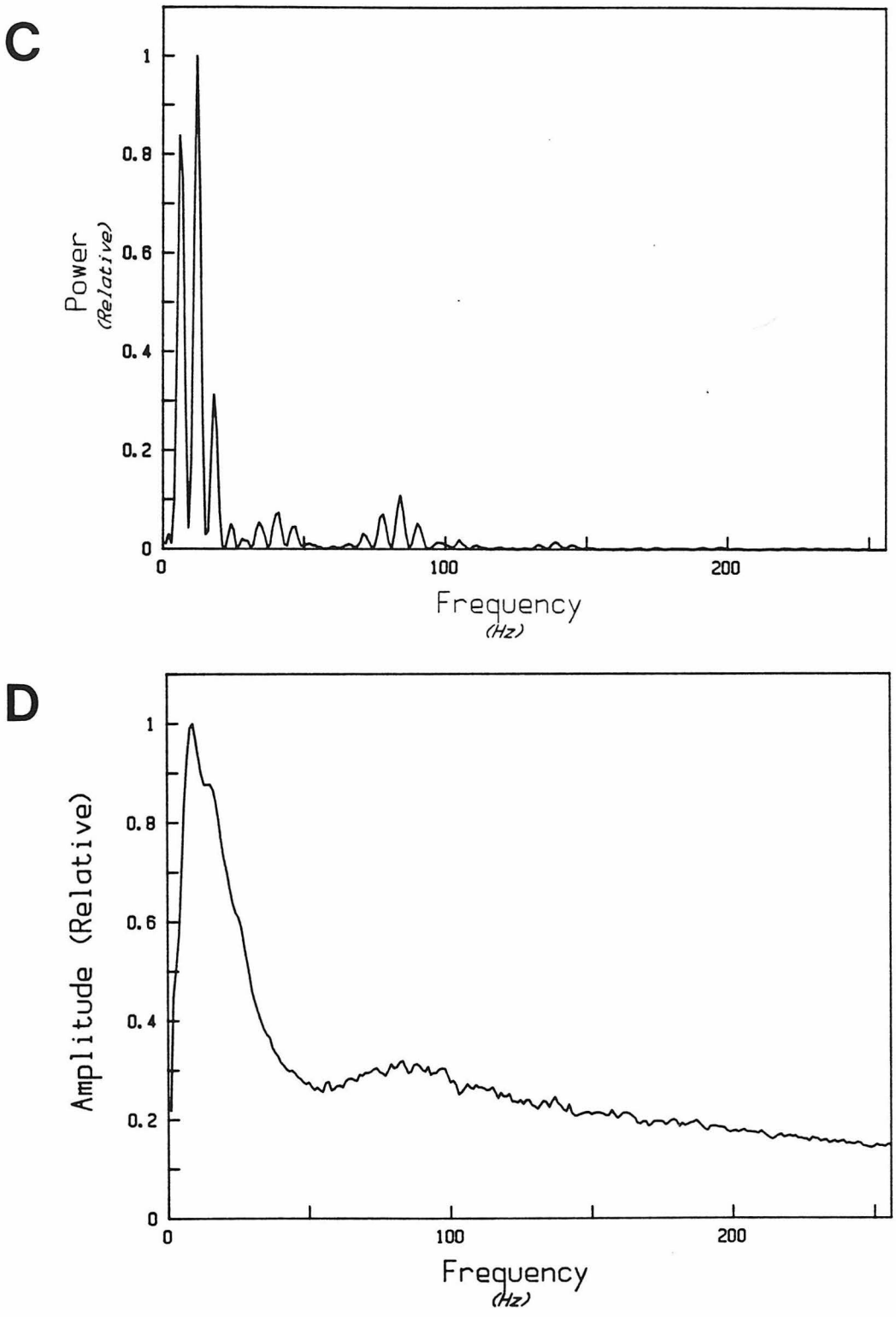
C
Power
(Relative)
1
0.8
0.6
0.4
0.2
0
0
100
200
Frequency
(Hz)
D
Amplitude (Relative)
1
0.8
0.6
0.4
0.2
0
0
100
200
Frequency
(Hz)

Figure 2.8

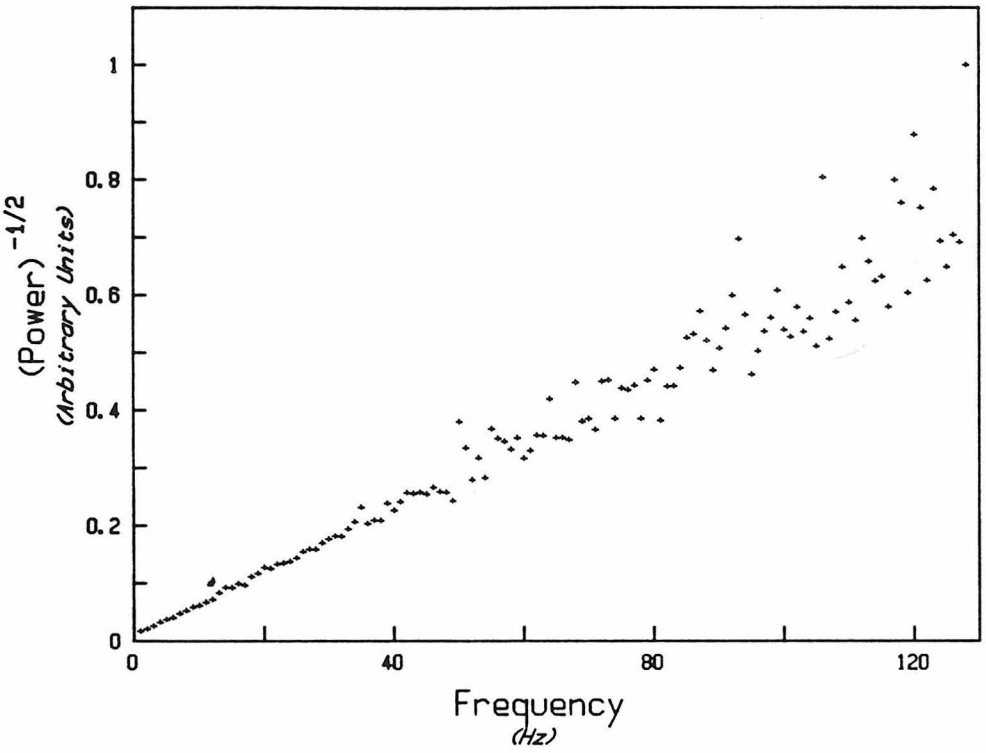

Figure 2.9. A plot of (Power)$^{-1/2}$ vs Frequency for Brownian motion.

The power spectrum was computed from the photocurrent noise generated by a suspension of de-energized cells. Experimental conditions correspond to those described in Fig 5.1. Data were sampled at 512 Hz and spectra corresponding to 200 one second data blocks were averaged. A noise spectrum which did not include any contribution from the motion of cell bodies was obtained from the static image of a grease smear adjusted to yield the same mean photocurrent as the cells. This spectrum was subtracted from that of the cells, and the result was divided by the measured transfer function for the filters. The slope of the line is inversely proportional to the R.M.S. value of the convolution of the detector response function, Φ, with the cell image structure factor, F (see §2.6).

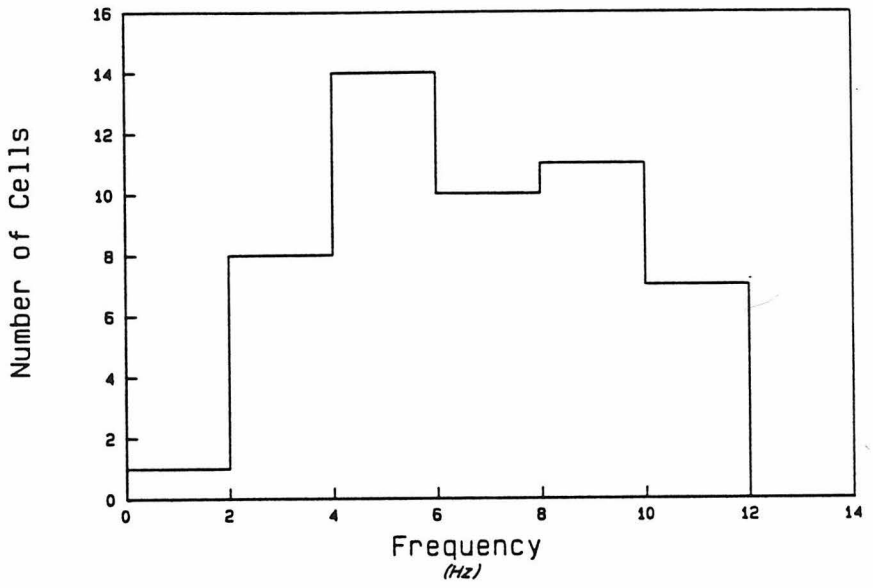

Figure 2.10. The body roll frequency distribution in swimming cells.

The distribution of body roll frequencies was measured for metabolizing Streptococcus SM197 in a phosphate buffer (Buffer T2 (pH 7.5) + 0.01 M D-glucose). Videotapes were made of inverse phase contrast images of energized, motile cells under the same conditions as in Fig 5.1 and frequencies were obtained during slow frame-by-frame playback by directly counting the number of wobbles executed in a known time interval for every measurable cell in a field defined by a common initial frame. A cell was deemed to be not measurable if its wobbles could not be observed because its trajectory took it out of the focal plane in subsequent frames or if its motion did not exhibit any periodicity during its passage through the focal plane. The histogram represents the pooled data from three individual experiments, with means and standard deviations of: 6.7 ± 2.4 Hz (19 cells, same culture as in Fig 5.1), 7.2 ± 3.0 Hz (17 cells) and 6.8 ± 2.8 Hz (15 cells).

CHAPTER 3

THE EFFECT OF VISCOSITY ON FLAGELLAR ROTATION

§3.1. Introduction

This chapter describes the experiments I conducted with swimming cells to study how the speed of the flagellar motor varies when the external load is changed. The corresponding experiments with tethered cells were done by Manson et al. (1980), who changed the viscosity, η, of the medium using Ficoll and found that the angular velocity of each cell was proportional to the fluidity, $1/\eta$. Since the torque, N, generated by the motor must be equal in magnitude to that exerted by external frictional forces, the following relation holds:

$$N = f_R \Omega = \eta G \Omega \qquad (3.1)$$

where Ω is the angular velocity of the cell, $f_R = \eta G$ is the frictional drag coefficient of the external load, and G is the geometric drag coefficient, a factor which depends on the shape and size of the load. Manson et al. deduced that, for the range of speeds over which tethered cells spin ($\lesssim$ ca. 13 Hz), N must be independent of speed. Preliminary studies done using hook mutants of E. coli, described in Berg et al (1982), showed that flagellar motors run at much higher speeds (ca. 100Hz) when f_R is made very small. These speeds did not change when 0.6 μm diameter polystyrene latex beads were attached to the hooks, an enormous increase in load. Hooks are only ~20 nm in diameter. For spheres, f_R scales as the cube of the diameter, implying that the torque must have increased by a factor of ca. 3×10^4. Thus, at small loads and high speeds, the speed appears to be independent of torque.

It is useful to picture the motor as a device which relates speed and torque at any given protonmotive force - if Δp is fixed and the motor is observed to run at a certain speed, then a unique torque must

be generated by the motor at that speed:

$$N = H(\Omega;\Delta p) \qquad (3.2)$$

The value of N for any given external load can be computed from equation (3.1). However, the function H is not dependent on the external load - it is a determined solely by internal parameters which characterize the torque generating machinery. For any given load, f_R, the operating point of the motor in the torque-speed plane is obtained by solving the equations (3.1) and (3.2) for N and Ω. The experiments mentioned above define the values of H close to the $N = 0$ axis and close to the $\Omega = 0$ axis. My experiments were aimed at defining the values of H at points intermediate between these two extremes by varying the load. This was done by varying the viscosity of the medium rather than the shape or dimensions of the load, since geometric drag coefficients are difficult to estimate accurately. Using the techniques described in Chapters 2 & 5, I measured the mean bundle frequency for suspensions of cells swimming in media whose viscosities varied from less than 0.1 cP to about 1 cP. As an independent control for these measurements, Howard used his tracking microscope to obtain mean swimming speeds for bacteria prepared in the same way as in my experiments, and swimming over the same range of viscosities. If the cell geometry (body plus bundle) does not change much over this range of viscosities, the swimming speed should be proportional to the bundle frequency and vary accordingly. This would, in turn, allow one to argue that the actual viscosity dependence of frequency was not simply an artifact resulting from geometry changes.

§3.2 Methods

§3.2.1 Viscous solutions.

The substance of choice for controlling the viscosities of solutions was Ficoll-400 (Pharmacia), a roughly spherical, branched synthetic molecule (M.W. 400,000 ± 100,000) formed by copolymerization of sucrose and epichlorohydrin. It is highly soluble in aqueous media (over 50% w/v) and its solutions are Newtonian (Berg & Turner, 1979). Due to its high molecular weight, very viscous solutions can be obtained at relatively low osmolarities (e.g. a 20% w/v aqueous solution is 0.5 mM and has $\eta \simeq 16$ cP). Stock solutions (20% w/v) were made up in a standard medium (either a buffer or KTY growth medium) as follows. Dry Ficoll (20 gm) was weighed out in a 100 ml volumetric flask, and about 60 ml of the buffer was added. This mixture was swirled on a gyrating shaker at room temperature (22°C) until optically homogeneous. Additional buffer added to give a volume of 100 ml. Alternatively, the Ficoll was dissolved in a beaker and then washed into the flask. Solutions of lower concentration were obtained by serial dilution of this stock solution into the standard medium. The problem of dispensing accurately known volumes of the highly viscous stock solution was solved by measuring its density and weighing out aliquots.

All measurements of viscosity were done using Cannon-Ubbelohde viscometers whose interior surfaces were cleaned with fuming nitric acid (70°C, 1 hour, the same treatment as used in cleaning coverslips, §2.3). A calibration curve relating viscosity to Ficoll concentration was obtained for solutions in E. coli motility medium (Buffer MM, also known as 1:3 motility medium) by measuring the viscosities of 0, 2, 3, 4, 6, 8, 10, 16.25 and 20 % (w/v) solutions. The temperature of the

viscometer was controlled at 32°C in a heated, stirred water bath. Between measurements, the viscometer was rinsed out with distilled water and ethanol, and dried in an oven at 150°C. Drainage times, T_d, were measured by eye and stopwatch and the dynamic viscosity, η, was computed from the mean of three consecutive measurements, with standard deviation less than 0.2 %, using the equation:

$$\eta = \rho K T_d \qquad (3.3)$$

where ρ is the density of the solution, and K the viscometer constant. The density was calculated by linearly interpolating between the density, $\rho_{20} = 1.067 \pm 0.001$, of the 20% solution, and the density, $\rho_0 = 0.995 \pm 0.004$, of the buffer, both measured at room temperature (22°C), and then correcting for thermal expansion by linearly interpolating data for H_2O taken from the AIP Handbook (Sec 2-152). For concentrations of 10% or less, viscometer 75L321 ($K = 8.13 \times 10^{-5}$ cm^2/s^2) was used, and for greater concentrations, viscometer 150K361 ($K = 3.289 \times 10^{-4} cm^2/s^2$) was used. The data were fit well by a relation of the form:

$$\ln\eta = a_0 + a_1 c + a_2 c^2 \qquad (3.4)$$

where c is the Ficoll concentration (%w/v), $a_0 = -0.255$, $a_1 = 0.179$, $a_2 = -1.35 \times 10^{-3}$. See Fig.3.1. (The Ficoll lot number is unknown.)

These measurements were repeated at 22°C on solutions made up in Buffer T2 + 10 mM glucose (used in experiments on Streptococcus) and a similar relation was found to hold. The values of the parameters a_1 and a_2 were almost identical (0.180 and -1.31×10^{-3} respectively) but the value of a_0 was different. The former two parameters appear to be characteristics of the Ficoll and are independent of both temperature

and buffer. The parameter a_2 changed when a different batch of Ficoll was used (Sigma Chemical Co., Batch No. F-4375, Lot 114F-0299, $a_2 = -1.01 \times 10^{-3}$). The parameter a_1 was unchanged. The parameter a_0 is the logarithm of the viscosity of the buffer, and for Buffer TM, used in artificial energization experiments (Chapter 6), its temperature dependence was measured and found to be described by the equation:

$$a_0 = -3.67 + \frac{569.7}{T+133.15} \qquad (3.5)$$

where T is the temperature in degrees Celsius. Once it had been determined that the calibration curve followed the form given in equation (3.4), the curve for any stock solution could be obtained by measuring the viscosity at three different concentrations. Thus the viscosity of any medium obtained by mixing cell suspensions with Ficoll solutions could be read off directly.

§3.2.2 Preparation of cells used in bundle frequency measurements.

For Streptococcus, cells of strain SM197 were grown as described in §2.3.1. Experiments were done on cells swimming in solutions of Ficoll in both KTY medium and in buffer T2 (pH 7.5) + 10 mM glucose. For observations in KTY, a 5 ml culture was divided into 5 equal aliquots and these were pelleted in microfuge tubes, the supernatant pipetted off, and resuspended in 0.4 ml volumes of Ficoll solution. For observations in buffer T2, cells were washed twice by centrifugation into this buffer, resuspended in the same buffer to a final density of 80 times the harvest density, and then diluted 10-fold into the Ficoll solution. Mixing was achieved by slow stirring with a capillary tube. In both media, noise spectra were obtained from cells de-energized by

addition of 2-4-dinitrophenol (DNP) to the Ficoll solutions. The DNP was added to each solution in solid form and allowed to dissolve to overnight to saturation at room temperature. The final concentration was less than 10 mM. All observations were conducted at room temperature (22°C) in 0.15 mm deep glass flow chambers constructed from coverslips using Apiezon-L grease. The ends of flow chambers were sealed with grease to prevent evaporation. Coverslips were cleaned in fuming nitric acid as described in §2.3.1. Prior to experiments in buffer T2, the chamber was exposed to KTY medium for about 30 minutes, a procedure which seemed to inhibit the attachment of cells to glass by glucose.

§3.2.3 Preparation of cells used in tracking experiments.

For E. coli, cells of wild-type strain AW405 were grown at 32°C in tryptone broth for 4 h to an absorbance of A = 0.2 (measured at 610 nm, in a cuvette of path length 10 mm, on a Perkin-Elmer 552 Spectrophotometer) and washed twice by centrifugation (480 g, 6 min) at 22°C in buffer MM. Such low speed spins produced rather diffuse pellets, so supernatant fractions were removed by suction instead of decanting. Resuspension was by slow manual swirling to minimize the threat of mechanical damage to flagellar filaments. This seems to be a greater problem for E. coli than it is for Streptococcus, whose vigor of motility, as judged by eye or by measurements of power spectra, is little affected by vortexing. Pelleted E. coli show a loss in motility even if the tube is tapped too hard (Berg, pers comm). The final supension, at 5 times the harvest density, was kept on ice until ready for tracking, because cells kept at 22°C change their size distribution over the 3 hour duration of the experiment, becoming uniformly smaller.

The temperature of the tracking stage was controlled at 32°C by using a heating coil combined with an ice water flow system. 10 μl volumes of cell suspension were mixed with 0.5 ml volumes of Ficoll solution, allowed to warm to room temperature for 5 min, then placed on the tracking stage. Tracking was commenced after a further wait of 5 min.

For Streptococcus, a 10 ml culture of wild-type strain V4051 was grown and harvested as in §2.3.1, pelleted at low speed (480 g, 6 min) and resuspended by slow manual swirling in 10 ml of buffer T2 (pH 7.5) + 10 mM glucose. The cells were pelleted again, then resuspended in 2 ml of the same buffer, where they were stored at 22°C until ready for tracking, at which time a 10 μl volume was mixed with 0.5 ml of Ficoll solution in this buffer. The temperature of the tracking stage was controlled at 22.5°C.

§3.2.4 Methylcellulose experiments.

Berg and Turner (1979) demonstrated that the microviscosity (on the length scale of a bacterium) of solutions of long chain unbranched polymers is very different from that of a solution of Ficoll having the same bulk viscosity (as determined by the passage of solutions through a macroscopic viscometer). For example, the helical bacterium Leptospira swims much faster in buffers which contain 1% w/v methylcellulose than it does in those that contain enough Ficoll (over 35% w/v) to have the same bulk viscosity. Similarly, Schneider and Doetsch (1974) observed increases in swimming speeds of a variety of bacteria upon addition to buffers of polyvinylpyrollidone, which increased the bulk viscosity by over 50%. E. coli swims smoothly with a reduced body roll amplitude in methylcellulose solutions. I was interested to see how Streptococcus

would swim in methylcellulose because it might be possible to use this reagent to improve the yield of swimmers in suspensions of artificially energized cells. At low applied protonmotive force, many cells tumble about erratically, presumably because they cannot generate enough torque to form a stable bundle. The polymer chains in a methylcellulose solution might exert lateral forces and stabilize the bundles of these sub-threshold cells.

A 1% w/v stock solution of Methocel 90 HG (Dow Chemical Co., MW ≃ 143,00) was made up by stirring overnight in distilled water. This solution was used to make up the following buffer: 0.1 M TES, 0.1 M TAPS, 0.1 M TAPS, 0.2 M KCl, 0.1 mM Tetren, 1 mM $MgCl_2$, 1 mM $CaCl_2$, 0.46% w/v Methocel. Buffers of lower Methocel concentration were made up by serial dilution. Cells of strain SM197 were grown and harvested as in §2.3.1, then washed 3 times into the above buffer without Methocel (corex tubes, 2,000 rpm spins for 15 min in a Sorvall swinging bucket rotor, 490 ×; resuspension by manual swirling in 1 ml volumes for 15 min). They were re-energized by addition of 10 mM glucose, then mixed with a Methocel buffer and observed in acid-cleaned glass flow chambers. Cells in these buffers did not adhere to the glass in the presence of glucose. Noise spectra were obtained from suspensions de-energized by addition of 10 μg/ml FCCP.

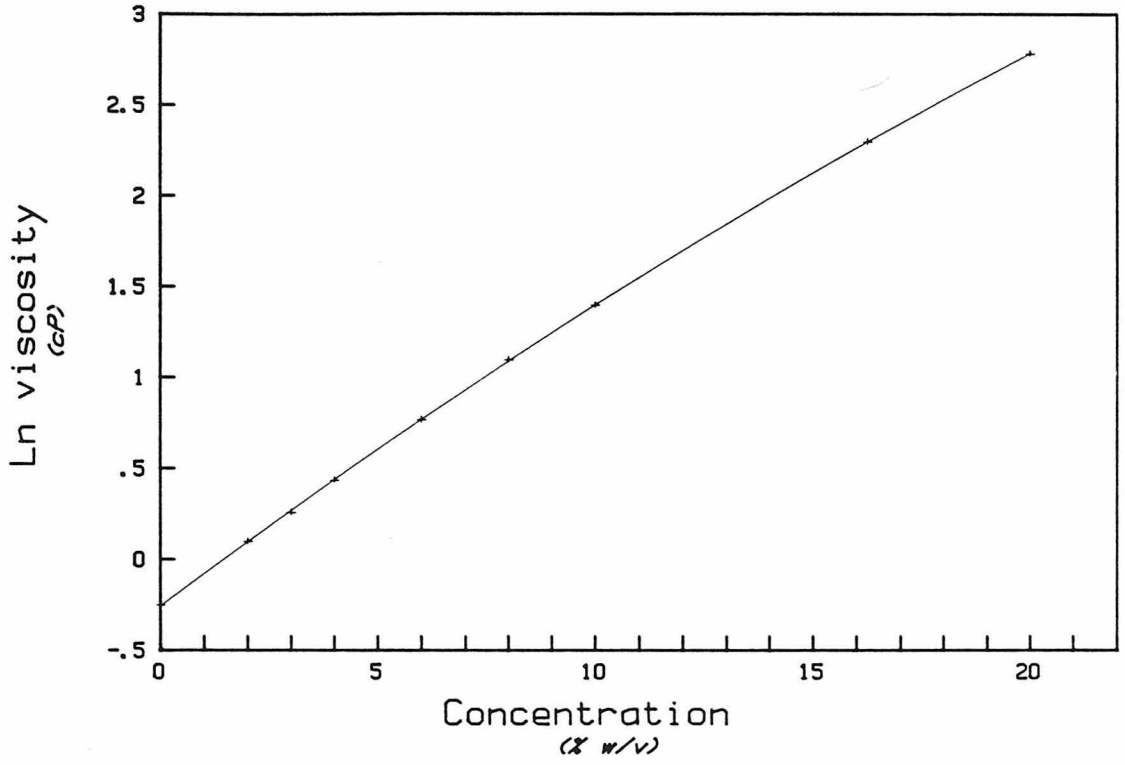

Figure 3.1. Calibration curve for viscosity as a function of Ficoll concentration.

A stock solution of 20% w/v Ficoll-400 was made up in buffer MM, lower concentrations were obtained by serial dilution, and viscosities were measured at 32°C as described in the text. The curve fit was obtained by least squares quadratic regression.

§3.3 Results

Power spectra obtained from cells swimming in Ficoll solutions were similar in shape to those for cells swimming in buffer without Ficoll. At high viscosities there was a decline in the bundle frequency, and peaks in the spectra shifted to lower frequency, with a proportionate reduction in their width (Fig.3.2). The signal to noise ratio, R_m (defined in §2.5), was noticeably diminished at high Ficoll concentrations ($\geq$ 10 %) due to two effects - a reduction in the number of cells passing over the detector per unit time, and a reduction in the image intensities of cells due to the higher refractive index of the solution. In such cases, about 2.5 times as many data scans were required to give a peak resolution comparable to that obtained for low Ficoll concentrations.

In Fig. 5.2A, the estimated mean bundle frequency, $\langle f_f \rangle$, is plotted as a function of the fluidity of the medium using results obtained from experiments on three different cultures of Streptococcus SM197. The open squares and triangles come from experiments done in KTY medium, and the open circles from cells in buffer T2 (pH 7.5) + 10 mM glucose. Apart from variation from culture to culture in the absolute values of the frequencies, there is good agreement in the shape of the curves followed by different sets of data points. Each set closely matches a hyperbolic fit obtained by a linear least squares regression using the variables $\langle f_f \rangle \eta$ and η (c.f. §3.4), with correlation coefficients greater than 0.90. The differences between frequencies of washed cells and those of cells observed directly in KTY are probably not due to mechanical damage suffered by flagellar filaments during centrifugation and resuspension. Variations of such a magnitude (ca. 20 %) were seen among different

cultures grown in the same way and observed directly in KTY medium. Also, cells which had been pelleted at high speed (6780 g, 1 min) and resuspended by vortexing (both much harsher treatments than those used above) exhibited a power spectrum very similar to that of untreated control cells from the same culture, with a bundle peak located in the same position.

In order to interpret the curves in Fig. 5.2A as representing the speed of the flagellar motor as a function of the reciprocal of the frictional drag coefficient of the external load, it is necessary to exclude the possibility that the geometric drag coefficient of the load is changing in an unknown manner as the viscosity changes. Macnab and Ornston (1977) made direct observations on the rotating bundles of swimming cells of small peritrichously flagellated bacteria (Salmonella typhimurium) using high-intensity dark-field light microscopy. No difference could be seen between the waveforms of detached flagella, flagellar bundles of cells swimming in buffer with the viscosity of water, and those of cells swimming in highly viscous solutions of Methocel 100 (2% w/v). There may be a 10 to 20 % error in the determination of the wavelength and radius of the bundle from their micrographs. However, the filaments of Salmonella may have elastic properties different from those of Streptococcus. The more fragile nature of E. coli filaments has already been noted. The following argument, based only upon observations on Streptococcus, implies that changes in the bundle geometry must be small. As an elastic, helical structure, the bundle can only change its shape if there is a change in the torque acting upon it. In Chapter 4 I show that the bundle frequency of swimming cells is strongly temperature dependent over the range 10°C

to 40°C. By simultaneously making bundle frequency measurements and video tape recordings of the same culture at different temperatures, I found that the ratio, r_2, of bundle frequency, f_f, to body roll frequency, f_b, is independent of speed over the range f_f = 52 Hz to f_f = 139 Hz (r_2 = 14.4 ± 0.9 for one culture examined). This was the basis of the method Markus devised (see his thesis) to estimate the mean bundle frequency of cultures in which excessive peak overlap prevented accurate power spectrum measurements. He also found that the ratio, r_1, of swimming speed to body roll frequency was independent of speed to within 20% (f_f ranging from 30 Hz to 85 Hz). Over this range, the torque changes by a factor of about 2.5 (taking into account the variation of the viscosity of water with temperature). Banks et al, (1975) obtained a similar result for E. coli (c.f. §4.1). Assuming that the total filament length is constant, the shape of the bundle helix is specified by two parameters, its radius, r, and its wavelength, λ. Since the two ratios r_1 and r_2 are functions only of the geometry, they uniquely determine the shape of the helix, which must therefore be unchanged. This conclusion can be applied to the Ficoll experiments where the torque (proportional to ηf_f) changes by a similar factor. The results of tracking experiments done at different Ficoll concentrations indicate that the ratio r_1 does not vary by more than 20 %, see Fig.5.2B (although the data shown are for different cultures). The data actually suggest a systematic reduction in $r_1/r_2 = r_3$ at high viscosities. By fitting a hyperbola to the bundle frequency data and evaluating $r_3(\eta)$ at the two extreme tracking fluidities, one obtains $r_3(12.05)$ = 0.15 ± 0.01, and $r_3(0.99)$ = 0.18 ± 0.01. Such a trend might simply reflect a difference in weighting between the two methods of measurement. For

example, consider again the hypothetical correlation (§2.6) between Δp and cell wall thickness. As the Ficoll concentration (and hence refractive index) increased, tracking would continue to weight all cells equally, while the bundle frequency method would detect relatively stronger signals from more refractile cells having higher Δp and faster bundles. A less exotic explanation of the trend is that, at higher torque, the bundle helix winds up, reducing its pitch angle and hence propulsive efficiency. Estimates of r_1 and r_2 can be computed from an approximate theory which describes the frictional force on each element of a long slender filament in terms of transverse and longitudinal drag coefficients (Gray & Hancock, 1955, Chwang & Wu, 1971, and Shimada et al., 1976). Although this theory does not take into account either the coupling between filament elements moving in nonparallel directions or the effect of the filament's motion on the cell body (and vice versa) it is useful in providing a first order estimate of how much the bundle geometry is allowed to vary under the assumption that the above ratios must remain constant to within a given error limit. Using formulae from the above theory, I found that, over ranges which included the values determined from measurements made on stained flagellar filaments (c.f. Markus's thesis), $r = 0.35\ \mu m$, $\lambda = 3.2\ \mu m$, if r_1 and r_2 varied by no more than 20%, then r and λ could not vary by more than about 10%. To first order, the geometric drag coefficient of the helix is expected to be independent of λ, and to vary as r^2, implying that it cannot change by more than about 20%. This represents an upper bound for the error in the abscissa of a plot of speed as a function of the reciprocal of the frictional drag coefficient.

The results of tracking experiments done on E. coli are shown in

Fig. 3.3. Swimming speed varies with fluidity in much the same way as for Streptococcus. If bundle geometry is again assumed to be approximately constant, the torque-speed diagram is well fit by a linear relation. Chapter 5 gives the results of bundle frequency measurements done on a smooth-swimming strain of E. coli, using techniques described in §4.4. The speeds seen were in the same range as speeds of spinning hooks on cells grown under almost identical conditions (Berg et al, 1982), showing that motor frequency is independent of load for swimming cells. All available evidence indicates that the motors of both species of bacteria have the same dynamic properties.

Fig. 3.4A shows the bundle frequency of SM197 as a function of methylcellulose concentration. In Fig. 3.4B, the frequency has been plotted as function of bulk fluidity (computed by fitting a logarithmic curve through the viscosity data of Berg and Turner (1979), who used the same Methocel in their experiments). There is a monotonic decrease in bundle frequency with increased bulk viscosity, and the speed saturation effect seen for Ficoll is absent. Swimming speed, on the other hand, has been shown to increase. The speed of tracked E. coli AW405 (grown in H1 medium and observed in buffer MM without methionine or lactate) at 32°C increased from 13.7 ± 3.0 μm/s (in 0 % Methocel) to 19.5 ± 6.0 μm/s (in 0.2 % Methocel) (Berg, 1972, unpublished data). Schneider and Doetsch (1974) reported a similar effect in other kinds of bacteria. The result supports the notion that propulsive efficiency (proportional to r_3^2) is enhanced by solutions of long chain polymers and reduced by solutions of spherical polymers.

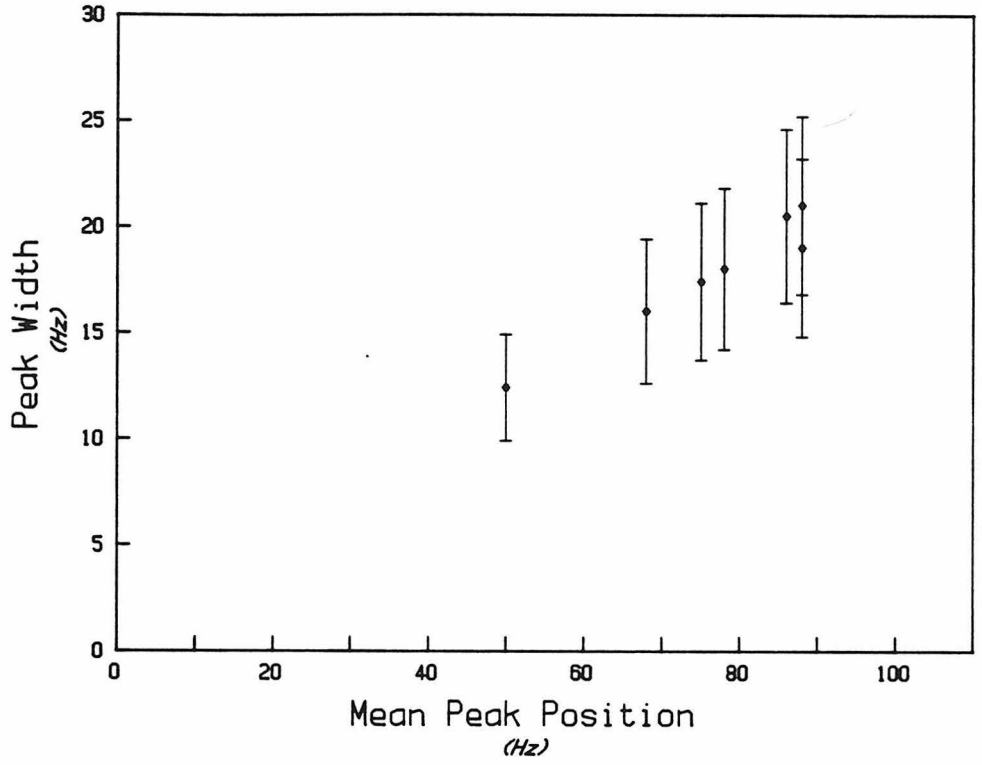

Figure 3.2. Scaling of bundle frequency peak width with position.

The data correspond to the viscosity experiment Streptococcus shown Fig.5.2 (open circles). Mean bundle frequency was estimated by f_1^*, as described in §2.6. Peak width was estimated by calculating the standard deviation over the same summation range.

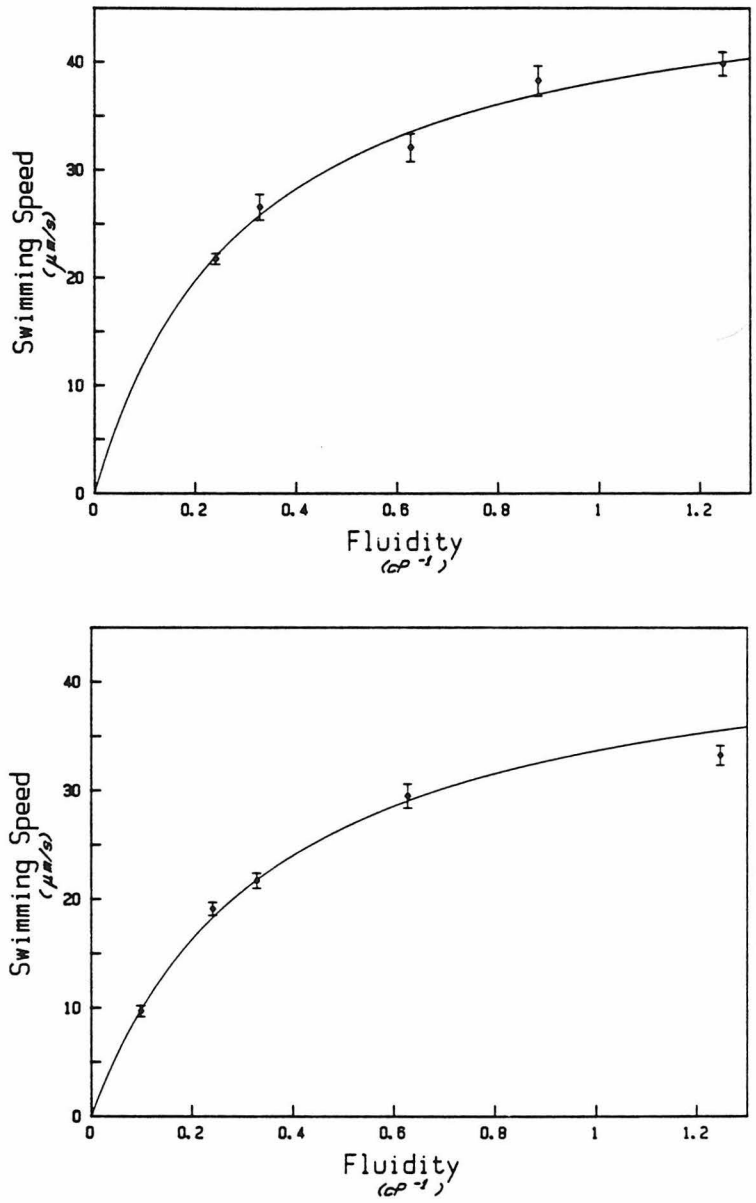

Figure 3.3. Swimming speeds of E. coli as a function of fluidity. The plots show results from tracking experiments done on two different cultures as described in §3.2.3. The hyperbolae were obtained by a least squares regression of 1/(swimming speed) on fluidity. Correlation coefficients were 0.94 (A) and 0.91 (B).

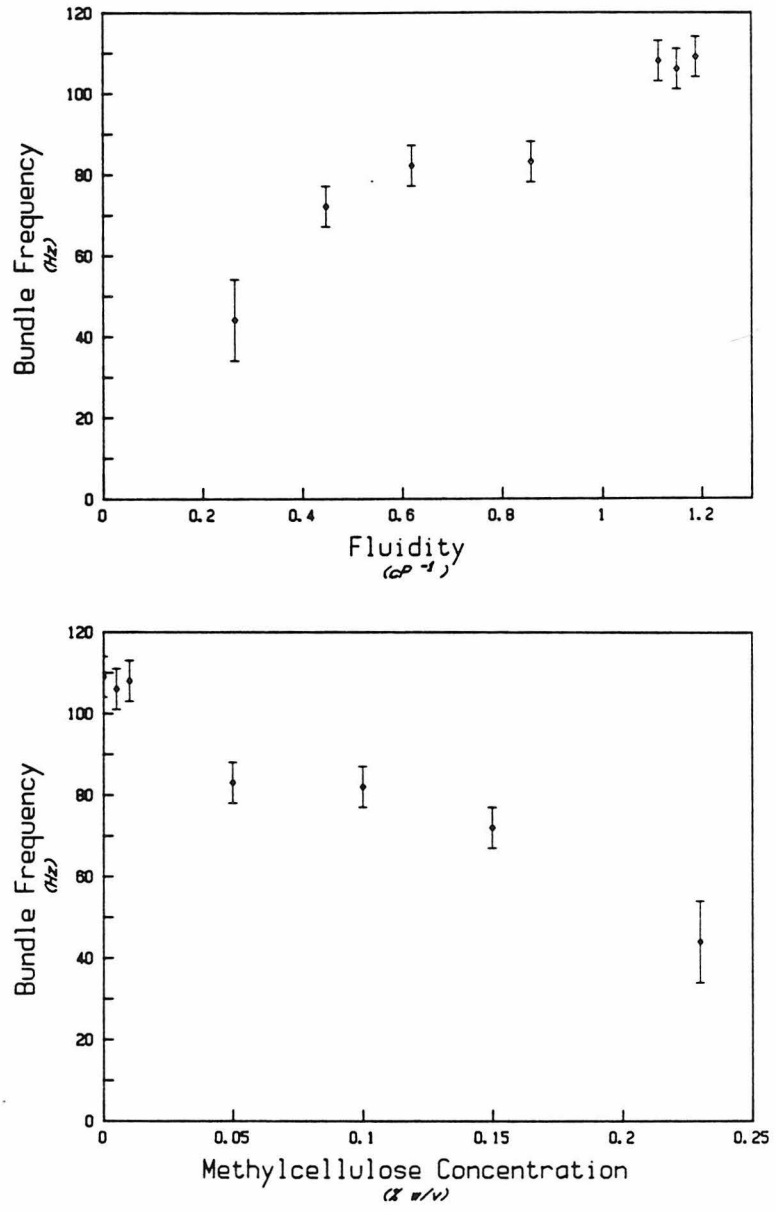

Figure 3.4. The effect of methylcellulose on bundle frequency.

Frequencies were determined for swimming Streptococcus SM197 at different methylcellulose concentrations. Bulk fluidities were determined from the data of Berg and Turner (1979).

§3.4 Discussion

The results of the Ficoll experiments can be recast in a form in which the function H, relating torque and speed, is explicitly plotted. The torque per motor in the bundle is proportional to $f_f\eta$ and is found to decrease linearly with increasing f_f. This can be seen in Fig.5.3, where the absolute torque has been computed for comparison with the torque generated by motors driving tethered cells at low speed. If there are n motors operating in a swimming cell, the total torque is given by:

$$nH(2\pi[f_f+f_b]) = 2\pi G_f \eta f_f \qquad (3.6)$$

$$= 2\pi G_b \eta f_b \qquad (3.7)$$

where G_f is the geometric drag coefficient of the bundle, and G_b that of the cell body. Using $f_f = r_2 f_b$, (3.7) implies that the absolute torque generated by a motor rotating at a frequency f_f+f_b relative to the cell body is given by:

$$N = \frac{2\pi G_b \eta f_f}{n r_2} \qquad (3.8)$$

The values of n and G_b were estimated as described in Fig.5.3, and r_2 was the value obtained from videotapes of swimming cultures. The major source of uncertainty in this formula is the value of G_b, which was computed from a a model in which a swimming cell body of average size and shape was assumed to have a fixed average orientation relative to the bundle axis. There is considerable variation in the shapes and orientations of swimming cells and the motion of some cannot be described simply as rotation about a fixed axis. Any correlation between bundle frequency and cell size would introduce a systematic

error into (3.8). A systematic study of such a correlation would require the ability to measure the bundle frequencies of single free swimming cells, a task which exceeds the capabilities of existing instrumentation. There is an additional uncertainty due to the crude approximation of cell bodies as cylinders. This also affects the absolute torques obtained for tethered cell geometries, and hence there is some doubt about the positions of the points representing these cells relative to those representing swimming cells on the torque-speed plot. All one can rigorously state is that such computations do not contradict the assumption of linearity over the entire speed range. Of course, these errors do not affect the relative torques derived from the bundle frequency data, which constitute strong evidence for linearity in the speed range between 50 Hz and 100 Hz. The similarity of the frequencies observed for spinning hooks and for bundles in E. coli (Chapter 5) shows that this behaviour extrapolates to the N = 0 axis.

What would cause a linear fall-off in the observed torque with increasing speed? Is it possible that such behavior is entirely due to processes unrelated to the mechanism of torque generation? For example, suppose that the torque generated is a constant, N_0, independent of speed, and that energy is being dissipated by frictional forces which are coupled to flagellar rotation but which are unaffected by changes in the external viscosity. Then the observed torque would be given by $N_0 - f_I\Omega$, where f_I represents an "internal" frictional drag coefficient. However, it is not likely that this internal drag can be due to friction between motor components and the cell wall and lipid bilayer, because such friction is estimated to be smaller than the drag on a tethered cell by a factor of about 3×10^{-4} (Berg, 1974). In this calculation a

0.5 nm gap was assumed between the M and S rings and between the rod and wall, and the M-ring was approximated as a 210 nm diameter sphere. Since the motor runs at 100 Hz at zero external torque and at 10 Hz in tethered cells, the predicted value of N_0 would be about 3×10^{-3} times too small. Nor could the only dissipation be due to friction between different filaments in the bundle, since this would imply that for isolated loads driven by a single motor, the speed should be inversely proportional to the frictional drag coefficient of the load, a conclusion which is inconsistent with the observation that beads and hooks spin at comparable speeds (Berg et al., 1982). One might still argue that internal friction is much higher due to close contact between the M-ring and protein structural components of the motor, but this seems to be a rather contrived and highly inefficient design. It would be like running an engine with the brakes permanently engaged, so that almost all the torque developed is used up in overcoming internal friction. It seems unlikely that most of the available free energy would be used up in wasteful dissipation after the torque generating step. It is also possible that the torque drops because there is dissipation of the free energy of protons before the torque generating step, at a rate which increases with the flux. For example, this might happen during passage through a transmembrane proton channel. As the speed increased, the flux would increase (assuming tight coupling) and the free energy available for torque generation would decrease.

The torque-speed diagram may directly reflect the dynamic characteristics of the force generation mechanism itself. In general, such a mechanism must rely upon an interaction potential, $V(\vec{x})$, between the stator and the rotor, where $\vec{x}$ represents internal configuration

coordinates. For example $\vec{x}$ might be the positions of elastic structures linking rotor and stator, or the reaction coordinates of a series of proton transfer reactions. V will have a local minimum at some value, $\vec{x}_0$, corresponding to zero force. At nonzero Δp and speeds near stall, the torque will be determined by an average state with $\langle\vec{x}\rangle = \vec{x}_a$. The torque will drop as the speed, Ω, increases if rotation of the stator is fast enough to change the average configuration $\vec{x}$, and if this shift reduces the force ∇V. This will happen when the rotation rate becomes comparable to the rate at which internal coordinates relax to their values at equilibrium (in the case of tightly coupled mechanisms) or at steady state at stall (in the case of loosely coupled mechanisms). These relaxation processes will then determine the speed. As Ω increases to the idle speed, the torque will fall to zero as $\vec{x}_a \longrightarrow \vec{x}_0$. The model of contraction in striated muscle is an example of a mechanism which exhibits this general property (Huxley, 1957). As the velocity of the myosin fibers relative to the actin increases, the mean extension of the elastic element of the myosin molecule decreases. The elastic element corresponds to the potential V, and the rate of association and dissociation of actin and myosin (with concomitant hydrolysis of ATP) to the internal relaxation rate. These rates depend on the position, x, of the elastic element, and the limiting speed at zero load is determined by the asymmetry of this dependence about the origin at $x = 0$. This is a loosely coupled mechanism - the ratio of the number of ATP molecules hydrolysed to the distance moved by the sliding filaments is not fixed. At high speeds, a small number of rate limiting steps dissipate most of the available free energy and the force-velocity diagram is nonlinear, in agreement with experiment (Hill, 1938). A similar mechanism in which

proton translocation is loosely coupled to flagellar rotation was proposed by Oosawa and Masai (1982). Force is exerted by an elastic linkage between the stator and a complex between a proton binding group and a site on the rotor. An approximately linear torque-speed plot is predicted (Oosawa and Hayashi, 1983), although the maximum rotation rates are an order of magnitude smaller than those observed experimentally. The model of Berg and Khan (1982) is an example of a tightly coupled device in which the torque drops with increasing speed. Again, there is an elastic element (spring) which is linked to the stator, and which stores the free energy of protons and exerts an average force on the rotor. The spring is attached to a transmembrane protein called a channel complex whose motion along an array of proton binding sites on the rotor is coupled to the transfer of protons across the membrane. The relaxation time in this case corresponds to the rate at which the spring is able to store the free energy of the proton chemical potential. This is determined by the frequency of dissociation of the channel complex from a given pair of binding sites and by the rate of transition (perhaps by lateral diffusion in the lipid environment of the membrane) from one site to another. At high speeds the spring is stretched less, so a smaller amount of free energy is required to step from one pair of binding sites to the next. Thus, more energy is dissipated in the course of interaction between the channel complex and rotor, and the torque drops in a nonlinear manner.

The kinds of models discussed above can be modified to accommodate torque-speed relations which are linear over most of their range. It should be emphasized that there is approximately a factor of two uncertainty in the relative positions of the tethered versus swimming

cell data points shown in Fig. 5.3 due to the difficulty in making precise computations of frictional drag coefficients, so linearity over the entire speed range has certainly not been rigorously demonstrated. Future experiments should focus on extending the swimming cell data to cover the lower half of the speed range using much higher viscosities (up the 50% w/v Ficoll). I was unable to make bundle frequency measurements under these conditions, but direct measurement of swimming speeds off videotape records should still be possible. However, in view of the comments in §3.3, a I think that it is important to devise a test of the assumption of constant bundle geometry for such extreme viscosities.

CHAPTER 4

THE EFFECT OF TEMPERATURE ON THE FLAGELLAR MOTOR

§4.1 Introduction.

Although several authors have studied the effect of varying temperature on bacterial motility, the relevance of such experiments for the mechanism of torque generation was not addressed. Banks et al. (1975) computed the autocorrelation function of the light scattered by cells of a smooth swimming strain of E. coli, cheC497, swimming through a 25 μm diameter focused laser beam, from 25°C to 35°C. They deduced that the root mean square swimming speed and body·roll frequency scaled together and increased linearly over this temperature range. Maeda et al. (1976) also looked at E. coli, obtaining swimming speeds directly by measuring the lengths of motility tracks recorded on film. They also reported a monotonic, approximately linear increase in speed, from 20°C to 40°C. Using similar techniques, Miller and Koshland (1977) demonstrated a linear increase in the average swimming speed of Salmonella typhimurium with temperature from 5°C to 42°C.

The above studies were all done with metabolizing cells so it is unclear whether the temperature dependence represents a property of the flagellar motor alone, or whether it also contains an unknown variation in the protonmotive force. The torque generated by the motor has been shown to increase linearly with the protonmotive force up to about 80 mV for tethered cells (Khan & Berg, 1983), and there is also evidence that it varies with Δp for swimming cells. It is therefore conceivable that the observed effect is at least partly due to changes in Δp with temperature. In the experiments of Khan and Berg (1983), designed to examine the effect of varying temperature on the torque generated by flagellar motors of tethered Streptococcus, this possibility was ruled out by using artificially energized cells whose Δp was defined by a

potassium diffusion potential and pH gradient. They found that at a fixed protonmotive force of $\Delta p = \Delta\psi = 77$ mV, the torque of tethered cells remained constant to within 10% over the range 4°C to 38°C. My original plan was to utilize the same system to observe the effect of varying the temperature upon motors driving small loads. However, for artificially energized cells, the method of using small markers attached to flagellar stubs (§2.2) proved to be unworkable, and peak overlap in power spectra derived from suspensions of swimming bacteria was too great to allow reliable estimates of the average rotation rate of bundles. Howard suggested a simple but elegant solution to this problem. Since the torque of tethered cells shows no thermal effect at fixed Δp, why not use this preparation as a control for bundle frequency measurements on metabolizing, swimming bacteria? Populations of metabolizing cells have a narrower distribution of bundle frequencies, allowing easy determination of the bundle frequency by the methods of Chapter 2. Any change in Δp with temperature should show up as a change in the torque generated by the tethered cells. This, then, was how we chose to do the experiment. Bundle frequency measurements were made on glycolysing swimming cells and the control was done in parallel on the same culture by Markus, our resident Strep-tethering guru. To control for changes in bundle geometry with varying torque, and as an independent test of the method, Howard tracked similar cultures over the same temperature range to obtain swimming speeds. In this way we were able to reproduce the same linear dependence of speed on temperature as had been observed for other species of bacteria.

§4.2 Methods.

§4.2.1 Temperature control.

In all bundle frequency measurements, temperature control was achieved by the method described in Khan and Berg, 1983. Cells were observed in acid cleaned glass flow chambers constructed on glass microscope slides (25 mm X 75 mm X 1 mm) which were attached by thermal contact grease (Thermacote, Thermalloy #250) to a special temperature controlled microscope stage consisting of an aluminum block composed of two pieces. The upper piece, 2.6 cm wide X 3.7 cm long, had a large circular opening into which fit a microscope objective (Nikon 40X BM outer casing removed), and the lower piece, 5 cm wide X 5 cm long, had a small circular opening (1.3 mm diameter) to allow the passage of light from the substage condenser. The two pieces were bolted together via vertical extensions to leave a horizontal gap, 4 mm high, into which fit the glass flow chamber. Insulating plastic tabs held the lower piece of the block onto an annular support, and an insulating plastic ring separated the objective from the upper part of the microscope. Temperature was controlled by a water-cooled peltier element (Melior MC 3.3-32-16) attached to the vertical extension (0.9 cm deep X 3 cm high) of the lower block. The temperature of the lower block was sensed by inserting a thermistor (Fenwall GB3J1) into a small hole drilled 0.8 cm from the plane of attachment of the Peltier element. The thermistor was connected to one arm of a bridge circuit which controlled the amount of current flowing through the Peltier element by negative feedback. The relation between thermistor voltage and temperature was calibrated by reference to standard mercury thermometer. The steady state temperature of the stage was set by a dial which controlled the position of contact

between a resistor in the second arm of the bridge circuit and the inverting input of an operational amplifier. All non-insulating stage junctions were sealed with Thermacote grease.

§4.2.2 Preparation of cells for the measurement of bundle frequency.

Cells of Streptococcus strain SM197 were grown as described in §2.3.1. in four 20 ml volumes of KTY each in a 250 ml flask. They were pelleted in eight 10 ml corex tubes at 480 X g for 6 min, the supernatant was removed by suction, and they were resuspended by slow swirling in 5 ml volumes of buffer T2 + 10 mM glucose; 5 ml of buffer T2 was then added to each tube and the treatment was repeated. A third, final spin left pellets which were resuspended in residual buffer, pooled and made up to a volume of 1 ml. Cells were stored in this dense suspension at room temperature for the duration of the experiment. Measurements of bundle frequency at a given temperature were conducted as follows. The control circuit was adjusted so as to attain the required stage temperature and, while steady state was being approached, 50 μl of the dense cell suspension was added to 450 μl of buffer T2 + 10 mM glucose. Cells were given 5 min to re-energize in the fresh glucose solution (control suspensions of starved cells reached maximal motility vigor in less than 5 min), and then a 60 μl aliquot was tranferred to an acid-cleaned glass flow chamber. The glass slide was attached to the stage and 4 min were allowed for it to reach the steady state temperature. Data acquisition and microscope optical arrangement followed the set-up described in Chapters 2 and 5. At each temperature a maximum of 600 or 800 spectra calculated from one second data blocks were averaged, with cumulative partial sums stored every 200 scans.

Examination of these partial spectrum averages revealed no systematic temporal drift in bundle frequency over the 10 to 15 minute duration of each measurement. At temperatures below 37°C, data were sampled at 512 points/s, and the computer required an average of 1.01 seconds/scan to acquire and process this information. At temperatures above 37°C, data were sampled at 1024 points/s, with a slower processing time of 1.34 seconds/scan. Noise spectra at each temperature were collected from suspensions of cells, de-energized with 10 μg/ml FCCP, by repeated accumulation of 200 scan sums.

Two minor difficulties were encountered at high temperatures. The Apiezon L grease used to construct the flow chambers began to melt and flow in some preparations, creating a temporary shot noise problem by pulling cells across the microscope field. The cell field was constantly monitored during the measurement to reject data during such episodes. I also found that prolonged exposure to high temperatures led to a cessation of motility. In one experiment, cells remained at 37°C for 13.4 min, maintaining a constant bundle frequency. They were then shifted to 42°C, and were found to have lost all motility after 15 min. Motility was restored upon addition of fresh buffer containing 10 mM glucose, indicating that the cells had previously used up all of the glucose in the medium. This problem could be overcome by using buffers with higher glucose concentrations or by limiting the time spent at high temperatures. Such accelerated starvation at high temperatures might be useful in speeding up protocols for preparing cells for artificial energization.

§4.2.3. Preparation of cells for tracking experiments.

Cells of wild-type Streptococcus strain V4051 were grown and harvested as described in §2.3.1, washed and resuspended as for the viscosity experiments (§3.2.3). Tracking proceeded as for the latter experiments, except that the buffers did not contain Ficoll.

§4.3 Results.

The position of the high frequency peak in the power spectrum exhibited a strong temperature dependence, and its width scaled with the mean peak location. Bundle frequency increased linearly with temperature over the range from 10°C to 42°C. Data from experiments on four separate cultures are shown in Fig.5.4 (open symbols). The scatter about the regression line is due in part to differences between cultures. The mean location of the low frequency peak, generated by body counter-rotation, also shifted to higher frequency and increased in width at higher temperatures. Its height increased relative to that of the bundle frequency peak due to reduced attenuation by the high pass filter, although the overlap between the two peaks remained small. Mean swimming speeds derived from tracking data showed a similar variation with temperature, increasing linearly from 16°C to 30°C (Fig.5.4, closed symbols, data from a single culture). These results are consistent with the assumption that the ratio of mean swimming speed to bundle frequency is approximately independent of speed over a wide range of speeds (and torques), as argued in §3.3.

Only a small part of the observed temperature effect can be due to the change in the viscosity of water, which, for example, decreases from 0.955 cP at 22°C to 0.627 cP at 42°C. Extrapolation of a hyperbolic fit to the speed vs. fluidity data obtained from viscosity experiments done at 22°C (Fig.5.2, continuous curve) predicts a 4% increase in speed for such a viscosity change if the torque were temperature independent, not the 108% increase actually seen. A change in Δp is ruled out, at least over the range from 16°C to 30°C, by measurements of the average torque of tethered cells rotating in the same buffer, which demonstrated

a variation of less than 10% (data quoted in Chapter 5, shown in Fig.4.1). In fact, Markus has measured the swimming speeds and body roll frequencies of artificially energized cells (directly off videotape recordings), in which the value of Δp does not change by more than about 14%, and has found a linear temperature effect very similar to that seen in glycolysing cells. Assuming that the bundle geometry does not change (§3.3), this implies that the bundle frequency shows a similar effect. Although I invested considerable time and effort in attempting to obtain a direct measurement of the bundle frequency in artificially energized cells (using the methods described in Chapter.6), I was not able to derive good estimates, apparently because there is a large spread in the speeds of such cells, leading to a wide peak in the power spectrum which overlapped with the harmonic tail of the body-roll peak. Both peaks were widened further by the rapid decrease in motility during the first few minutes after application of the artificial Δp. Even so, it was evident from major changes in the shape of the spectra that there was a strong thermal effect.

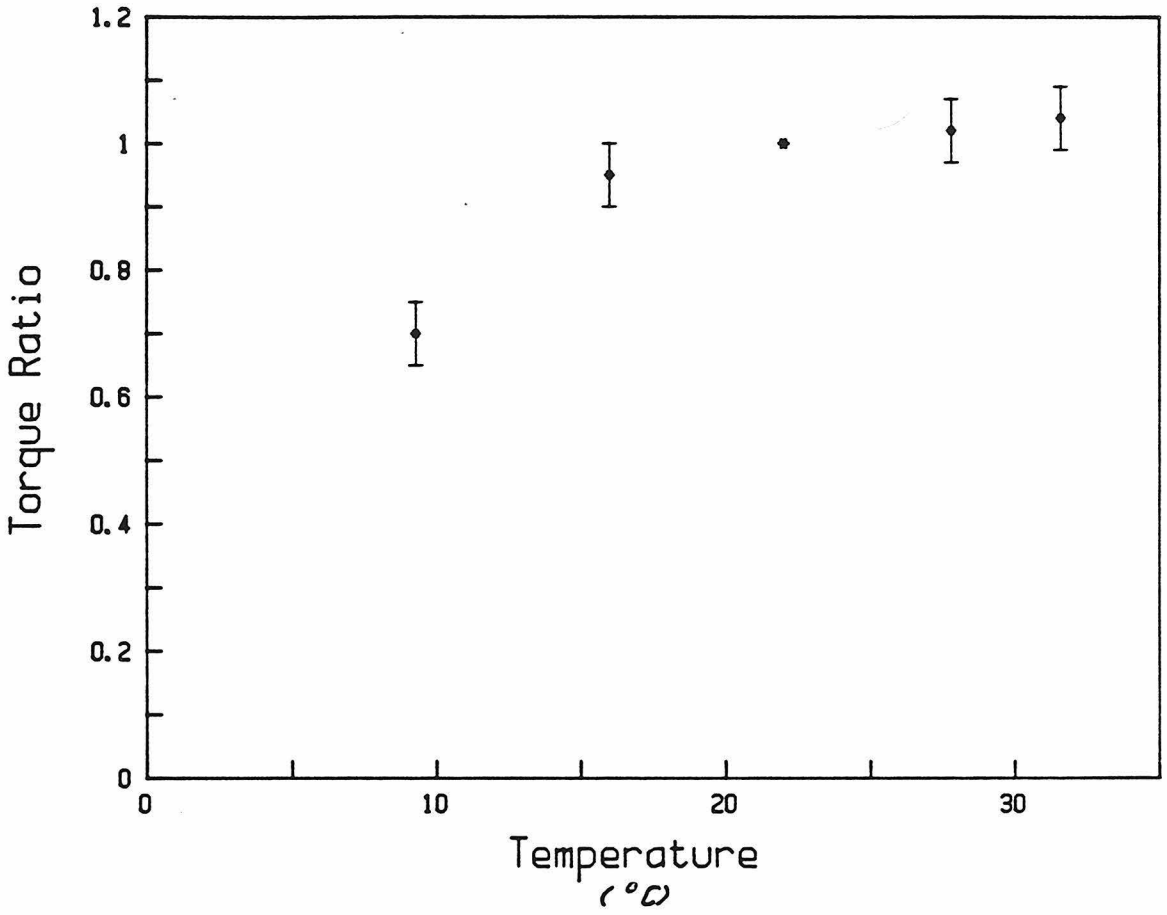

Figure 4.1. Torque of tethered glycolysing Streptococcus SM197 as a function of temperature.

Torques were scaled to the torque at 22°C and averaged. Means and standard deviations are shown. The data are cited in Chapter 5.

§4.4 Measurements on *E. coli*

Bundle frequency measurements on populations of swimming *E. coli* were difficult, even at room temperature, because, at the cell densities required to obtain a good signal-to-noise ratio, oxygen was rapidly depleted, leading to a loss in motility. This problem was alleviated considerably by observing cells in motility medium (buffer MM) rather than in growth medium (tryptone broth), where the rate of oxygen utilization is about two orders of magnitude greater. However, there is a risk of damaging flagellar filaments while washing cells into this buffer from growth medium. In the 150 μm deep observation chambers there was a significant reduction in motility near the center of the chamber, while cells continued to swim vigorously at the edge near the meniscus where oxygen was available from the surrounding air. In measurements made by focusing on cells near the edge, continual monitoring was required to maintain a fixed distance from the meniscus as water evaporated from the chamber. A temperature experiment using this method was not feasible because the effects of oxygen depletion and evaporation became more severe as the preparation was warmed.

I found an alternative way of measuring motor speed as a function of temperature by examining single cells. When a culture in growth medium was injected directly into an uncleaned glass flow chamber, a small number of cells stuck to the dirty coverslips, perhaps by one or more pili or flagellar filaments. The unattached cells were washed out by a flow of motility medium, and the attached cells were examined individually using a pinhole, as described in §2.2, in this case positioned over the edge of each cell body. The bodies of many stuck cells vibrated visibly, presumably in response to forces generated by a

freely rotating flagellar bundle projecting from the side of the each cell. Power spectra of the photomultiplier output resembled those for rotating markers, exhibiting a low frequency peak with harmonics and a high frequency peak (Fig. 4.2A). The former is probably due to the vibratory motion of the body being pushed by the bundle. The high frequency peak admits only one simple interpretation - it has the same origin as in swimming cells, being centered at the rotation frequency of the free bundle. For all cells examined, this frequency showed a steep monotonic increase with temperature from 22°C to 35°C (Fig. 4.2B), although its magnitude varied from cell to cell at a fixed temperature. The speed record for flagellar motors is held, at the time of writing, by one of these cells. At 35°C (the growth temperature), a cell was observed to vibrate at 420 Hz, almost an order of magnitude faster than the old "standard" filament frequency of 50 Hz derived from Spirillum volutans (Metzner, 1920). These data are consistent with the results of previous studies of the swimming speed of E. coli if it is assumed that the ratio of bundle frequency to swimming speed is independent of torque. Unfortunately there is no control experiment telling us how Δp varies over this temperature range, since E. coli cannot be starved and artificially energized. It is tempting to postulate that the motor of this species behaves in a similar way to that of Streptococcus and that the basic mechanism of torque generation is highly conserved among different taxonomic groups.

Figure 4.2. Bundle frequency measurements on single cells of E. coli HCB437.

A. Amplitude spectrum obtained by averaging 50 power spectra of one second scans of the photomultiplier output. The inverse phase contrast image of an intact cell stuck to a coverslip was positioned over the edge of a pinhole (0.37 mm diameter). Stage temperature was set at 27°C.

B. Temperature dependence of bundle frequency for a second single cell. The stage temperature was changed in the following order: 25°C, 22°C, 25°, 32°C, 35°C, 25°C, with the following respective peak locations: 245 Hz, 210 Hz, 250 Hz, 327 Hz, 426 Hz, 258 Hz. For the first three points, filter settings were the same as in Figure 5.1. For the last three points, the high pass filter was set with 3dB cutoff at 133 Hz. In both (A) and (B) the cells were strain HCB437, grown in tryptone broth at 35°C to an absorbance of 0.912 (as measured on a Perkin Elmer 552 Spectrophotometer at 610 nm, using a cuvette with a path length of 10 mm), and washed into in buffer MM as in §3.2.3.

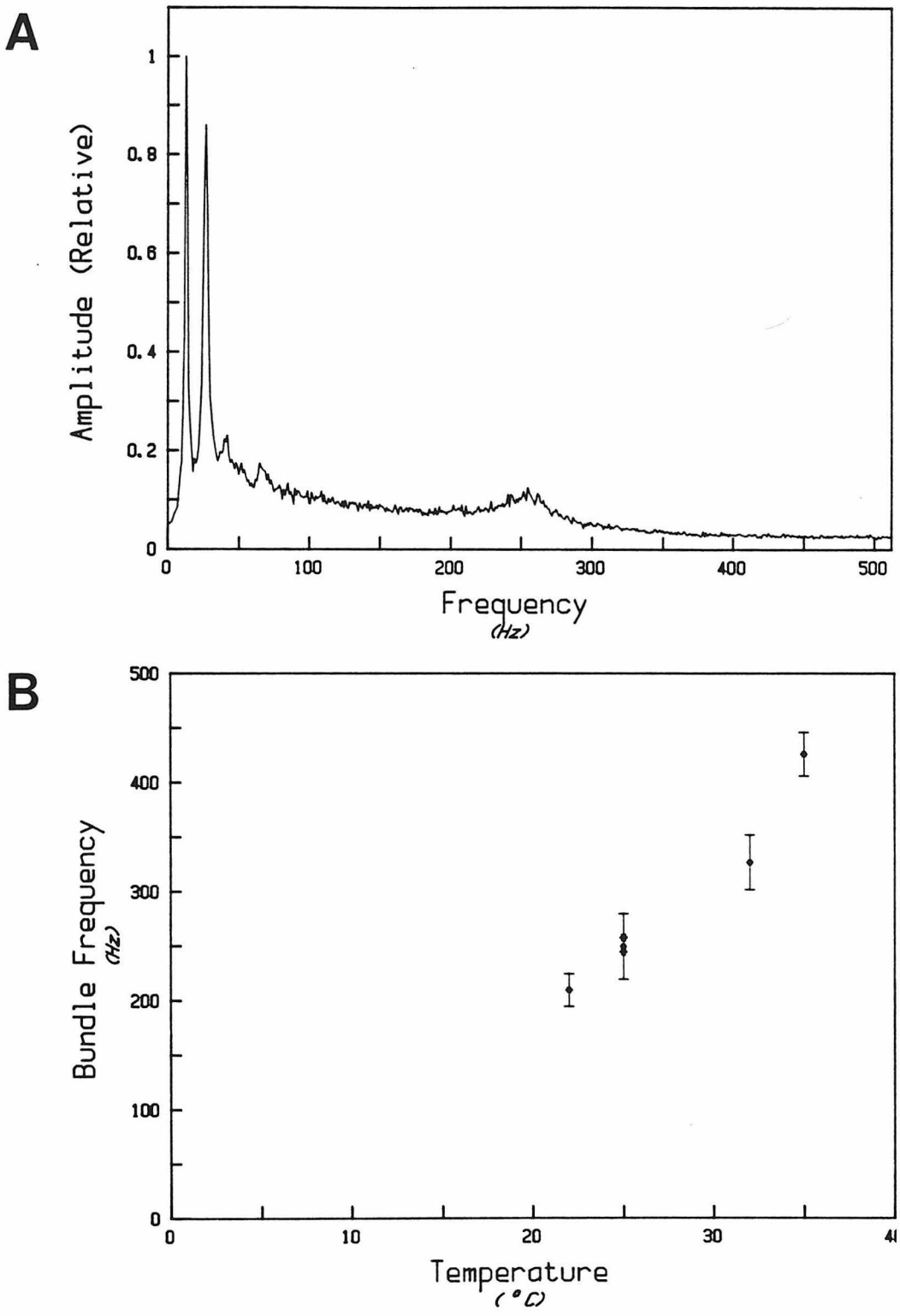
A
Amplitude (Relative)
1
0.8
0.6
0.4
0.2
0
0
100
200
300
400
500
Frequency
(Hz)
B
Bundle Frequency
(Hz)
500
400
300
200
100
0
0
10
20
30
Temperature
(°C)

Figure 4.2

§4.5 Discussion

The torque of the flagellar motor of Streptococcus increases steeply with increasing temperature, at constant protonmotive force, from 16°C to 32°C. Fig.4.3 shows the relative torque computed as function of temperature by multiplying observed speeds, f_f, by the viscosity of the buffer, η. To estimate the temperature-dependence of the idle speed (speed at zero torque), f_o, assume that the motor is characterized by a linear torque-speed diagram (§3.4), in which the stall torque (the torque at zero speed), N_o, is temperature independent (Khan & Berg, 1983).

$$\frac{N}{N_o} + \frac{f}{f_o} = 1 \qquad (4.1)$$

where f is the observed speed relative to the cell body, and N is the torque per motor. Using equation (3.8), the idle speed is given by:

$$f_o = \frac{N_o f}{N_o - \gamma\eta f_f} \qquad (4.2)$$

where $\gamma = 2\pi G_b/nr_2$, and $f = (1 + 1/r_2)f_f$. For the calculation, I took experimentally determined values, r_2 = 14.4 (from video recordings), n = 3.5, $N_o = 3 \times 10^{-11}$ dyn cm (from tethered cells), $G_b = 2.6 \times 10^{-11}$ cm^3 (using the geometry assumed in Chapter 5), f_f as measured above, and η according to Touloukian et al. (1975). The result of this calculation is shown in Figure 4.4. Over the range from 16°C to 32°C, where Δp is known to be approximately constant, the idle speed increases linearly. It should be noted that the experiments of Chapter 2 only provide evidence for a linear torque-speed diagram at a fixed temperature, 22°C, not over a range of temperatures, as I have assumed above. Future experiments

should be done to test this assumption.

What are the implications of these results for the mechanism of torque generation? It is not difficult to imagine how the difference in behavior between tethered cells, whose motors are running near the stall torque, and swimming cells, whose motors are running near the idle speed, might arise in tightly coupled mechanisms. At stall, there is no net flux of protons through the motor and the internal states of the device assume equilibrium populations. Although these occupancies vary with temperature, it is possible to construct simple models in which the predicted stall torque does not depend on temperature - for example the model of Khan & Berg, 1983. At a nonzero rotation rate, there is a net flux of protons through the motor, and the speed may be determined by the steady state rates of (1) proton translocation, (2) cyclic transformations of protein components in the motor which couple flux to rotation, or (3) the movement of structural components through the cytoplasmic membrane. Each of these types of processes might show some kind of temperature dependence. At slow rotation rates, their relaxation times may be fast enough to maintain populations of internal states close to their equilibrium values, so no temperature effect would be detected. At high speeds they may become rate limiting. Although the temperature data alone do not favor any particular type of process, the linear behaviour might seem to suggest that the speed is not being determined by the rate of a single reaction obeying a simple exponential temperature dependence. However, the Arrhenius plot is roughly linear from 16°C to 32°C, and if allowance is made for a reduction in Δp below 16°C, in accordance with Fig.4.1, then the plot becomes linear over the wider range from 10°C to 32°C (Fig.4.5A). For this calculation I made

the further assumption that both N_o and f_o are proportional to Δp:

$$N_o = \beta.\Delta p \tag{4.3}$$

$$f_o = \alpha.\Delta p \tag{4.4}$$

where β is independent of temperature, T, and the factor α contains the temperature dependence of f_o at fixed Δp. The idle speed is still given by equation (4.2), but with N_o replaced by $N_o\epsilon(T)$, where $\epsilon(T)$ is plotted in Fig.4.1. The idle speed at fixed Δp (equal to its value at $\epsilon(T) = 1$) is thus:

$$\frac{f_o}{\epsilon(T)} = \frac{N_o f}{N_o\epsilon(T) - \gamma\eta f_f} \tag{4.5}$$

No data on $\epsilon(T)$ is available for $T > 32°C$, but the protonmotive force would have to drop at higher temperatures in order to preserve the linearity of the plot of Fig.4.5B. It should be noted that there is good evidence that stall torque is proportional to Δp (Equation 4.3), but that the evidence for proportionality between idle speed and Δp (Equation 4.4) is very weak. In fact there are reasons for believing that idle speed may show nonlinear saturation at high Δp (c.f. §7.1).

The simplest picture which would account for these results is that of a tightly coupled model in which the rotation speed is being determined by the rate of a single reaction step described by the transition-state formalism. In this theory (Eyring, 1935) the rate constant of a chemical reaction is given by:

$$k_T = \nu \exp\left(- \frac{V_o}{kT} \right) \tag{4.6}$$

where the prefactor ν is interpreted as a vibration frequency of the initial state along the reaction coordinate, and V_o is the activation

energy, the free energy difference between the transition state and the initial state. The prefactor is temperature independent if $h\nu \ll kT$ and depends only weakly on the absolute temperature if $h\nu \tilde{>} kT$, giving the Arrhenius plot a slight upward curvature that would not be detectable within the scatter of the data points. The slope of the Arrhenius plot gives an activation enthalpy of ca. 17 kT, which is about twice the average energy required to break hydrogen bonds but much smaller than that required to break a covalent bond (about 140 kT for a C-C bond).

An expression similar to equation (4.6) was found by Kramers (1940) for the highly damped case in which the energy of motion of the reactants is dissipated by friction with the surrounding medium. In this case the prefactor is inversely proportional to the viscosity of the medium. Since viscosity decreases exponentially with increasing temperature, the final temperature dependence is still exponential, but with a reduced energy barrier. Thus, viscous damping may or may not play an important role in determining the rate of motor rotation. In the extreme case in which diffusion of membrane proteins alone limits the rotation rate, the ratio of speeds at two different temperatures would be approximately equal to the ratio of the diffusion coefficients at those temperatures (Berg and Khan, 1982). For example, the ratio of lateral diffusion coefficients measured by fluorescence microphotolysis for bacteriorhodopsin in synthetic lipid membranes at 24°C and 32°C was found to be about 2.75 (Peters and Cherry, 1982). This is about twice the ratio of flagellar rotation rates at the same temperatures. If membrane fluidity has a role in limiting the speed of the motor then one might expect to see a sharp transition in speed with increasing temperature corresponding to a phase transition of the lipid bilayer.

Phase transitions have been revealed in E. coli membranes of defined composition by differential scanning calorimetry (Haest et al., 1974), fluorescent probes, light scattering, and the study of membrane transport systems (Overath and Trauble, 1973). Miller and Koshland (1977) studied swimming speeds of E. coli and found no differences when membrane fluidity was changed by varying the growth temperature or by supplementing fatty acid auxotrophs with specific lipids. They also failed to detect any sharp transitions in swimming speeds.

The data discussed in this chapter do not allow any definite statements to be made about the processes which limit the motor speed in swimming cells mainly because there is sufficient scatter over a relatively limited temperature range to accomodate more than one kind of fit. Further work needs to be done to investigate whether the exponential fit can be maintained over a wider temperature range under conditions of constant Δp. The correct approach would be to utilize the artificially energized system (Chapter 6) and the video technique of obtaining swimming speeds, calibrated by bundle frequency measurements on glycolysing cells. Tethered cell controls on the same cultures would provide an independent check of any variation of Δp with temperature.

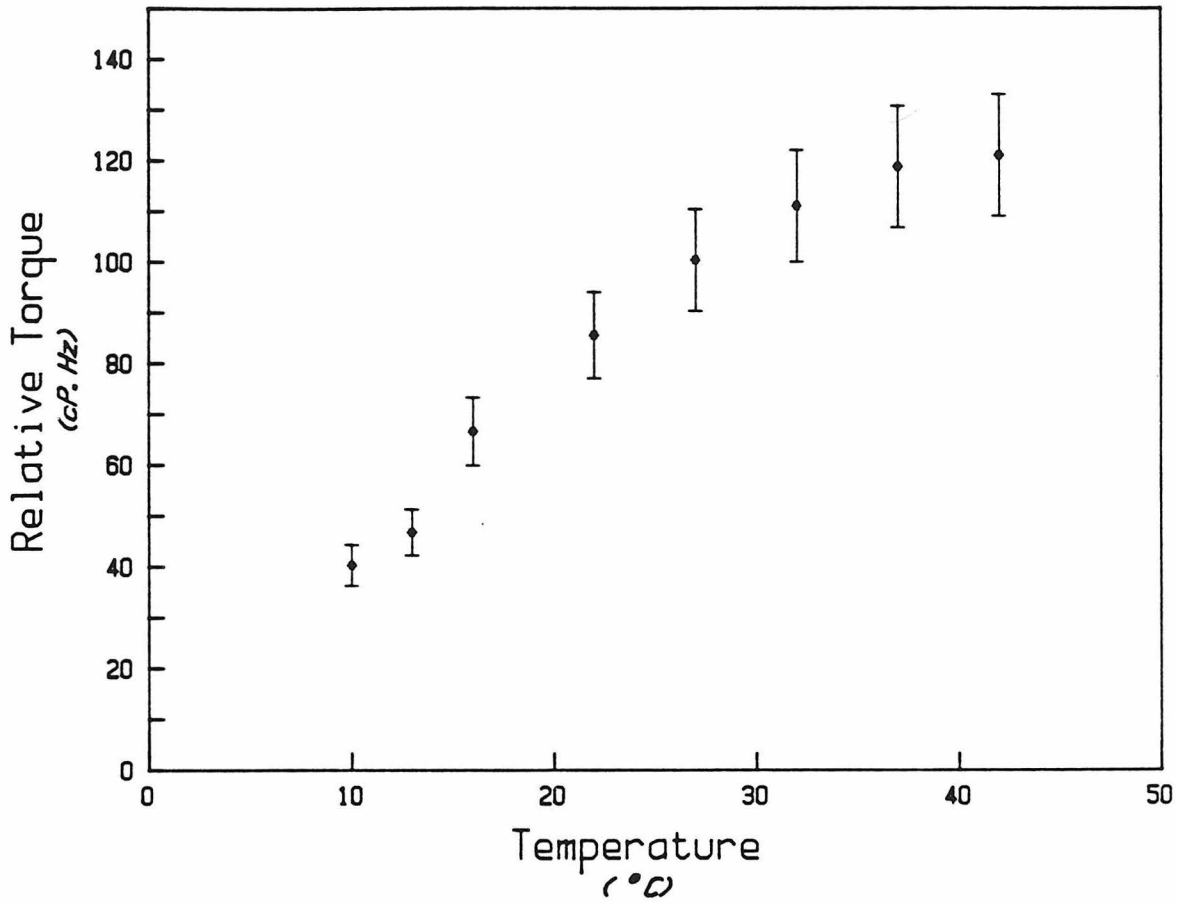

Figure 4.3. Torque of swimming Streptococcus SM197 as a function of temperature.

Relative torque was computed as the product of bundle frequency and viscosity of the medium from data obtained from a single culture.

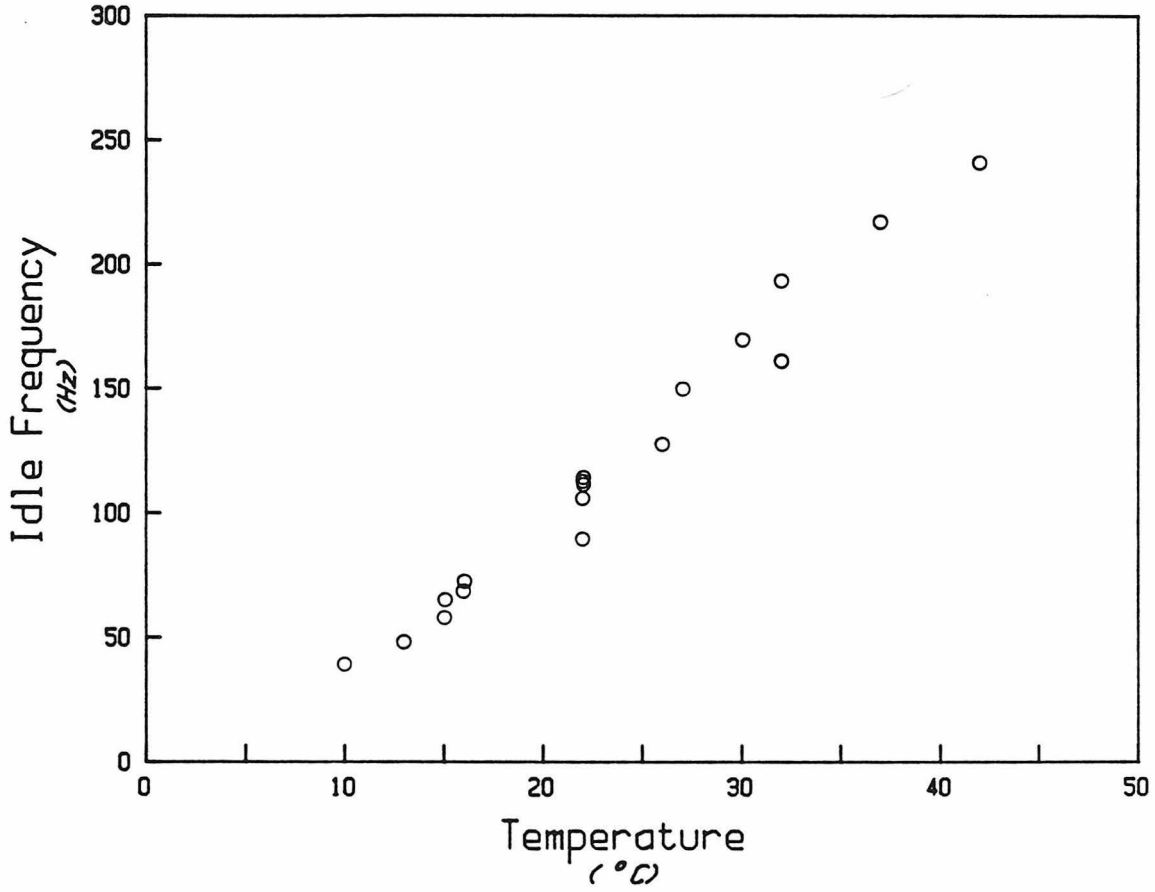

Figure 4.4. Temperature dependence of the idle frequency.

Idle frequency was computed from the data of Figure 5.4, assuming the validity of the linear fit to the points of Figure 5.3. The protonmotive force is constant from 16°C to 32 °C.

Figure 4.5. Hypothetical temperature dependence of the idle frequency at fixed Δp.

A. The idle frequency as a function of temperature at fixed Δp, computed from the data in Figure 5.4 (excluding points above 32°C) and Figure 4.1., assuming that both stall torque and idle frequency are proportional to Δp (see text), and that the constants of proportionality do not depend on speed. The open symbols in this plot are unaffected by these assumptions and essentially coincide with the corresponding points in Figure 4.4. The closed symbols fall into the temperature range over which there is a significant drop in Δp.

B. The natural logarithm of the hypothetical idle frequency plotted as a function of the reciprocal of the absolute temperature. The line is a least squares fit. The slope corresponds to an activation energy of ca. 17 kT for a single step reaction.

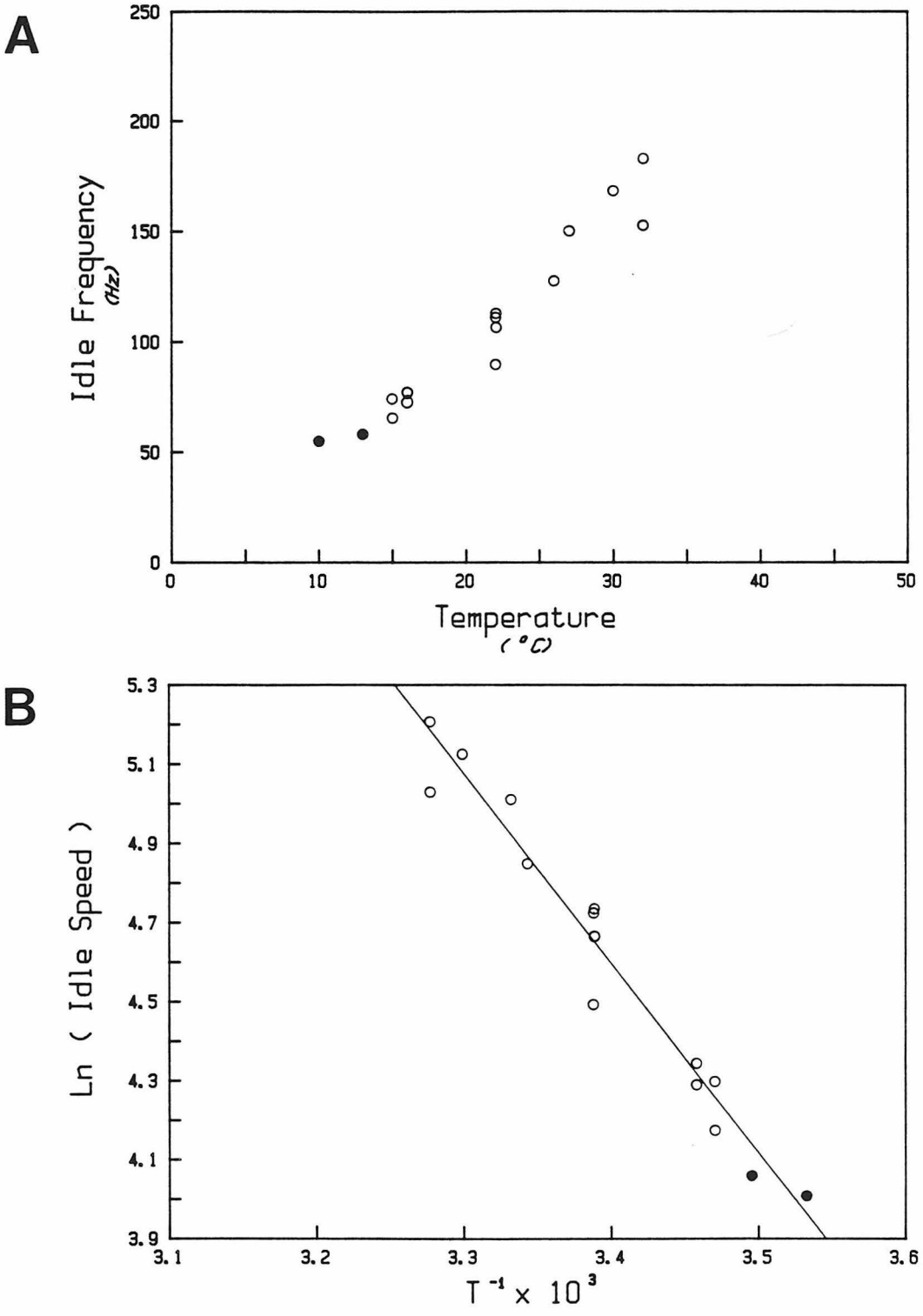
A
Idle Frequency (Hz)
250
200
150
100
50
0
0
10
20
30
40
50
Temperature (°C)
B
Ln (Idle Speed)
5.3
5.1
4.9
4.7
4.5
4.3
4.1
3.9
3.1
3.2
3.3
3.4
3.5
3.6
T -1 x 10 3

Figure 4.5

CHAPTER.5

RAPID ROTATION OF FLAGELLAR BUNDLES IN SWIMMING BACTERIA

Nature, 1987 (in press)

Rapid rotation of flagellar bundles in swimming bacteria

Graeme Lowe, Markus Meister & Howard C. Berg

Division of Biology 216-76, California Institute of Technology,
Pasadena, California 91125, USA

A bacterial flagellum is driven by a reversible rotary motor[1-3]. The power input is determined by protonmotive force and proton flux, the power output by torque and speed. Interrelationships between these parameters provide important clues to motor mechanisms. Here we describe the relationship between torque and speed at constant protonmotive force. The measurements are analogous to those that could be made by plugging an electric motor into a constant-voltage outlet, varying the external load, and determining the torque delivered at different speeds. We used suspensions of metabolizing cells of a motile Streptococcus, varied the external load by changing the viscosity of the medium, determined motor speed from the frequency of vibration of the cell body, and inferred motor torque from the rate of body rotation. The flagellar bundles rotate more rapidly than formerly supposed, at rates that increase linearly with temperature. The torque delivered by the flagellar motor drops linearly with speed. At high speed, the torque-generating cycle associated with the transfer of one proton appears to dissipate free energy in a series of small steps.

The helical bundle of a swimming bacterium generates thrust, and the cell translates at a velocity at which this force is balanced by viscous drag on the body. The bundle also generates torque, and the body counter-rotates (or rolls). If the longitudinal axes of the bundle and the cell body are not collinear, then the

image of the body wobbles from side to side. If there is a net imbalance in the forces perpendicular to the axis of the helix, e.g., if the bundle does not contain an integral number of wavelengths[4], then the cell body also vibrates (or gyrates) at the rotation frequency of the bundle. The presence of such motion was postulated long ago by Reichert[5], who referred to it as "die Trichterbewegung," or funnel movement[6].

We measured these frequencies by projecting the images of swimming cells onto the photocathode of a photomultiplier tube whose sensitivity is spatially inhomogeneous. The output was passed through a bandpass filter, and the power spectral density was computed with the fast Fourier transform. The spectra of many successive one-second data blocks were averaged. The top curve of Fig. 1 shows the amplitude of this spectrum (the square-root of the power spectrum) obtained from a field of smooth-swimming cells of Streptococcus. The low-frequency peak is due to the roll of the cell body and the high-frequency peak to its funnel movement. The other spectra in Fig. 1 characterize noise arising from changes in the number of cells imaged on the detector, Brownian movement, and photoelectron statistics.

In order to better interpret these spectra, we simulated the measurements by computer, moving a vibrating spot across a detector with a radial Gaussian sensitivity and filtering the output. We concluded from this analysis that the low-frequency peak (Fig. 1) is skewed toward high frequencies because of harmonics of the body-roll frequency that arise from the nonlinear relation between displacement and detector output at large wobble amplitudes. The high-frequency peak, on the other hand, while broadened somewhat by sidebands generated by mixing with the low-frequency signal, remains centered at the mean bundle frequency, provided (as in Fig. 1) that the two peaks do not strongly overlap. Both peaks are broadened and smoothed by variations over the cell

population[10].

The correct body-roll frequency corresponding to each amplitude spectrum was determined by examining video recordings made of the same cell suspensions. An average was computed from the wobble frequencies of all the cells in a video field, as measured by eye and stopwatch during slow-speed playback. For the culture used in the experiments of Fig. 1, the body-roll frequency was 6.7 ± 2.4 Hz (mean ± SD for 20 cells). Given a bundle frequency of about 95 Hz (Fig. 1), this yields a value for the speed of the flagellar motor relative to the cell body of about 100 Hz.

Figure 2 shows the dependence of bundle frequency (A) and swimming speed (B) on the fluidity of the medium, adjusted by addition of Ficoll, a highly-branched viscous agent whose solutions are Newtonian[11]. A ten-fold increase in viscosity was required to halve the bundle frequency. Swimming speeds closely paralleled bundle frequencies, but they were slightly lower at higher viscosities: the ratio of swimming speed to bundle frequency decreased from 0.18 ± 0.01 μm to 0.15 ± 0.01 μm for the data shown. A possible explanation for this trend is that the bundle winds up slightly as the torque increases, decreasing its propulsive efficiency. We also measured bundle frequencies of Streptococcus as a function of fluidity using methylcellulose and found that the frequencies decreased monotonically with increasing viscosity (data not shown). Thus, increases in swimming speed observed on the addition of small amounts of this agent[15] must arise from enhancement of the efficiency of flagellar propulsion, as argued previously[11], not from changes in the speed of the flagellar motors.

Figure 3 shows the torque generated by the flagellar motor as a function of its rotation rate. The open symbols are a different representation of the data of Fig. 2A: their position on the abscissa is the sum of the body-roll and bundle frequencies, equal to the motor rotation frequency, while their position on the

ordinate is proportional to the product of the body-roll frequency and the viscosity of the medium. The proportionality constant is determined by a geometrical drag factor and the number of filaments per bundle. The same constant was assumed for all the experiments on swimming cells. For each of the three cultures, the torque appears to drop linearly with increasing speed, although the relationship varies somewhat from culture to culture. The closed symbols represent the torque for tethered cells, calculated in the same fashion, but with a different geometrical drag factor. These torques correspond well to the linear extrapolation of the data for swimming cells. However, it should be noted that the ratio of the two drag factors, and thus the position on the ordinate of the closed symbols relative to the open symbols, is subject to considerable uncertainty, probably up to 40%. The implications of Fig. 3 for the mechanism of torque generation are discussed below.

Figure 4 shows the dependence of bundle frequency (open symbols) and swimming speed (closed symbols) of Streptococcus on temperature. Both increase linearly over the range 10 to 40°C. To check for a possible temperature dependence of the protonmotive force, we tethered cells from the culture used for the bundle-frequency measurements. Their torques were compared at 9.3, 16.0, 22.0, 27.8, and 31.6°C and found to fall in the ratios 0.7, 0.95, 1.00, 1.02, and 1.04, respectively (torques for each of 14 cells were scaled to the torque at 22°C and then averaged; the standard deviation for the population was about 0.05; the mean speed at 22°C was 6.3 Hz). Artificially-energized cells generate a torque that is essentially independent of temperature over the range 4-38°C[21]. Assuming a linear dependence of torque on protonmotive force[16,21], we conclude that the protonmotive force of metabolizing cells increases by at most 10% over the temperature range 16-32°C. The bundle frequencies of the swimming cells increased by a factor of 2.4 (Fig. 4), corresponding to an increase

in torque by a factor of 1.7. A linear dependence of swimming speed on temperature was observed earlier for Escherichia coli by Banks et al.[22], using number-fluctuation spectroscopy, and by Maeda et al.[23], using cinematography. Similar results were obtained for Salmonella typhimurium by Miller and Koshland[24], who recorded motility tracks.

We also measured the bundle frequencies and swimming speeds of E. coli. The mean bundle frequency of a smooth-swimming strain (HCB437) grown at 35°C on glycerol in a minimal salts medium, harvested at mid-exponential phase, and then studied in motility medium[25] at 22°C--these were the conditions used for the measurements of rotational frequencies of hooks described earlier (mean ± SD for 20 cells 104 ± 29 Hz)[2]--gave a result in the same range, 113 Hz. The mean bundle frequency for these cells was higher at 32°C, 156 Hz. We also determined mean bundle frequencies for cells grown at 35°C in tryptone broth and harvested at mid-exponential phase. These frequencies were higher still, 191 Hz at 22°C, and 268 Hz at 32°C. All of these measurements were made near the open edge of the chamber[8] to ensure that the cells were well oxygenated. Cells of wild-type strain AW405 (ref. 26) were grown on tryptone broth and tracked at 32°C in motility medium containing varying amounts of Ficoll. The dependence of swimming speed on fluidity was essentially identical to that observed for Streptococcus (Fig. 2B), except that the swimming speeds were higher (mean ± SEM for 79 cells at fluidity 1.25 cP^{-1}, 36.4 ± 1.0 μm/s).

What can these measurements tell us about the physics of flagellar propulsion? The motor's torque drops monotonically with increasing speed, and the relationship appears to be approximately linear over a wide range, Fig. 3. These results do not favor a mechanism by which the motor runs at constant power: in that case the torque would be inversely proportional to speed, and the fits would be hyperbolic. This conclusion is reinforced by two additional

observations, namely, that the stall torque of a tethered cell is approximately equal to its running torque (M. Meister and H. C. Berg, in preparation), and that the speed observed with hooks approximates the speed observed with flagellar bundles (see above). The frictional drag coefficient of a hook is very much smaller than that of a filament in a bundle. Therefore, the intercepts of the linear fits with the axes of Fig. 3 are confirmed experimentally.

In the framework of thermodynamics, one can treat the flagellar motor as a system coupling two flows: the flux of protons and the rotation of the rotor. If the system operates close to thermodynamic equilibrium, then the flows are linear functions of the pair of conjugate driving forces, namely, the protonmotive force and the torque acting on the rotor[27]. When the protonmotive force is held constant, as it was in the measurements of Fig. 3, one predicts that torque decreases linearly with speed, as observed. Chemical processes occur close to equilibrium when the difference in the free energies of reactants and products (dissipated as heat) is small compared to kT, where k is Boltzmann's constant and T is the absolute temperature. The linear relationship between torque and speed appears to extend to the point where the motor generates essentially no torque and, thus, performs no mechanical work. At this speed, all of the free energy available per proton (ca. 8 kT) is dissipated by processes internal to the motor. The motor would still operate in the linear regime if the torque-generating cycle associated with the transfer of one proton involved a series of many reactions, each of which entailed only a small free energy loss.

A mechanism that has this feature has been proposed by Läuger[28]. In this scheme protons are translocated from the external medium into the cytoplasm along binding sites at the intersections between rows of ligands on the faces of the M- and S-rings. The two sets of rows are tilted with respect to each other,

so proton movement is coupled to motor rotation. Läuger discussed the operation of this device at low speeds and suggested that the torque should be independent of speed up to about 10 Hz. At the much higher speeds observed in swimming cells, finite proton transfer rates might lead to considerable dissipation of free energy in conduction along the ligand chain and thus limit the torque. If each row contains 10 or more sites, one would expect the torque to vary linearly with speed.

In a model proposed by Berg and Khan[29], a single torque-generating step utilizes all of the electrochemical energy of a proton and stores it as elastic energy in a spring. This process becomes rate-limiting at high speeds and accounts for all of the internal dissipation. A preliminary analysis of this mechanism at steady-state predicts a nonlinear dependence of torque on speed that is inconsistent with the data of Fig. 3. However, the model can be altered successfully by assuming that protons reach the rotor by stepping along a series of sites in a membrane channel, provided that the latter process is rate-limiting at high speeds.

An approximately linear torque-speed relationship can be obtained from mechanisms that work far from thermodynamic equilibrium, but only by explicit construction. An example is the model proposed by Oosawa and Hayashi[30], in which proton transfer and rotation are loosely coupled. Measurements of torque at high speed place strict requirements on all models for the bacterial motor and deserve further attention.

We thank R. D. Smyth for help with the tracking experiments, D. F. Blair for discussions, and E. M. Purcell for comments on the manuscript. Development of the new technology was inspired by the light-scattering experiments of C. Ascoli and C. Frediani and their colleagues, although the physics turned out to be different[31]. This work was supported by grants from the US NSF (DMB8518257)

and the Gustavus and Louise Pfeiffer Foundation. G. L. and M. M. were recipients of Earle C. Anthony Fellowships.

References

1. Berg, H. C. & Anderson, R. A. Nature **245**, 380-382 (1973).
2. Berg, H. C., Manson, M. D. & Conley, M. P. Symp. Soc. Exp. Biol. **35**, 1-31 (1982).
3. Macnab, R. M. & Aizawa, S.-I. Ann. Rev. Biophys. Bioeng. **13**, 51-83 (1984).
4. Berg, H. C. Random Walks in Biology, pp. 78-79 (Princeton University Press, Princeton, New Jersey, 1983).
5. Reichert, K. Zentr. Bakteriol. Parasitenk. Infektionskr. Abt. 1 Orig. **51**, 14-94 (1909).
6. Berg, H. C. Ann. Rev. Biophys. Bioeng. **4**, 119-136 (1975).
7. Berg, H. C. & Block, S. M. J. gen. Microbiol. **130**, 2915-2920 (1984).
8. Segall, J. E., Ishihara, A. & Berg, H. C. J. Bact. **161**, 51-59 (1985).
9. Berg, H. C. Adv. Opt. Elect. Micros. **7**, 1-15 (1978).
10. Lowe, G. Ph.D. thesis (California Institute of Technology, Pasadena, 1987).
11. Berg, H. C. & Turner, L. Nature **278**, 349-351 (1979).
12. Reinsch, C. H. Numer. Math. **10**, 177-183 (1967).
13. van der Drift, C., Duiverman, J., Bexkens, H. & Krijnen, A. J. Bact. **124**, 1142-1147 (1975).
14. Berg, H. C. & Brown, D. A. Nature **239**, 500-504 (1972).
15. Schneider, W. R. & Doetsch, R. N. J. Bact. **117**, 696-701 (1974).
16. Manson, M. D., Tedesco, P. M. & Berg, H. C. J. molec. Biol. **138**, 541-561 (1980).
17. Tirado, M. M. & de la Torre, J. G. J. Chem. Phys. **71**, 2581-2587 (1979).
18. Tirado, M. M. & de la Torre, J. G. J. Chem. Phys. **73**, 1986-1993 (1980).
19. Heimbrook, M. E., Wang, W. L. L. & Campbell, G. Abstracts of the Annual Meeting of the American Society for Microbiology, 1986, 240 (American

Society for Microbiology, Washington, DC, 1986).

20. Berg, H. C. in Cell Motility, Vol. 3, Bk. C. (eds. Goldman, R., Pollard, T. & Rosenbaum, J.) 47-56 (Cold Spring Harbor Laboratory, New York, 1976).

21. Khan, S. & Berg, H. C. Cell **32**, 913-919 (1983).

22. Banks, G., Schaefer, D. W. & Alpert, S. S. Biophys. J. **15**, 253-261 (1975).

23. Maeda, K., Imae, Y., Shioi, J.-I. & Oosawa, F. J. Bact. **127**, 1039-1046 (1976).

24. Miller, J. B. & Koshland, D. E., Jr. J. molec. Biol. **111**, 183-201 (1977).

25. Ishihara, A., Segall, J. E., Block, S. M. & Berg, H. C. J. Bact. **155**, 228-237 (1983).

26. Armstrong, J. B., Adler, J. & Dahl, M. M. J. Bact. **93**, 390-398 (1967).

27. Prigogine, I. Introduction to Thermodynamics of Irreversible Processes, 2nd Ed. (Interscience, New York, 1961).

28. Läuger, P. Nature **268**, 360-362 (1977).

29. Berg, H. C. & Khan, S. in Motility and Recognition in Cell Biology (eds. Sund, H. & Veeger, C.) 486-497 (Walter de Gruyter, Berlin, 1983).

30. Oosawa, F. & Hayashi, S. J. Phys. Soc. Japan **52**, 4019-4028 (1983).

31. Angelini, F., Ascoli, C., Frediani, C. & Petracchi, D. Biophys. J. **50**, 929-936 (1986).

Fig. 1 Amplitude spectra of swimming cells of Streptococcus (top curve), of de-energized cells moving at the speed of the swimming cells (second curve), of de-energized cells undergoing Brownian movement (third curve), and of the background illumination at the same total light intensity (bottom curve). **Methods:** Cells of a smooth-swimming mutant, SM197, were grown at 35°C in KTY medium[2], harvested at late exponential phase, washed twice by centrifugation (480 x g , 6 min) in an equal volume of 0.1 M sodium phosphate (pH 7.5), 0.2 M KCl, 0.1 mM EDTA, 0.01 M D-glucose, and then resuspended in this medium at a density of about 4×10^8 cells/ml. An aliquot of this suspension was drawn into a flow chamber[7] (0.4 mm deep) and examined at 22°C under an inverse phase contrast microscope (see below), yielding the spectrum shown in the top curve (swimming speed: mean ± SEM 15.7 ± 1.1 µm/s for 17 cells, as judged from slow-speed playback of a video recording, made as in ref. 8). Another aliquot was de-energized by the addition of the uncoupler FCCP (trifluoromethoxycarbonylcyanide phenylhydrazone, 10 µg/ml) and either drawn through the chamber at a speed of 14.4 µm/s (measured at the middle of the chamber), yielding the spectrum shown in the second curve, or examined when stationary, yielding the spectrum shown in the third curve. The microscope (Nikon S-Ke) was equipped with a 100-W tungsten-halogen lamp (type FCR, driven by a constant-voltage DC power supply), a heat-transmitting mirror (Optical Industries 03MCS007), a CF BM 40X objective, a 20X eyepiece, a ½X PFM photomicrographic attachment, and a photomultiplier tube (RCA 4886, run at 300 V). The focal plane was located midway between the top and bottom windows of the flow chamber to minimize wall effects. The diameter of the photocathode (1.8 cm), referred to the focal plane, was about 39 µm. The output of the photomultiplier was passed through a current-to-voltage converter (10^7 ohm feedback), a difference amplifier (to remove the DC offset and amplify

the AC signal), a double-pole low-pass filter, and a single-pole high-pass filter. The 3 dB cutoff points of these filters were set at 200 and 72 Hz, respectively. A 12 bit A/D converter sampled data at 512 points/s for 1 s intervals and a PDP-11/34 computer computed and averaged the corresponding power spectra (400 times for the data shown). The signals arose from lateral motion of images on the photocathode, which was exposed to light from only a small region of the flow chamber, and which when scanned with the image of a cell that was stuck to glass, was found to have an output (signal less background) that rose and fell 3 or 4 times across a diameter, varying in amplitude by as much as 50%. Contributions from out-of-focus components of the images were significant, since useful spectra could be obtained on moving the plane of focus beyond the limits of the flow chamber. The basic features of the spectra, including sidebands due to non-linearities encountered with large displacements (see text), could be reproduced by mounting the detector on the tracking microscope[9], suspending de-energized cells in the tracking chamber, and moving it sinusoidally with the tracker drive. Much larger signals were obtained on moving the tracking chamber sideways than up and down. De-energized cells and monodisperse polystyrene latex spheres (1.3 μm diameter) gave identical spectra.

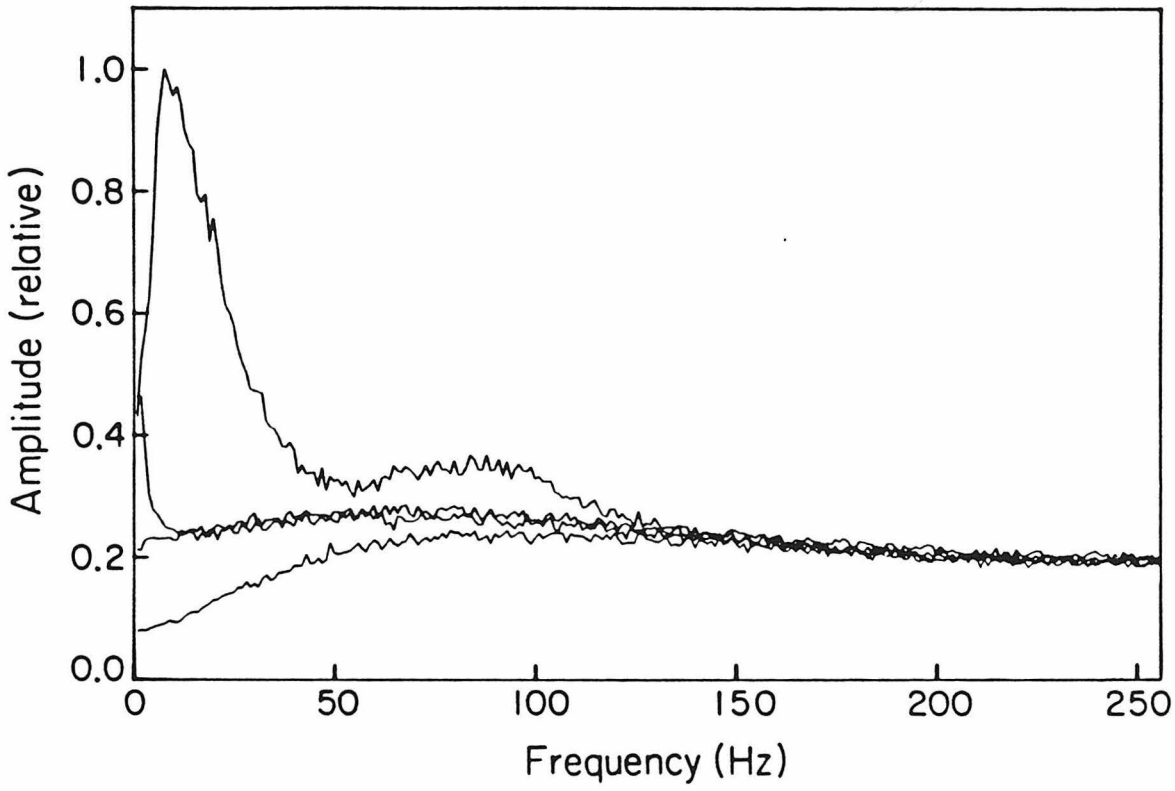
Amplitude (relative)
1.0
0.8
0.6
0.4
0.2
0.0
0
50
100
150
200
250
Frequency (Hz)

Figure 5.1

Fig. 2 Bundle frequencies (A) and swimming speeds (B) of Streptococcus as a function of the fluidity of the medium. The different symbols refer to cells from different cultures. The values shown at each point are means for the cell population determined from the power spectrum or the tracking data, respectively (see below). In either case, the spread (SD divided by the mean) was about 25%. The fits to the data in (A) were determined in Fig. 3. The solid curve is redrawn in (B) and scaled to approximately match the swimming speeds at high fluidity. **Bundle frequencies:** Open circles: cells of strain SM197 were grown, harvested, and washed as described in Fig. 1 and then resuspended at 80 times the harvest density. An aliquot was mixed with 9 volumes of a solution of Ficoll 400 (Pharmacia) of known concentration. Open triangles and open squares: cells were pelleted once, as before, and resuspended in a solution of Ficoll in KTY medium. All spectra were taken as described in Fig. 1, except in a shallower chamber (0.15 mm deep)[8]. Ficoll standards were prepared by serial dilution of a 20% w/v stock prepared in the medium in which the cells were suspended. The viscosities of these solutions were measured at 22°C in a Cannon-Ubbelohde viscometer (viscometer constant 8.13×10^{-5} cm^2/s^2). The same stock was used to prepare all of the Ficoll solutions. The position of the center of the high-frequency peak was found as follows. The power spectrum for non-motile cells was smoothed with a cubic spline procedure[12] and subtracted from the power spectrum for the swimming cells. The difference spectrum was smoothed in the same way, and its low-frequency peak was fitted by a curve generated by computer simulation (see text). This curve was subtracted out, and the center of the remaining (high-frequency) peak was found by eye. **Swimming speeds:** Cells of the wild-type strain V4051 (ref. 13) were grown, harvested, and washed as described in Fig. 1, and then resuspended at 2.5 times the harvest density. An aliquot was mixed with 50 volumes of a solution of Ficoll of known

concentration, and the swimming speeds of 20-30 cells were found by tracking[9]. Note: tracking results for Streptococcus were very similar to those reported earlier for E. coli[14]. The following data (mean ± SD, unless otherwise noted) were obtained for a population of 60 bacteria in the absence of Ficoll (compare ref. 14, Table 1): speed 16.8 ± 3.7 μm/s (mean ± SEM), tumble length 0.18 ± 0.07 s, run length 1.71 ± 0.90 s, change in direction from run to run 63 ± 14°, and change in direction during runs 26 ± 8°. The run-tumble statistics also were Poisson.

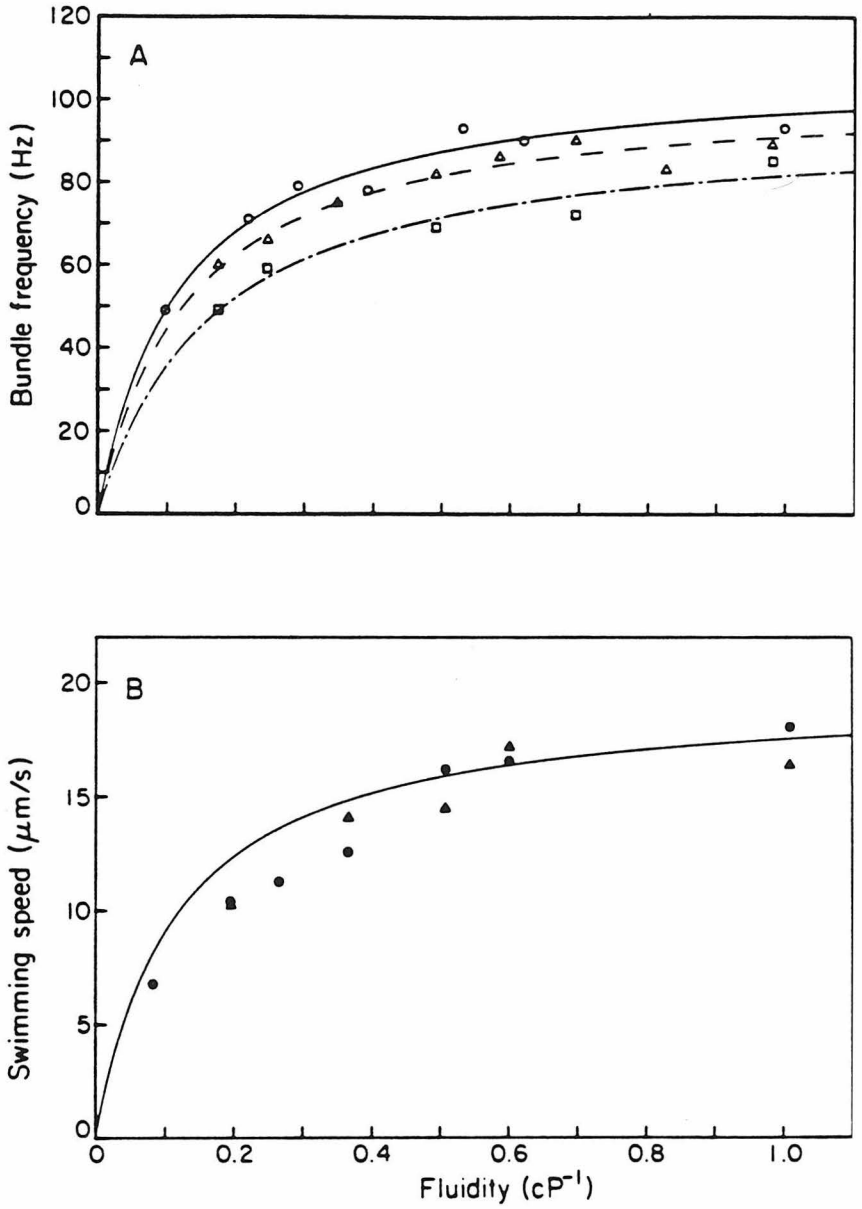
A
Bundle frequency (Hz)
120
100
80
60
40
20
0
B
Swimming speed (μm/s)
20
15
10
5
0
0
0.2
0.4
0.6
0.8
1.0
Fluidity (cP⁻¹)

Figure 5.2

Fig. 3 Torque of the flagellar motor of Streptococcus as a function of speed. The open symbols are values derived from the data of Fig. 2A. The lines are least-squares fits to these data. The closed symbols are values derived from experiments on cells tethered by a flagellar filament[16]. **Swimming cells:** The torque exerted by the bundle on the cell body is given by the product of the body-roll frequency, the viscosity of the medium, and a geometrical factor that depends on the shape of the cell and its axis of rotation. We approximated the cell body as a cylinder of length 3.27 μm and width 1.27 μm rolling about an axis that intersects the cylinder axis 1.09 μm from one end of the cell at an angle of 22°. Cell sizes were determined from photomicrographs of cells that had settled on a glass surface, while other parameters related to the geometry were estimated by inspecting the trajectory of several cells on the video record. The corresponding drag coefficient was computed from formulae given by Tirado and de la Torre [17,18]. No correction was made for the additional viscous drag on the body due to the counter-rotation of the flagellar bundle or for loss of torque due to interactions of flagella within the bundle; the latter assumption is justified by the observation that free hooks[2] or flagellar stubs[10] spin at rates comparable to those of flagellar bundles (see text). We visualized the flagellar filaments with a modified Ryu stain[19] and found an average of 3.5 ± 0.2 flagella per cell, all of which were assumed to join in a single bundle. **Tethered cells:** Cells from three cultures were prepared as described in Fig. 1 and tethered to a silanized cover slip[16]. We approximated the cell body as a cylinder of length 3.04 μm and width 1.36 μm spinning about an axis perpendicular to the cylinder axis 0.32 μm away from the center of the cell. No correction was made for the additional viscous drag due to the proximity of the cover slip [20].

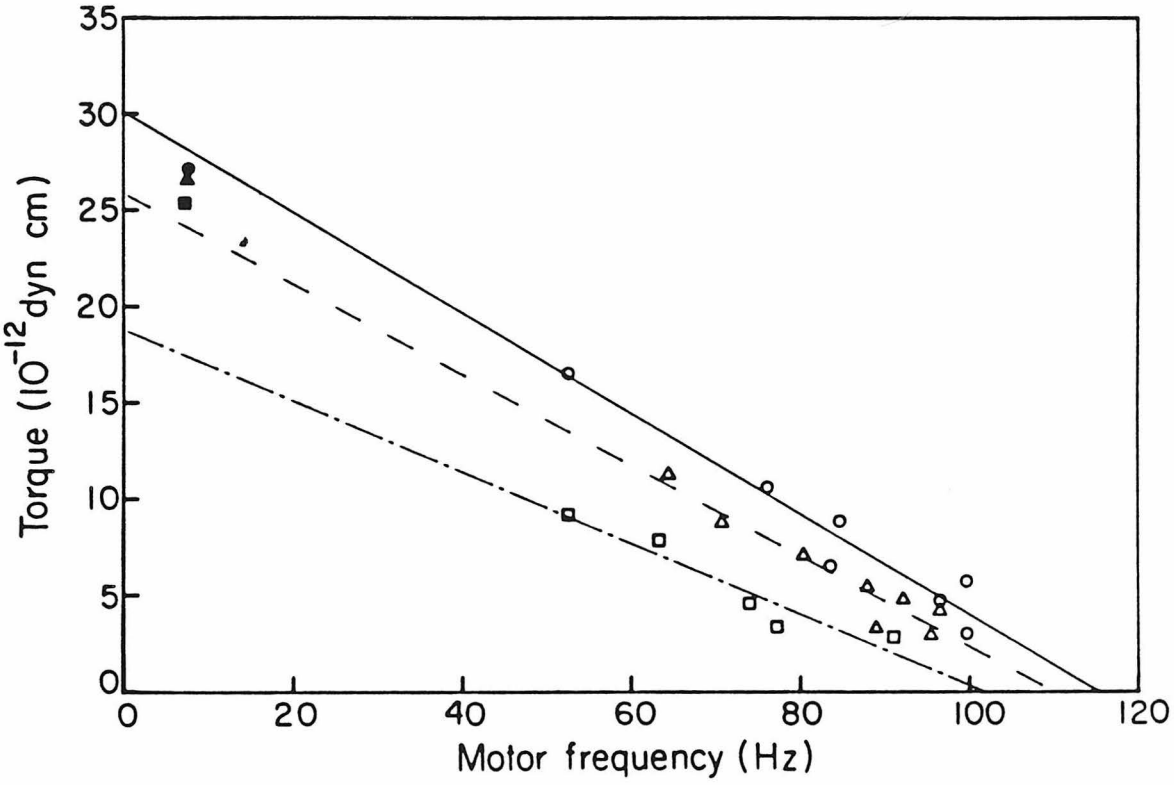
35
30
25
20
15
10
5
0
0
20
40
60
80
100
120
Torque (10^{-12} dyn cm)
Motor frequency (Hz)

Figure 5.3

Fig. 4 Bundle frequencies (o) and swimming speeds (o) of Streptococcus as a function of temperature. The values shown are the means for the cell population, determined at each point from the power spectrum or the tracking data, respectively. In either case, the spread (SD divided by the mean) was about 25%. The temperature was controlled as described previously[21]. Other conditions were as in Fig. 2 (with cells prepared in phosphate buffer). The line is a least-squares fit to the bundle-frequency data. The swimming-speed scale was adjusted so that the swimming-speed data fell along the same line.

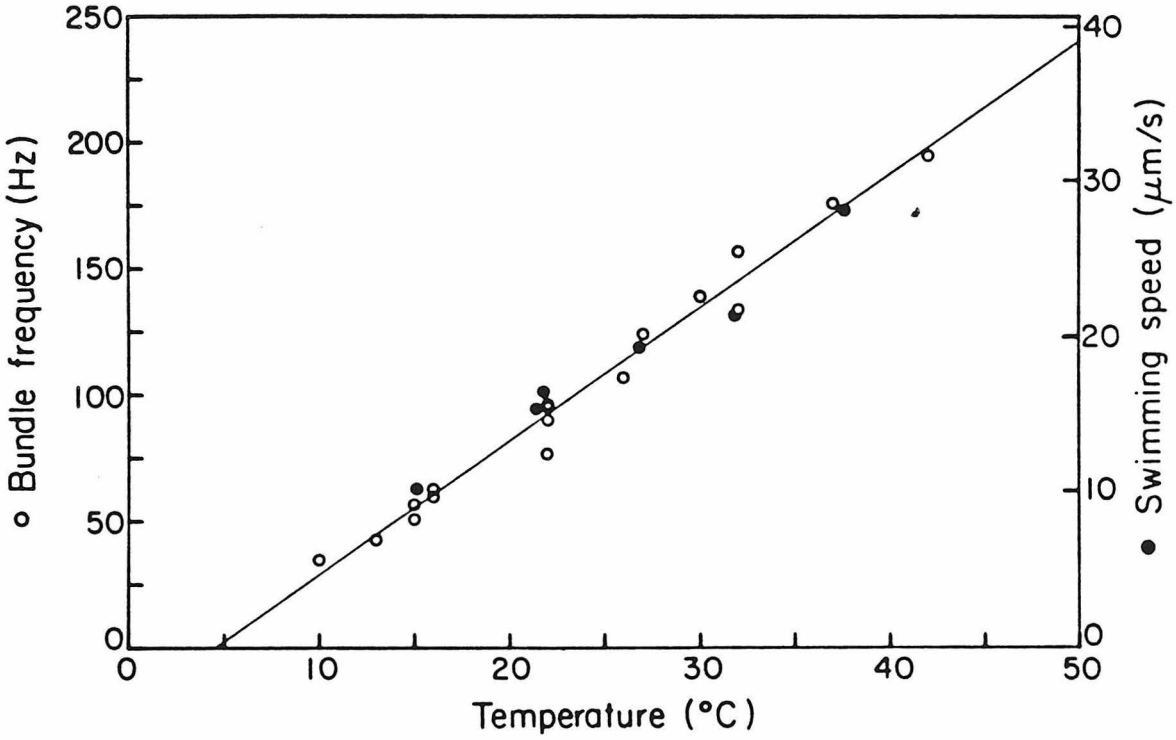
250
200
150
100
50
0
o Bundle frequency (Hz)
40
30
20
10
0
• Swimming speed (μm/s)
0
10
20
30
40
50
Temperature (°C)

Figure 5.4

CHAPTER 6

ARTIFICIALLY-ENERGIZED SWIMMING CELLS

§6.1 Introduction

This chapter contains a summary of the techniques I developed to obtain suspensions of swimming cells by imposing an artificial membrane potential and a pH gradient on starved Streptococcus. The primary motivation behind this work was to reach a stage where I could rigorously define the value of Δp and thereby study the effect of varying temperature and isotope substitution on the torque generated by the motor at fixed protonmotive force. Measurement of flagellar rotation rates in this system would also be useful, in conjunction with experiments being done by Markus, for determining the number of rotation-coupled protons flowing through the motor per revolution, and hence for calculating the efficiency of energy transduction. As I have already explained in previous chapters, I was unable to obtain accurate estimates of mean bundle frequency for such cells by the direct methods of Chapter 2. Instead, those methods were used to calibrate, from glycolysing cells, the ratios of swimming speed and body roll frequency to bundle frequency, and the former parameters were then measured from videotapes. The numerical accuracy and high time resolution of the video method makes it well suited for use on artificially energized cultures.

I first began to tackle the problem of making artificially energized cells swim while attempting to observe motility in cells which had been energized according to protocols used by Shahid Khan in preliminary proton flux measurements. Cells were starved in buffer T2 (pH 7.5) and shifted by dilution to a pH of 6.0 (Δp = 82 mV), with a simultaneous sudden drop in temperature from 22°C to 4°C. No swimming cells were seen. Was the temperature shock inhibiting motility or was Δp too small? Although tethered cells spin vigorously when energized with such pH

gradients, a larger Δp is apparently required to induce swimming, possibly due to a threshold torque required for the formation of a stable bundle (ca. 75 mV, c.f. Manson et al, 1980, p.557). I found that at 22°C, a combination of potassium diffusion potential (77mV) and ΔpH (7.5 to 6.5) gave a small yield of weakly motile swimmers, but there was no motility when this was combined with a rapid drop in temperature from 22°C to 10°C. The original purpose of including a temperature drop was to attempt to reduce transmembrane proton fluxes not coupled to rotation, thereby increasing the signal-to-noise ratio for measurements of the rotation coupled flux. At the time that this protocol was devised it was known that the torque generated by motors of tethered cells was temperature independent, but it was not known that motor speed is strongly temperature dependent for swimming cells. This illustrates clearly the danger in making untested assumptions about the behaviour of a system under one set of conditions based on observations made under quite different conditions.

During our efforts to obtain a preparation of vigorously swimming artificially energized cells, Markus and I tested many combinations of buffer composition, membrane potential and pH shift. Although Manson et al. (1980) had used sodium phosphate buffers to energize cells, we decided to eliminate sodium from the buffers in order to prevent fluxes through a putative sodium-proton antiport pathway in the membrane. When the external potassium concentration is reduced to generate a diffusion potential, the ionic strength of the buffer must be maintained by a positive counterion. We first chose choline for this role, assuming it to be inert and membrane impermeant. However, observations on tethered cells energized in choline buffers seemed to be inconsistent with these

assumptions (Meister, 1987) so we eventually settled on Mg^{2+} as the counterion. Phosphate was replaced by large, hopefully membrane impermeant, organic sulfonic acid ions. EDTA was unsuitable as a chelator because of its affinity for magnesium. It was replaced by tetraethylenepentamine (Reilly and Vavoulis, 1959). Using these buffers and a combination of a pH shift of 2 units and a potassium diffusion potential of at least 70 mV, we were able to generate vigorous swimming, although motility ran down after a period of 1-2 minutes.

§6.2 Methods for artificial energization

The first step is to grow a culture of vigorously motile Streptococcus (I used strain SM197 in all my experiments). I created a working stock, stored at -20°C, by growing a culture to saturation from a master stock stored at -20°C in 20% v/v glycerine in KTY medium. Current master stocks are stored in 10% v/v DMSO in KTY medium at -70°C, and should work equally well. The working stock was divided into 10 μl aliquots, each stored in a sterile plastic pipette tip. On the day before an experiment, a saturated culture was grown by inoculating 5 ml of KTY medium using one of these tips, and this culture was used to inoculate, by 100-fold dilution, a large volume of KTY medium, typically 100 ml, sometimes up to 1 liter. In the description below I shall assume that the culture volume is 500 ml. Large numbers of cells were required because (1) the process of energization involves dilution by a factor of about 20 or more, but the density after dilution must still be high enough to permit bundle frequency measurements, and (2) repeated energizations were required to average data since motility decayed rapidly after energization. Cultures were grown with swirling at 35°C for 4 h, and appeared to grow more rapidly in a single large volume.

All manipulations after harvest were done at room temperature (22°C). Cells were washed from growth medium into the following buffer (buffer TMK) at pH 8.5: 10 mM TAPS, 10 mM MES, 200 mM KCl, 1 mM $MgCl_2$, 0.1 mM Tetren. A solution made up with these ingredients has a pH of about 4. The pH was adjusted by titrating with: 10 mM TAPS, 10 mM MES, 200 mM KOH, 0.1 mM Tetren. To avoid precipitation at high pH, magnesium is omitted from the buffer until the final pH has been set. The culture was washed three times in four 250 ml capacity plastic screwtop bottles

(each with 125 ml) in the GSA rotor of the Sorvall centrifuge, spinning at 5,000 rpm (4080 X g) for 3 min. Cells continued to pellet over the 7 min required for the rotor to stop spinning. The pellet in each bottle was subjected to rapid manual swirling in 60 ml volumes until all the cells had been resuspended, then 65 ml of buffer were added. The final volume was 60 ml, and cells remained at this density until 2 h after harvest to complete starvation.

In the next step cells were concentrated to about 250 times their harvest density by dividing into 30 ml aliquots and pelleting in eight 50 ml capacity plastic tubes at 5,000 rpm (3090 X g) in the SS34 rotor in the Sorvall centrifuge, and resuspended in 7 ml volumes of buffer TMK (pH 8.5). They were transferred to glass corex tubes, pelleted again, and resuspended into the same buffer at a total pooled volume of about 2 ml. For energization at a series of different temperatures, aliquots remained separate, and the final resuspension buffer also contained the appropriate quantity of Ficoll to offset any temperature dependence in the viscosity (see below). The final suspensions were thick and milky due to the high cell density. Although starved, cells continued to extrude protons and acidify the buffer, so it was necessary to monitor the pH of these suspensions with an electrode and add small volumes of 1 M KOH to maintain the pH at 8.5. Another way to overcome this problem was to use a high buffering strength, e.g. 100 mM TAPS.

Cells were energized as follows. A 0.3 ml aliquot of the dense cell suspension was transferred to a plastic Eppendorf microfuge tube and 3 μl of a 0.5 mg/ml solution of valinomycin in methanol was added (giving 5 μg/ml of valinomycin). After waiting for 3 min, an aliquot of this was diluted (the dilution factor depending on the desired $\Delta\psi$, e.g. 50-fold

for 100 mV) into the following buffer: 10 mM TAPS, 10 mM MES, 67 mM $MgCl_2$, 0.1 mM Tetren (buffer TMg) at pH ≃ 6.45. The precise value of the pH depended on the dilution ratio, but it was adjusted to set the final pH after mixing at 6.5. The pH of this buffer was set by titrating with the following solution: 10 mM TAPS, 10 mM MES, 11 mM $Mg(OH)_2$, 56 mM $MgCl_2$, 0.1 mM Tetren, which has a pH between 9.0 and 9.5. The magnesium hydroxide was added last, in excess as a powder, to the solution containing all of the other components in the correct concentration. It dissolved slowly to saturation on a stirrer at room temperature over a period of several hours, and by titration back to the original pH with HCl, was found to be at about 11 mM concentration. Excess undissolved base was removed by centrifugation and passage through 0.45 μm pore diameter filters. The magnesium concentration was chosen to maintain a constant ionic strength.

Cells energized in this way initially swam vigorously but ran down after 1 to 2 min. Even with large nominal protonmotive forces (2 pH units and 2 decades of $[K^+]$ dilution), I never saw cells swim faster than about one half the speed of glycolysing cells. The maximal protonmotive forces that can be applied to cells by these techniques is apparently limited to values considerably less than those generated metabolically. Since 5 to 10 s were required to mix cells with the buffer of low pH and to transfer them to a glass flow chamber for observation, it is possible that Δp decays very rapidly from large values in the first few seconds. However, this assumption would call for a markedly biphasic decay in Δp, because simple extrapolation of the slow, approximately exponential drop in speed observed after the initial 10-second interval does not give a much larger speed at zero time.

§6.3 Temperature experiments.

In my initial observations on artificially energized cells at different temperatures, I followed the protocols described in §6.2. In later experiments I made two additional refinements: (1) Ficoll was added to the buffers to maintain a constant viscosity as the temperature was varied, and (2) the dilution factor was varied to maintain a constant Δp as kT varied. The errors in bundle frequencies incurred by neglecting these factors were expected to be small, no more than 10% over physiological temperature ranges.

The amount of Ficoll to be added was computed according to the relations given in §2.3.1. 20°C was taken as a reference temperature at which no Ficoll was added and all other measurements were at higher temperatures. The Ficoll supplied by the manufacturer (Pharmacia or Sigma Chemical Co.) contains metabolizable impurities which can be utilized as an energy source by Streptococcus. In particular, starved tethered cells will spin when exposed to a solution of unpurified Ficoll. In order to remove metabolizable contaminants, all buffers containing Ficoll were run through gel filtration columns (Sephadex G-50 Medium, Pharmacia). Columns were made up by soaking the gel overnight in buffer TMK (pH 8.5) or TMg (pH 6.45). The diameter of the column was 2.4 cm and its height was 12.5 cm. Stock solutions of 15% (w/v) Ficoll in these buffers were run through the column (12 ml each run). The column was calibrated with a Ficoll solution containing 0.6 mg/ml Bromophenol blue which was assumed to comigrate with low molecular weight contaminants. Calibration using a mixture of blue dextran and bromophenol blue dissolved in the buffer alone (which gave a void volume of 21.2 mls) was inaccurate, because the columns behaved very

differently when highly viscous solutions were eluted. There was extensive compactification with a 10-15% reduction in bed volume during passage of the Ficoll, and considerable vertical mixing between different levels of the column. During collection of the viscous fractions, allowance was made for this mixing as seen during the dye calibration runs. I tried running more viscous solutions on the columns (30% w/v Ficoll) but encountered severe problems in controlling the homogeneity of the flow. The bed penetration profile was extremely non-uniform and varied from one run to another. Sometimes large gaps were formed where the solution had penetrated the column without percolating through the Sephadex particles, and this was usually accompanied by the formation of vertical fissures. For concentrations of Ficoll greater than 15%, the preferred method of purification would be dialysis. The pooled fractions collected from one run of a 15% solution had a Ficoll concentration 6.6% as determined by viscometry (§2.3.1). These were diluted to give 2% w/v stock solutions which were tested on tethered cells and found to be free of the metabolizable contaminants. For energization at a temperature T (°C), the stock was diluted to give the concentration, c, of Ficoll required, determined by the equation:

$$a_2c^2 + a_1c + a_0(T) = a_0(T_0) \qquad (6.1)$$

where a_1 and a_2 are given in §3.2.1, $a_0(T)$ is given by equation (3.5), and T_0 is the reference minimum temperature (I used 20°C).

Since Δp is proportional to the absolute temperature, from 20°C to 35°C it increases by a factor of 308/293 = 1.05. To compensate for this 5% increase, I reduced the dilution factor at higher temperatures. I approximated the dependence of the pH of the final buffer on the mixing

ratio by linear interpolation. Thus if x mls of cells in pH 8.5 buffer are mixed with 1 minus x mls of cells in pH 6.5 buffer, the resultant pH is approximately Ax+B, where A = 2.02, B = 6.39 and $0.056 \leq x \leq 0.081$. Then x is a root of the equation:

$$\log_{10}x - (8.5 - Ax - B) = -3.25 \frac{293}{273+T} \qquad (6.2)$$

where I have assumed that at 20°C Δp is composed of 2 units of ΔpH and and a $\Delta\psi$ generated by 1.25 decades of $[K^+]$ dilution, and that the Nernst equation is valid.

The temperature of the microscope stage was controlled as described in §4.2.1. Instead of using glass flow chambers, observations were made in a stainless steel flow chamber (Berg & Block, 1984) which was attached to the aluminum stage using Thermacote grease. Prior to energization at any given temperature, cells were warmed or cooled to this temperature in glass shell vials inserted into a second aluminum block. This block was 9.5 cm square, 3.8 cm tall, with a 4 X 4 grid of cylindrical holes (1.5 cm diameter) for holding the vials. All of its outer surfaces except the top were insulated with a 1 cm thick layer of polystyrene foam. The temperature of the block was regulated by attaching, to its rear side, a peltier module driven by a current injection circuit controlled by a thermistor. The thermistor sensed the temperature of the block 1.5 cm from the attachment surface of the module. Cooling was provided by a water line connected in series with the block on the microscope stage. The block was placed on a magnetic stirrer (Magnestir 1250, Lab-line Instruments Inc.) and small 0.9 cm long teflon-coated stir bars were used to mix suspensions in the vials.

For energization, cells in a plastic microfuge tube were first

exposed to valinomycin at 22°C and, after a 3 min wait, placed into one of the holes in the block and allowed to warm for 4 min. A volume, x ml, of this suspension was then pipetted into 1 minus x ml of the pH 6.5 buffer in a glass vial in another hole, the stirrer switched on for 3 s, and the mixed suspension drawn into the flow chamber via a 16 cm length of polyethylene tubing (I.D. 0.58 mm, O.D. 0.965 mm, Intramedic), at a flow rate of 128 μl/s, for 5 s. Most of the length of the tubing was not in contact with a temperature regulated surface but was suspended in air at room temperature (ca. 22°C). I assumed that cooling of the suspension as it was drawn through the tubing did not significantly affect the results. To justify this, note that for the flow rates used, (1) an element of fluid requires ~0.3 s to traverse the total tubing length, and (2) the volume in the flow chamber between the point of connection with the tubing and the point of observation is small and traversed in much less than a second. Therefore, cells observed 5 seconds after the start of the flow were passing through the tubing at about the same time as the time of observation. By this time the flow of warm (or cool) buffer has warmed up (or cooled down) the tubing to about the same temperature, so that loss of heat from the suspension is not a problem. This follows from a rough estimate of the time required for heat to diffuse across the tubing wall of width $w \simeq 0.03$ cm, $t \simeq w^2/\kappa$, where κ is the thermal diffusivity of polyethylene. The thermal conductivity of polyethylene is $K = 0.0042$ $Wcm^{-1}\cdot K^{-1}$, its specific heat is $c = 0.3$ J $g^{-1}\cdot K^{-1}$, and its density $\rho = 0.92$ g cm^{-3} (Boysen, 1981); so $\kappa = K/c\rho = 1.6 \times 10^{-3}$ cm^2/s, and $t \simeq 0.6$ s, which is much shorter than the total flow duration. The rate of heat loss from the tubing into the surrounding air by convection and radiation is probably much smaller.

Flow was switched on and off by linking the outgoing end of the flow chamber to a three way stopcock attached to a vacuum line. The stopcock was lubricated with silicone grease (Dow Corning). In the "off" position, the vacuum line pulled air through the third (open) connector of the stopcock, thus relieving the suction on the grease seal. When Apiezon L grease was used to seal the upper window of the flow chamber, bulk flow of the cell field continued for many seconds after switching off the vacuum, as the grease seal relaxed. This problem was solved by sealing both the upper and lower windows onto the flow chamber with Histowax (Granular HX 480 (L910C), Matheson Coleman & Bell) which has a melting point of 50 - 52°C. The empty flow chamber was heated to 56°C on the exposed block of an Eppendorf 5320 Thermostat, clean slips were placed on the chamber ledges, and flecks of wax were applied to their edges. The wax melted and was drawn into the gap between slip and ledge by capillary action. When cooled, a tight seal was formed. This method would not be suitable for bottom window attachment in general flow chamber experiments as the wax is highly soluble in heptane. The chamber was pre-filled with buffer before the experiment. Between energizations, the chamber was flushed with buffer (maintained at the appropriate temperature) and cells which had stuck to the windows were removed by pulling through a few air bubbles.

Cells which have been artificially energized as described above run down rapidly during the first minute. To collect data from such preparations, I wrote a modified Fourier transform program which computed N_{int} average power spectra for a series of consecutive time intervals. Each interval was Mt_s seconds long, where M was the number of successive spectra averaged during that interval, and t_s was the time

required to collect and process a one second data block. By repeating the energization routine N_e times, N_eM spectra would be averaged for each interval. I found that, using the apparatus and settings described in Chapter 5 for measurements on glycolysing cells, with a digitization rate of 512 Hz (t = 1.01 s), and with M = 15, bundle peaks could be resolved after 15 energizations. Peaks were smeared to an extent determined by the drop in speed during the interval duration (about 15 s). Greater time resolution could be achieved by reducing M and increasing N_e, at the expense of considerably increased labor on the part of the experimenter. The number of measurements needed and the total time over which cells may be kept starved at pH 8.5 and still retain viability limited the resolution attainable.

The bundle frequency peaks in power spectra obtained from suspensions of artificially energized cells were about twice as wide as those seen for glycolysing cells. There was a large overlap between the low frequency half of the peak and the harmonic tail of the body roll peak. This prevented accurate estimates to be made of the mean bundle frequency. The computer simulations described in §2.6 indicated that, for such large overlap, an error of 30% or more could be expected using the procedure involving subtraction of the noise spectrum and simulated body roll spectrum. The peak shifted to higher frequency at elevated temperatures in a manner consistent with the large thermal effect observed in glycolysing cells. Swimming speed measurements made by Markus from videotape recordings confirm the presence of a monotonic, approximately linear increase in speed in artificially energizeed preparations. This technique is now the preferred one for studying artificially energized cells because of greater accuracy and time

resolution. Since cells run down in about a minute after energization at 22°C, and since the rate of decay increases at higher temperatures (about twice as fast at 35°C), it is important to obtain speeds at a series of consecutive times and to extrapolate back to zero time to obtain an accurate speed estimate.

§6.4. Isotope substitution experiments.

Khan and Berg (1983) energized tethered cells both by a transmembrane pH gradient and by a potassium diffusion potential and found that the torque of tethered cells does not change when deuterons are substituted for protons. This suggests that the rates of proton transfer reactions do not determine the speed of the motor when it is operating close to stall. To test whether the same might hold true for motors running near the idle speed, I attempted to compare bundle frequencies of swimming cells artificially energized in buffers made up in H_2O with those made up in D_2O.

A valid comparison required that I be able to energize cells in D_2O buffers with a deuteronmotive force equal in magnitude to the protonmotive force applied to cells artificially energized according to the method of §6.2. Thus it was necessary to determine the initial cytoplasmic pD of cells which had been starved in an H_2O buffer at a known initial pH, and then shifted to a D_2O buffer. In order to duplicate the conditions used for the H_2O energization, an internal pD of about 8.5 was required. Khan and Berg (1983) found that cells starved at pH 7.5 and then shifted to D_2O had an internal pD of 8.0, a shift up of half a unit. I therefore starved tethered cells at pH 8.0, shifted to buffers with pD values ranging from 6.5 to 10.0, and observed their rotation rates. Streptococcus strain SM197 was grown and washed as described in §6.2, this time into buffer TMK at pH 8.0. After starving in this buffer for 3 h at the harvest density (at 22°C), cells were sheared and tethered in the same buffer according to the method of Manson et al (1980). Coverslips were cleaned by exposure to a saturated solution of KOH in 99% ethanol for several minutes (22°C) before

silanization. Cells were exposed to 1 μg/ml of valinomycin in the same buffer for several minutes, then shifted to a buffer in D_2O. The pD values of the latter buffers were measured by adding 0.4 units to the readings obtained from a glass and potassium-calomel pH electrode (Gandour & Schowen, 1978, Chapter 6). They were made up by dissolving the same reagents as for H_2O buffers into D_2O. These reagents contribute a negligbly small number of hydrogen ions to the solutions. All D_2O solutions were covered with parafilm to hinder absorption of atmospheric moisture. Rotation rates of tethered cells were measured as in Khan et al (1983). The results (Fig. 6.1) are consistent with the assumption that the pD immmediately after energization lies between 8.4 and 9.0. I therefore settled on a procedure of energization by starvation at pH 8.0 followed by a shift to a buffer with a pD of 6.5 combined with a nominal potassium diffusion potential of 100 mV (1/50 dilution in $[K^+]$). Energizations were carried out at 27°C using the methods of §6.3. A concentrated cell suspension in H_2O buffer (pH 8.0 or 8.5) was diluted into D_2O buffer (pD 6.45) or H_2O buffer (pH 6.45) respectively.

Spectra obtained for cells of the same culture energized in H_2O and D_2O buffers are shown in Fig.6.2. The bundle peak of the deuterium spectrum shows a clear shift to lower frequencies. Although the peaks are too wide for accurate determination of a mean frequency, computer simulated spectra showed a comparable change in shape when frequencies were reduced by 30-50%. Such a large drop in frequency cannot be accounted for by the increase in solvent viscosity ($\eta(D_2O) = 1.24\eta(H_2O)$) since small changes in external load do not affect the rate of flagellar rotation at low loads (Chapter.3). This conclusion was confirmed by comparing power spectra obtained from artificially energized cell

suspensions with and without Ficoll, added (§6.3) to give a similar or greater increase in viscosity. No significant differences in bundle frequency peak location were noted. Cells from the same culture as in Fig. 6.2 which were tethered, energized, and exposed to D_2O buffers did not show the same dramatic reduction in speed. Markus has made a more accurate determination of the deuterium isotope effect by measuring swimming speeds from a videotape recording of artificially energized cells (pH shift from 8.5 to 6.5 combined with a 1/40 $[K^+]$ dilution) and observed a drop in motor speed from 33.57 ± 2.17 Hz to 26.11 ± 2.18 Hz (Meister, 1987).

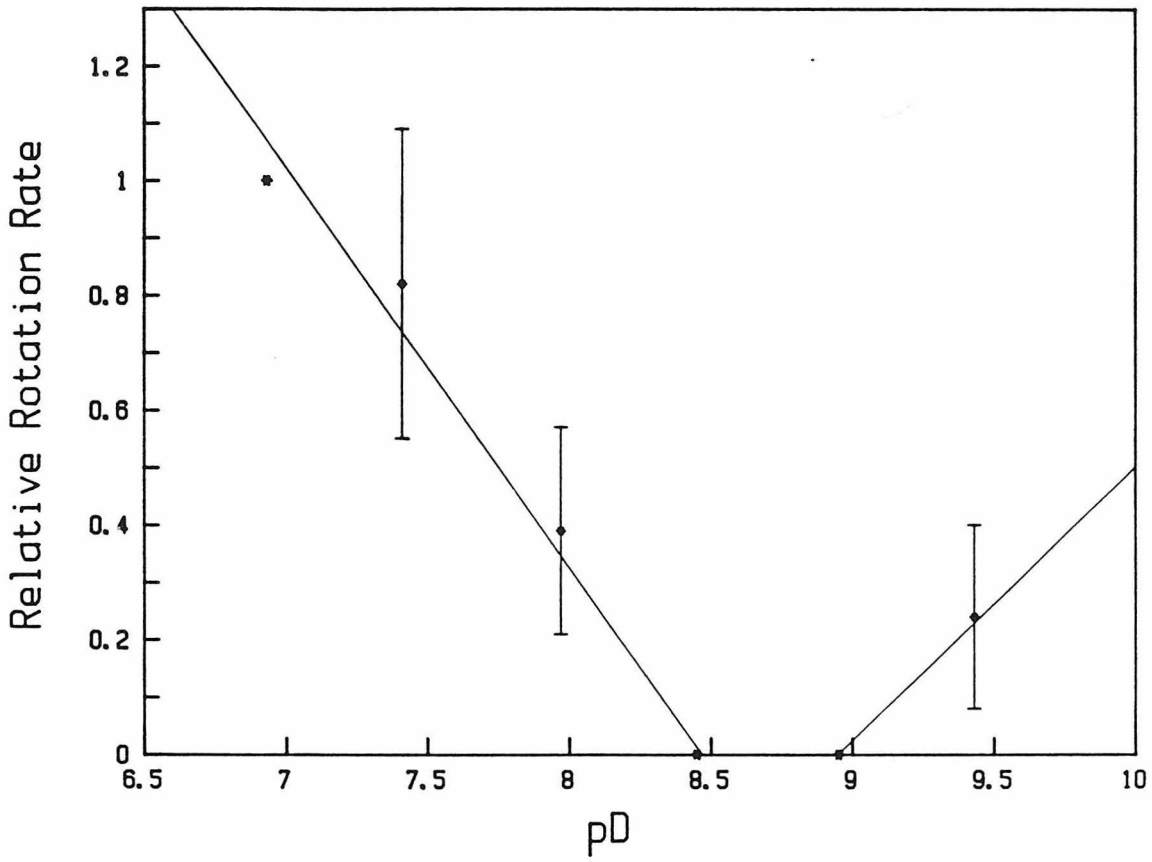

Figure 6.1. Rotation rates of tethered cells of SM197 in D_2O.

Cells were prepared and starved as described in the text, then energized by shifting to a D_2O buffer of known pD. Relative rotation speeds were normalized relative to the speed of each cell at pD 6.93 and plotted as a function of final external pD.

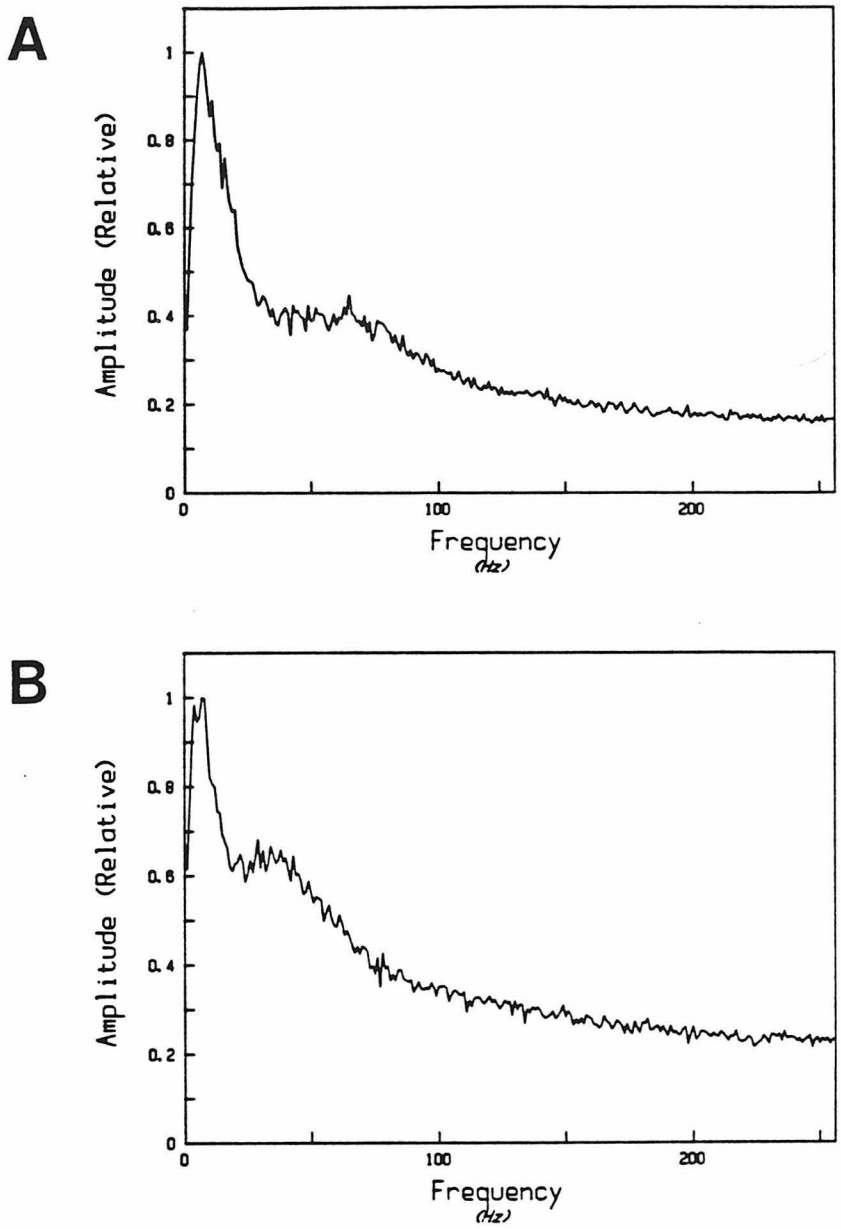

Figure 6.2. Isotope effect for swimming cells.

Cells were prepared and energized as described in §6.4 Power spectra for cells energized in H_2O buffer (A) and D_2O buffer (B) were obtained by averaging M = 15 consecutive one second data blocks collected over the first 15.3 seconds after energization, mixing and flow. This was repeated N_e = 12 times. Data collection rate was 512 Hz.

CHAPTER 7

SUMMARY AND OUTLOOK

§7.1 Summary and discussion.

First let me summarize what has been learnt so far about the behavior of the motor at high speeds, as seen in swimming cells. As before, I shall refer to the torque at zero speed as the stall torque, and the speed at zero torque as the idle speed. These results refer specifically to Streptococcus.

(1) At 22°C and fixed Δp (glycolysing cells), the torque generated by the motor decreases linearly with increasing speed. This is known to be true for speeds greater than about half the idle speed. There is good evidence (tracking data and observations on beads) that property **(1)** also holds for E. coli. I failed to observe hook rotation in putative Streptococcus hook mutants (strain V4055), but hook rotation speeds observed directly in E. coli show that the linear drop in torque extrapolates to almost zero torque.

(2) At fixed Δp (glycolysing cells and artifically energized cells), close to the idle speed, torque is a steeply rising function of temperature. With property **(1)**, this implies that the idle speed is a steeply rising function of temperature. This has been established over the temperature range 16°C to 32°C.

(3) At 22°C and fixed Δp (artificially energized cells), close to the idle speed, the motor runs 1.5 to 2 times as fast on protons as it does on deuterons. Properties **(1)** and **(2)** have not been tested for motors run on deuterons.

Properties **(1)** to **(3)** contrast with the following behavior seen at low speeds (close to stall, around 10 Hz or less) in tethered cells:

(4) At 22°C, and fixed Δp (glycolysing cells), the torque generated is independent of speed. This has been determined for rotation rates

from stall (Meister, 1987) up to about 8 Hz (Manson et al., 1980), when the motor is run on protons.

(5) At fixed Δp (artificially energized cells, 77mV) close to the stall torque, the torque generated is independent of temperature (Khan and Berg, 1983). This holds over the range 4-38°C, when the motor is run on protons.

(6) At 22°C and fixed Δp (artificially energized cells), close to the stall torque, the torque generated does not change when D_2O is substituted for H_2O.

As noted in Chapters 3 and 5, the observations **(1)** and **(2)** can be pieced together to give a tentative torque-speed relationship which is linear over the entire speed range. The energy per revolution available to perform useful work at the output (i.e. rotating the load) decreases linearly with increasing speed. In loosely coupled mechanisms no general conclusions can be drawn from this. However, in the special case of tight coupling, where the free energy available per revolution at the input to the motor is independent of speed, the fraction of this energy dissipated by internal processes increases linearly with speed, up to 100 % at idle. Such linear behavior is characteristic of systems near-equilibrium, where the free energy dissipated in reactions is much less than the thermal energy, kT. This would appear to be inconsistent with the fact that in glycolysing cells the free energy available per proton is large (ca. 8kT). One possible explanation is that the free energy is dissipated in many steps of size much less than kT, as suggested in Chapter 5. This might correspond, for example, to transport of protons through an ion channel by hopping along a series of binding sites (Meister, 1987). One way to test this hypothesis would be to check for a

break down in linearity for sufficiently large Δp. Unfortunately, it is not obvious how one would generate values of the protonmotive force much greater than those in glycolysing cells when current methods seem barely able to produce values one half as large. Even the problem of measuring and calibrating Δp appears to be a source of difficulty. Another test of the near equilibrium hypothesis might be a measurement of speed as a function of Δp. Again, for a sufficiently large driving force we would expect to see nonlinear effects and eventual speed saturation. Although it has been established that speed is proportional to Δp in tethered cells (e.g. Khan et al., 1985), a similar result is lacking for swimming cells. I have attempted to tackle this question by measuring bundle frequencies of glycolysing cells at varying external pH values, assuming that the only effect is to change Δp by an amount equal to the change in external pH. I found that speed varies nonlinearly, being maximal between pH 6.5 and pH 7.5 and decreasing monotonically at lower or higher pH values. Unfortunately, these kinds of experiments are difficult to interpret because there may be an unknown effect of external pH on the motor due to titration of proton binding sites accessible to the bulk solvent. The pH might also affect metabolic processes which contribute to Δp generation, or have a direct effect on the proton translocating ATPase itself.

Observation **(3)** strongly suggests that the steps which are rate limiting at high speeds involve transfer of protons. Such an interpretation implicitly assumes that deuteration causes little change in the structure of the motor. It is always possible to imagine that when proteins in the motor have had their rapidly exchangeable protons replaced by deuterons, they alter their tertiary or quaternary

structure, with consequent changes in their dynamic properties. Thus the permeability of a proton channel might be reduced, not because of a direct effect on proton hopping in a narrow conduction chain, but by a reduction in the diameter of a wide channel, resulting in a greater interaction between the solvation shell of the cation and the channel walls. Brink (1983) presented evidence for such an effect on gap junctions in giant axons of the earthworm. The radius of the solvation shell would also be expected to increase in D_2O. The translocation of protons might be coupled to the motions of side chains of motor component molecules through the solvent, and therefore be affected by solvent viscosity. However, this cannot account for the large observed reduction in the speed of swimming cells. Only a 20 % decrease in speed would be predicted if solvent viscosity alone were controlling the rate of proton translocation. Finally, there could even be major effects on the torque-generating machinery leading to an altered torque-speed diagram in D_2O - e.g. one in which the torque is a more slowly varying function of speed in swimming cells. Performing viscosity experiments on artificially energized cells in deuterium buffers would be an obvious way to test this hypothesis.

It appears that a mechanism which is operating close to equilibrium (in the sense that speed and proton flux are linear functions of torque and Δp), and in which proton transfer is rate limiting, can accommodate all of the known facts about the flagellar motor. This includes the result, from proton flux measurements, that the flux coupled to motor rotation is directly proportional to speed (Meister, 1987). However, the assumption of tight coupling is appealing because it explains such proportionality in a natural way and minimizes the number of free

parameters available to fit data. In this case, the motor's resistance to the proton current is ohmic, suggesting an arrangement whereby energy is lost in many small steps rather than in a few large steps.

Future experiments should focus on testing the linear behavior of the system under a wider range of conditions. Clearly there are many more combinations of parameters one could vary to define in more detail the speed as a function of other parameters, $\Omega = \Omega(T,\Delta p,N,J,i)$, J being the flux and i the isotope. In particular, we would expect deviations from linearity to occur at high Δp, so the determination of idle speed as a function of Δp has a high priority rating. This would, in turn, require the accurate calibration of membrane potentials generated by artificial energization.

§7.2 Outlook.

In the past, quantitative measurements of cell motility have relied mainly on three kinds of techniques: (1) high-speed cinematography, in which a large quantity of data is gathered using elaborate instrumentation and much effort is required to extract a small number of interesting parameters (see e.g. Shimada et al., 1976), (2) video recording or recording of motility tracks on film, both utilizing simple instrumentation to gather much data, with low time resolution, which is analysed later with much effort to obtain few parameters, and (3) laser light scattering, in which the equipment can be sophisticated but a few interesting parameters may be convoluted in a complicated way with other uninteresting parameters to yield the observed scattering and correlation functions. These methods have been complemented by some more specialized techniques well suited for the measurement of specific parameters - e.g. intensity fluctuation spectroscopy (Banks et al., 1975) and the tracking microscope (Berg, 1978). In this thesis I have presented a further addition to this repertoire, a system especially designed for extracting the frequencies of periodic motions of motile microorganisms. The apparatus is simple and can be easily assembled from inexpensive, commercially available equipment and software packages. Signal processing is done on line and population averaged frequencies are computed quickly without tedious analysis. Motions of very small amplitude (compared with that of Brownian motion) can be detected by averaging many power spectra. Single cells or organelles can be singled out using a pinhole.

Although I have mainly focused on bundle frequency measurements of smooth swimming peritrichously flagellated bacteria, there are other

potential applications. I have used the system to examine cells of Streptococcus strain SM29, a mutant in which the motor is locked in a clockwise (CW) mode, and which therefore tumbles incessantly (Berg et al., 1982). Fig.7.1 shows the amplitude spectrum obtained from these cells. There is a clear high frequency peak in the range 30 - 50 Hz, although the amplitude is smaller than that seen for swimming cells where the lateral forces generated by rotation of the filaments add coherently. In swimming cells, typical bundle frequencies lie in the 100 Hz range for cells observed under the same conditions. This difference can be combined with other observations to estimate the ratio of the rotational drag coefficients of the filaments in the tumbling case and in the swimming case. If n is the number of filaments in the bundle, N is the torque per motor, f is the rotational drag coefficient of the bundle, f^* is the rotational drag coefficient of a counterclockwise (CCW) rotating filament, (assumed to be the same for a bundle as for a single filament), Ω is the angular velocity, and * denotes the tumbling case, then:

$$\frac{f}{f^*} = \frac{nN\Omega^*}{N^*\Omega} \qquad (7.1)$$

Using the values n = 3.5 (Meister, 1987), $N^*/N \simeq 5$ (c.f. Fig. 5.3), $\Omega^*/\Omega \simeq 0.4$, the result is: $f/f^* \simeq 0.3$, i.e. the average drag on CW rotating filaments is about three times as large as that on CCW rotating filaments. This is the opposite of what one would expect, given that the latter have a smaller helix radius and wavelength (Macnab and Ornston, 1977), and are also thinner than the bundle. Could the torque-speed diagram depend on the sense of rotation?

Fourier analysis of signals transduced by a pinhole apparatus (§2.4, §4.4) is a powerful method for detecting small amplitude vibrations. The pinhole has already been applied to measure hook frequencies (Berg et al., 1982). Examination of intact single cells of Streptococcus stuck to glass revealed strong vibrations associated with bundle rotation (Fig. 7.2). I also looked at a motile cyanobacterium, Synechococcus WH8103, which exhibits a unique kind of motility (Waterbury et al., 1985). This organism swims in three dimensions in aqueous media apparently without the aid of propulsive organelles - motility is unaffected by blending and no flagella can be seen under the electron microscope. Swimming is accompanied by a low frequency "twirling" motion of the cell body. My attempts to detect high frequency vibrations in these cells using the pinhole were unsuccessful (Fig. 7.3). A high frequency peak was also absent from spectra obtained from cell suspensions without a pinhole. This is not surprising since the signal-to-noise ratio is smaller for swimming populations. The mechanism of motility remains obscure. Could it be related to that of the gliding bacteria which move along phase boundaries? It is noteworthy that all three modes of bacterial locomotion - flagellar, gliding and twirling - appear to be driven by protonmotive force.

The dynamics of the bacterial motor away from steady state is not accessible by time-averaged studies if the averaging intervals are greater than the relaxation times of the processes of interest. Studies on single tethered cells under normal physiological conditions suggest that these relaxation times may be small. Wild-type cells reverse their direction of rotation and achieve a new steady speed in times much shorter than a second (less than 10 ms; see Berg, 1976). Preliminary

studies of the response of tethered cells to rapid steps in Δp were complicated by proton buffering effects of the cell wall and the finite time taken to wind up the elastic tether (Shimada and Berg, in press). The former problem could be eliminated by using an intracellular pH jump (perhaps with an envelope preparation of the type developed by Eisenbach and Adler, 1981) and the latter problem by detecting hook vibrations using a pinhole system. I was unable to detect hook vibrations in Streptococcus but it is possible that the strain I used (V4055) was not a bona fide hook mutant.

An alternative way of measuring the idle speed might involve the use of phosphoresence depolarization. A high quantum yield probe molecule would be linked to a group in the interior of a protein molecule (to protect the triplet state from quenching by molecular oxygen) which would, in turn, be linked to a hook by an antibody. Unfortunately, the probe concentration would be rather low - 10 probe complexes might fit on the surface of a hook, giving an average of 35 per cell. In a dense suspension (ca. 10^{10} cells/ml) this gives a probe concentration of about 0.5 nM, which is three orders of magnitude smaller than the levels used in experiments which rely on current technology (see e.g., Bartholdi et al., 1981). Even the most sensitive methods available for measuring the rotational motions of fluorescently labelled molecules on single cells (Johnson and Garland, 1982) require about 10^3 - 10^4 probe molecules per square micron of membrane area. Nevertheless, the theory for this experiment has been expounded in great mathematical detail (Hoshikawa and Asai, 1984).

Finally, I would like to propose some possible applications to the study of chemotaxis. At present it is not known how the individual

motors of bacteria coordinate their senses of rotation to form the flagellar bundle. Ishihara et al. (1983) showed that the motors are not synchronized by a global signal. Their conjecture, that a stable bundle might exist only when more than a certain fraction of the motors generate counterclockwise torque, was not able to reconcile the observed mean run and tumble times in swimming cells with the observed reversal statistics in tethered cells. Another prediction of this hypothesis, step changes in swimming speed at high torque, was not borne out by the tracking experiments in Ficoll (Chapter 3). A more sophisticated model invoking some kind of mechanical feedback to the directional switch of the motor seems to be required. For example, the reversal statistics might be a function of torque. This could be a potential application for the pinhole system. While working with the bead preparations (§2.3) I sometimes observed transitions between two modes of vibration (distinguished by their different frequencies and amplitudes) in spinning markers on wild-type cells (V4051). If these represent reversals, their statistics should be analysed and compared with those of tethered cells. Addition of Ficoll to the medium might change these statistics. An easier experiment would be to look for a correlation between rotation rate and CCW/CW bias in tethered cells. The observation that cells become biased towards CCW rotation at lowered Δp (Khan and Macnab, 1980) may simply be a manifestation of this effect. Load dependent bias suggests an intimate connection between the directional switch and the force-generating units of the motor. It is not inconceivable that the study of the chemotactic switch might someday provide clues about the mechanism of force-generation itself.

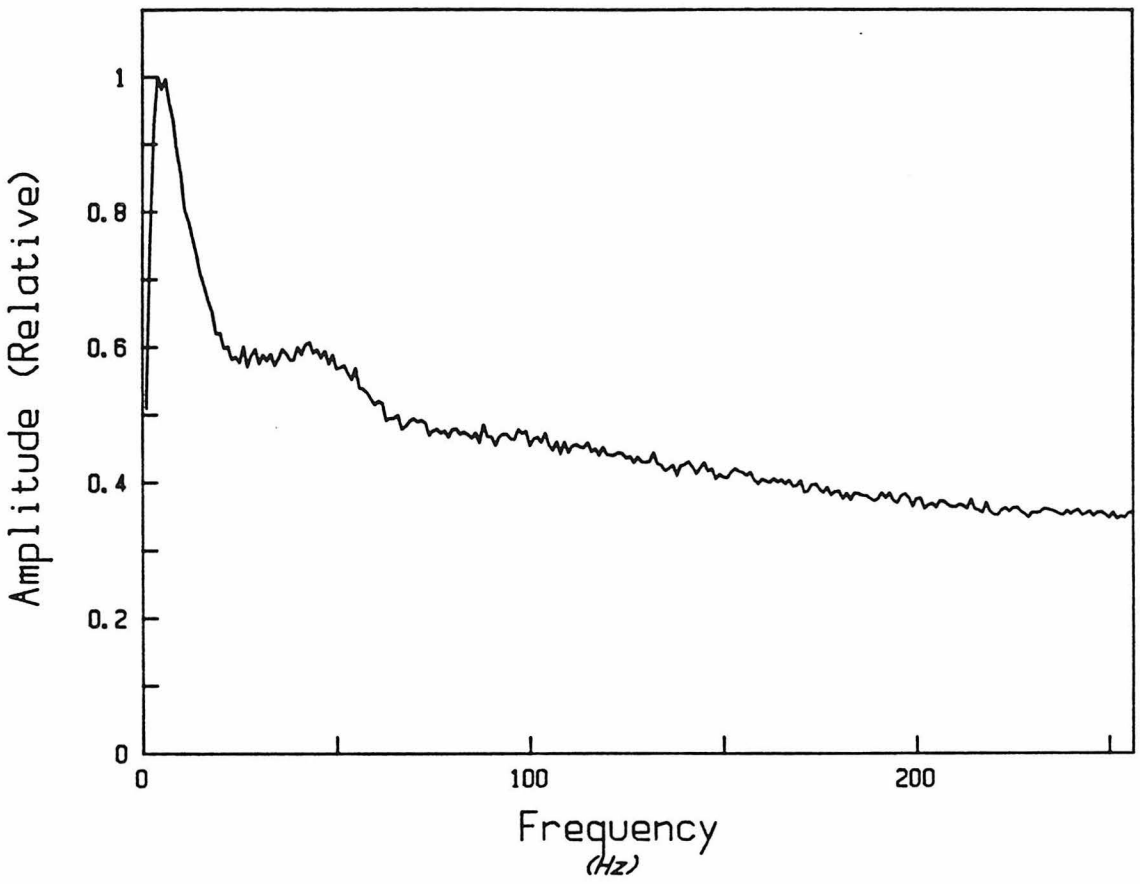

Figure 7.1. Amplitude spectrum of tumbling cells.

Streptococcus strain SM29 was grown to late exponential phase and examined in KTY growth medium. The culture consisted primarily of tumbling diplococci, with a small number (< 10 %) of short chains. 1200 consecutive one second data blocks were averaged. The data collection rate was 512 Hz.

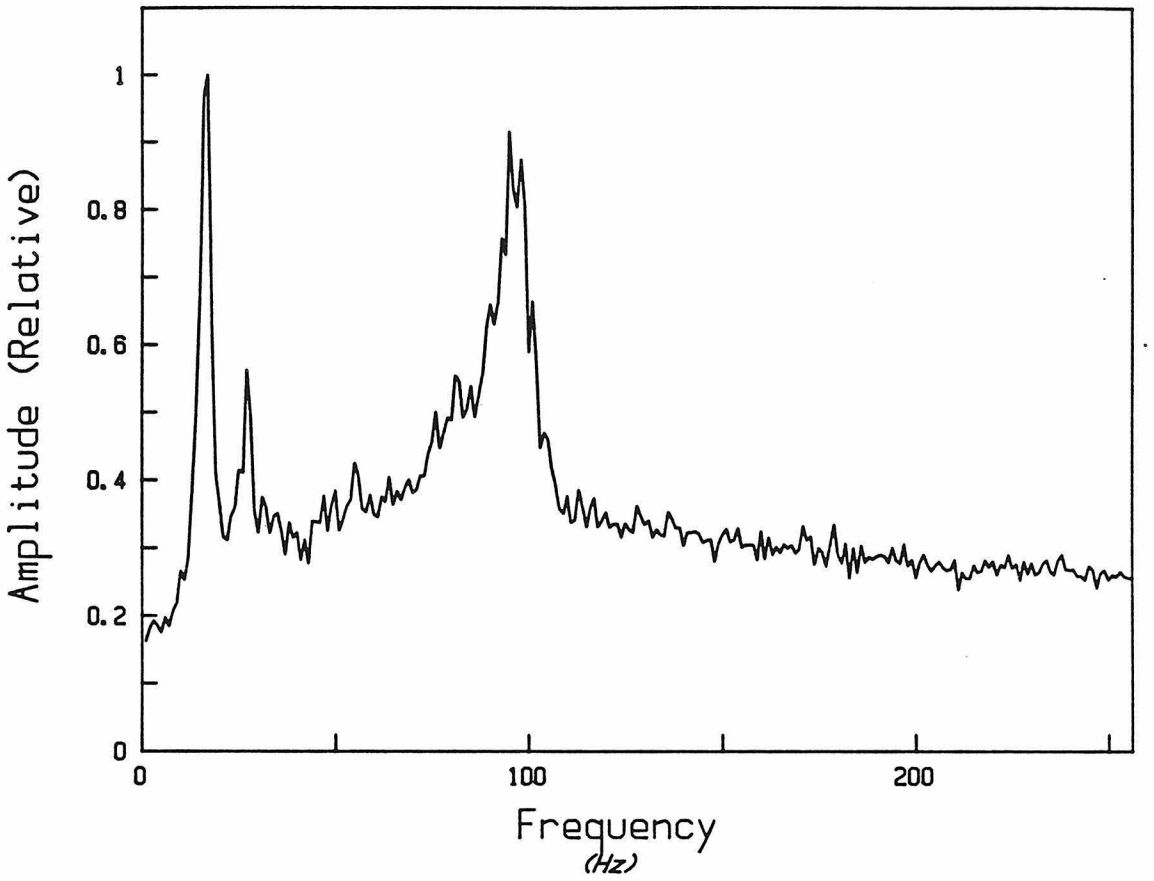

Figure 7.2. Bundle frequency measurement on a single cell of Streptococcus.

SM197 was grown to late exponential phase and examined in an uncleaned glass flow chamber in KTY medium. After about 10 min, the chamber was flushed with buffer TMK (pH 7.5) + 10 mM glucose to rinse out most unstuck cells. The image of a cell stuck with its symmetry axis close to vertical was positioned at the edge of a large pinhole (14 μm diameter at the focal plane). Spectra from 100 one second data blocks were averaged.

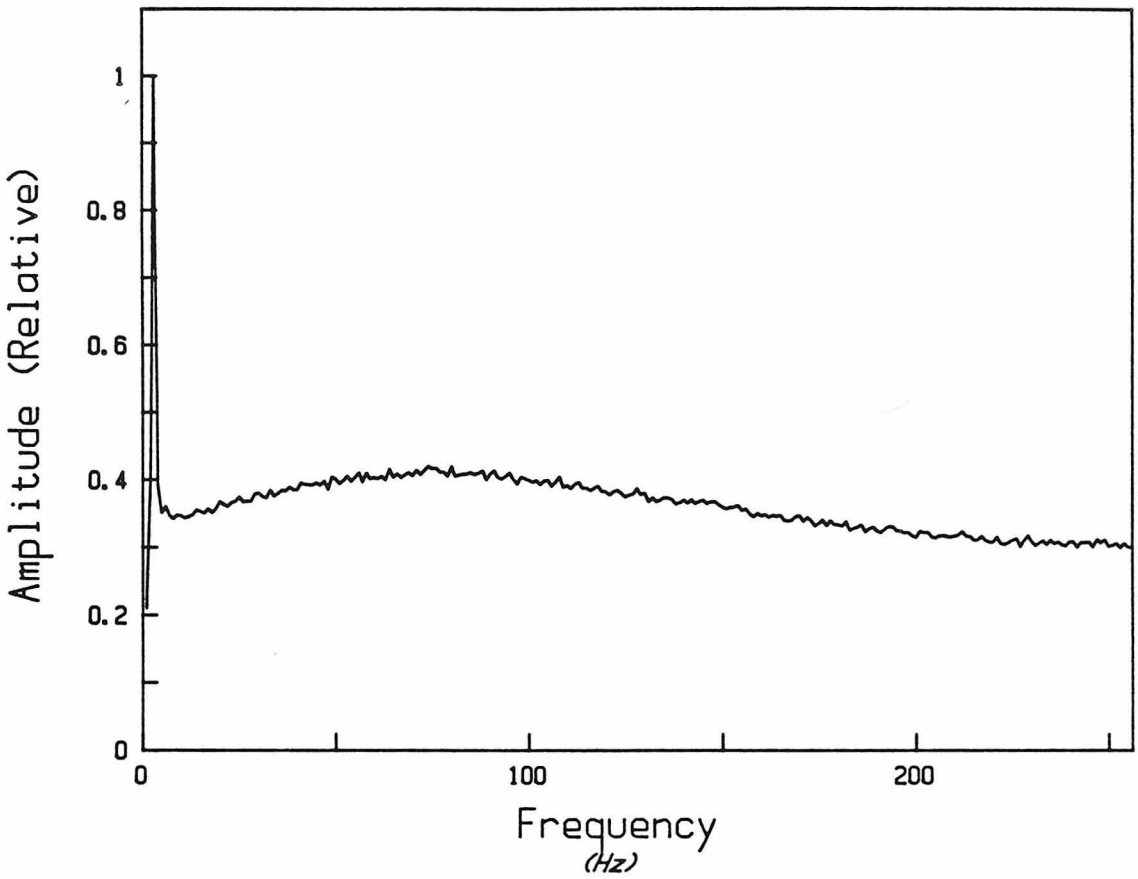

Figure 7.3. Pinhole spectrum of a motile cyanobacterium.

Synechococcus WH8103 was grown at room temperature (22°C) in artificial seawater supplemented with trace metals (0.34 M NaCl, 28 mM $MgSO_4$, 18 mM $MgCl_2$, 8.7 mM KCl, 9.9 mM $CaCl_2$, 0.087 mM K_2HPO_4, 0.013 mM Na_2EDTA, 0.094 mM Na_2CO_3, 0.88 mM $NaNO_3$, 0.3 nM Vitamin B_{12}, 1.0 ml per liter of cyano trace metal solution). The cyano trace metal solution was made by dissolving the following (gm/l) in double distilled water: $ZnSO_4.7H_2O$ 0.222, $MnCl_2.4H_2O$ 1.4, $Co(NO_3)_2.6H_2O$ 0.025, $Na_2MoO_4.2H_2O$ 0.39, citric acid.H_2O 6.25, ferric ammonium citrate 6.000. The image of a cell stuck to glass but undergoing twirling motion was positioned at the edge of a pinhole. Spectra from 2000 one second data scans were averaged.

APPENDIX.1 STANDARD SOLUTIONS, REAGENTS AND MEDIA.

1. Buffers.

All buffers were made with reagent-grade chemicals and glass distilled water. If the pH is not specified below, it is given in the text when reference is made to the buffer.

Buffer T : 10 mM NaH_2PO_4/HPO_4, 0.2 M KCl, 0.1 mM EDTA.

Buffer B : 10 mM NaH_2PO_4/HPO_4, 0.1 mM EDTA.

Buffer C : 10 mM NaH_2PO_4/HPO_4 (pH 6.5), 10 mM KCl, 0.1 mM EDTA, 0.2 M D-glucose.

Buffer T2 : 0.1 M NaH_2PO_4/HPO_4, 0.2 M KCl, 0.1 mM EDTA.

Buffer TMg : 10 mM TAPS, 10 mM MES, 67 mM $MgCl_2/(OH)_2$, 0.1 mM Tetren

Buffer TMK : 10 mM TAPS, 10 mM MES, 0.2 M KCl/OH, 0.1 mM Tetren, 1 mM $MgCl_2$

Buffer MM : 10 mM KH_2PO_4/HPO_4 (pH 7.0), 67 mM NaCl, 0.1 mM Na_4EDTA 1 μM methionine, 10 mM sodium lactate

2. Reagents.

MES = 2-(N-morpholino) ethanesulfonic acid

TAPS = tris [hydroxymethyl] methylaminopropanesulfonic acid

Tetren = tetraethylenepentamine

DNP = 2,4-dinitrophenol

FCCP = trifluoromethoxycarbonyl-cyanide phenylhydrazone

3. Growth Media.

KTY medium: 1% w/v Difco Bacto-Tryptone, 0.5% w/v Difco Bacto-Yeast Extract, 0.87% w/v K_2HPO_4, 1% w/v D-Glucose. Autoclaved for 30 min.

Tryptone Broth: 1% w/v Difco Bacto-Tryptone, 0.5% w/v NaCl. Autoclaved for 30 min.

REFERENCES

Armstrong, J. B., Adler, J. & Dahl, M. M. (1967). Nonchemotactic mutants of Escherichia coli. J. Bacteriol. **93**, 390-398.

Banks, G., Schaefer, D. W. and Alpert, S. S. (1975). Light-scattering study of the temperature dependence of Escherichia coli motility. Biophys. J. **15**, 253-261.

Bartholdi, M., Barrantes, F. J. and Jovin, T. M. (1981). Rotational molecular dynamics of the membrane-bound acetylcholine receptor revealed by phosphorescence spectroscopy. Eur. J. Biochem. **120**, 389-397.

Berg, H. C. (1971). How to track bacteria. Rev. Sci. Instrum. **42**, 868-871.

Berg, H. C. (1974). Dynamic properties of bacterial flagellar motors. Nature **249**, 77-79.

Berg, H. C. (1975a). Bacterial behaviour. Nature **254**, 389-392.

Berg, H. C. (1975b). Chemotaxis in bacteria. Ann. Rev. Biophys. Bioengin. **4**, 119-136.

Berg, H. C. (1976). Does the flagellar rotary motor step? In: Goldman, R., Pollard, T. and Rosenbaum, J. (eds.) Cell Motility. Cold Spring Harbor, New York: Cold Spring Harbor Laboratory.

Berg, H. C. (1978). The tracking microscope. Adv. Opt. Elect. Micros. **7**, 1-15.

Berg, H. C. (1983). Random Walks in Biology. Princeton University Press, Princeton, New Jersey.

Berg, H. C. & Anderson, R. A. (1973). Bacteria swim by rotating their flagellar filaments. Nature **245**, 380-382.

Berg, H. C. & Block, S. M. (1984). A miniature flow cell designed for rapid exchange of media under high-power microscope objectives. J. Gen. Microbiol. **130,** 2915-2920.

Berg, H. C. & Brown, D. A. (1972). Chemotaxis in Escherichia coli analysed by three-dimensional tracking. Nature **239,** 500-504.

Berg, H. C. and Khan, S. (1982). A model for the flagellar rotary motor, p.485-497. In Sund, H. and Veeger, C. (ed.). Mobility and recognition in cell biology. de Gruyter, Berlin.

Berg, H. C., Manson, M. D. and Conley, M. P. (1982). Dynamics and energetics of flagellar rotation in bacteria. Symp. Soc. Exp. Biol. **35,** 1-31.

Berg, H. C. & Turner, L. (1979). Movement of microorganisms in viscous environments. Nature **278,** 349-351.

Block, S. M. and Berg, H. C. (1984). Successive incorporation of force generating units in the bacterial rotary motor. Nature **309,** 470-472.

Boysen, R. L. (1981). Olefin polymers (High pressure polyethylene). In Encyclopedia of Chemical Technology. **16.** John Wiley and Sons. 3rd edition.

Brink, P. R. (1983). Effect of deuterium oxide on junctional membrane channel permeability. J. Membrane Biol. **71,** 79-87.

Chwang, A. T. and Wu, T. Y. (1971). A note on the helical movement of micro-organisms. Proc. Roy. Soc. London B **178,** 327-346.

Conley, M. P. and Berg, H. C. (1984). Chemical modification of Streptococcus flagellar motors. J. Bacteriol. **158,** 832-843.

Coulton, J. W. and Murray, R. G. E. (1978). Cell envelope asociations of Aquaspirillum serpens flagella. J. Bacteriol. **136,** 1047-1049.

DePamphilis, M. L. and Adler, J. (1971). Fine structure and isolation of the hook-basal body complex of flagella from Escherichia coli and Bacillus subtilis. J. Bacteriol. **105,** 384-395.

Eisenbach, M. and Adler, J. (1981). Bacterial cell envelopes with functional flagella. J. Biol. Chem. **256,** 8807-8814.

Eyring, H. (1935). The activated complex in chemical reactions. J. Chem. Phys. **3,** 107-116

Gandour, R. D. and Schowen, R. L. (eds.) (1978). Transitions states of biochemical processes. Plenum Press, New York.

Gray, D. E. (ed.) (1972). American Institute of Physics Handbook. Third edition. McGraw-Hill.

Haest, C. W. M., Verkleij, A. J., de Geir, J., Scheek, R., Ververgaert, P. H. J. and Van Deenen, L. L. M. (1974). The effect of lipid phase transitions on the architecture of bacterial membranes. Biochim. Biophys. Act. **356,** 17-26.

Harold, F. M., Baarda, J. R., Baron, C. and Abrams, A. (1969). Inhibition of membrane-bound adenosine triphosphatase and of cation transport in Streptococcus faecalis by N,N'-dicyclohexyl-carbodiimide. J. Biol. Chem. **244,** 2261-2268.

Harold, F. M. & Papineau, D. (1972). Cation transport and electrogenesis in Streptococcus faecalis. 1. The membrane potential. J. Membr. Biol. **8,** 27-44.

Hazelbauer, G. L., Mesibov, R. F., & Adler, J. (1969). Escherichia coli mutants defective in chemotaxis towards specific chemicals. Proc. Nat. Acad. Sci. U.S.A. **64,** 1300.

Hazelbauer, G. L. and Harayama, S. (1983). Sensory transduction in bacterial chemotaxis. Int. Rev. Cytol. **81,** 33-70.

Higgins, M. L. and Shockman, G. D. (1976). Study of a cycle of cell wall assembly in Streptococcus faecalis by three-dimensional reconstructions of thin sections of cells. J. Bacteriol. **127,** 1346-1358.

Hill, A. V. (1938). The heat of shortening and the dynamic constants of muscle. Proc. Roy. Soc. B **126,** 136-195.

Hoshikawa, H. and Asai, H. (1984). On the rotational brownian motion of a bacterial idle motor. I. Theory of time-dependent fluorescence depolarization. Biophys. Chem. **19,** 375-379.

Huxley, A. F. (1957). Muscle structure and theories of contraction. Prog. Biophys. Biophys. Chem. **7,** 255-318.

Iino, T. (1969). Genetics and chemistry of bacterial flagella. Bacteriol. Rev. **33,** 454-475.

Iino, T. (1974). Assembly of Salmonella flagellin in vitro and in vivo. J. Supramol. Struct. **2,** 372-384.

Ishihara, A., Segall, J. E., Block, S. M. & Berg, H. C. (1983). Coordination of flagella on filamentous cells of Escherichia coli J. Bacteriol. **155,** 228-237.

Johnson, P. and Garland, P. B. (1982). Fluorescent triplet probes for measuring the rotational diffusion of membrane proteins. Biochem. J. **203,** 313-321.

Julesz, B. (1971). Foundations of cyclopean perception. University of Chicago Press.

Kagawa, Y. (1984). Proton motive ATP synthesis. In: Ernster, L. (ed.) Bioenergetics. Chapter 5. 149-186. Elsevier Science Publishers B.V.

Khan, S. and Berg, H. C. (1983). Isotope and thermal effects in chemiosmotic coupling to the flagellar motor of Streptococcus. Cell **32,** 913-919.

Khan, S. and Macnab, R. M. (1980). The steady-state counterclockwise/clockwise ratio of bacterial flagellar motors is regulated by protonmotive force. J. Mol. Biol. **138,** 563-597.

Khan, S., Meister, M. and Berg, H. C. (1985). Constraints on flagellar rotation. J. Mol. Biol. **184,** 645-656.

Kramers, H. A. (1940). Brownian motion in a field of force and the diffusion model of chemical reactions. Physica **7,** 285-304.

Lauger, P. (1977). Ion transport and rotation of bacterial flagella. Nature **268,** 360-362.

Macnab, R. M. (1978). Bacterial motility and chemotaxis: The molecular biology of a behavioral system. CRC Crit. Rev. Biochem. **5,** 291-341.

Macnab, R. M. (1979). Bacterial Flagella. In: Haupt, W. & Feinleib, M. E., eds. Encyclopaedia of Plant Physiology, New Series, Vol.7, Physiology of Movements. Springer Verlag, Berlin.

Macnab, R. M. & Aizawa, S. -I. (1984). Bacterial motility and the bacterial flagellar motor. Ann. Rev. Biophys. Bioeng. **13,** 51-83.

Macnab, R. M. & Ornston, M. K. (1977). Normal-to-curly flagellar transitions and their role in bacterial tumbling. Stabilization of an alternative quaternary structure by mechanical force. J. Mol. Biol. **112,** 1-30

Maeda, K., Imae, Y., Shioi, J. & Oosawa, F. (1976). Effect of temperature on motility and chemotaxis of Escherichia coli. J. Bacteriol. **127,** 1039-1046.

Manson, M. D., Tedesco, P., Berg, H. C., Harold, F. M. and van der Drift, C. (1977) A protonmotive force drives bacterial flagella. Proc. Natl. Acad. Sci. U.S.A. **74,** 3060-3064.

Meister, M. (1987) Studies on flagellar rotation: the angular symmetry, the stall torque, and the proton consumption of the bacterial flagellar motor. PhD Thesis, California Institute of Technology, Pasadena.

Metzner, P. (1920). Die Bewegung und Reizbeantwortung der bipolar begeißelten Spirillen. Jahrb. Wiss. Bot. **59,** 325-413.

Miller, J. B. and Koshland Jr, D. E. (1977). Membrane fluidity and chemotaxis: effects of temperature and membrane lipid composition on the swimming behavior of Salmonella. J. Mol. Biol. **111,** 183-201.

Oosawa, F. and Hayashi, S. (1983). Coupling between flagellar motor rotation and proton flux in bacteria. J. Phys. Soc. Jpn **52,** 4019-4028.

Oosawa, F. and Masai, J. (1982). Mechanism of flagellar motor rotation in bacteria. J. Phys. Soc. Jpn **51,** 631-641.

Overath, P. and Trauble, H. (1973). Phase transitions in cells, membranes, and lipids of Escherichia coli. Detection by fluorescent probes, light scattering, and dilatometry. Biochemistry. **12,** 2625-2634.

Parkinson, J. S. (1981). Genetics of bacterial chemotaxis. Symp. Soc. Gen. Microbiol. **31,** 265-290.

Reichert, K. (1909). Uber die Sichtbarmachung der Geisseln und die Geisselbewegung der Bakterien. Zentr. Bakteriol. Parasitenk. Infektionskr. Abt.1 Orig. **51,** 14-94.

Reilly, C. N. and Vavoulis, A. (1959). Tetraethylenepentamine, a selective titrant for metal ions. Anal. Chem. **31,** 243-248.

Reinsch, C. H. (1967). Smoothing by spline functions. Numer. Math. **10,** 177-183.

Schneider, W. R. & Doetsch, R. N. (1974). Effect of viscosity on bacterial motility. J. Bacteriol. **117,** 696-701.

Segall, J. E., Ishihara, A. & Berg, H. C. (1985). Chemotactic signalling in filamentous cells of Escherichia coli J. Bacteriol. **161,** 51-59.

Shimada, K., Ikkai, T., Yoshida, T. & Asakura, S. (1976). Cinemicrographic analysis of the movement of flagellated bacteria. II. The ratio of the propulsive velocity to the frequency of the wave propagation along flagellar tail. J. Mechanochem. Cell Motility **3,** 185-193.

Shimada, K. and Berg, H. C. (in press). Response of the flagellar rotary motor to abrupt changes in extracellular pH. J. Mol. Biol.

Silverman, M. & Simon, M. (1974). Flagellar rotation and the mechanism of bacterial motility. Nature **249,** 73-74.

Swan, M. A. (1982). Trailing flagella rotate faster than leading flagella in unipolar cells of Spirillum volutans. J. Bacteriol. **150,** 377-380.

Taylor, B. L. (1983). Role of proton motive force in sensory transduction in bacteria. Ann. Rev. Microbiol. **37,** 551-573.

Touloukian, Y. S., Saxena, S. C. and Hestermans, P. (1975). Thermophysical properties of matter. Viscosity. TPRC Data Series, Purdue Research Foundation, Plenum.

van der Drift, C., Duiverman, J., Bexkens, H. & Krijnen, A. (1975). Chemotaxis of a motile Streptococcus toward sugars and amino acids. J. Bacteriol. **124**, 1142-1147.

Waterbury, J. B., Willey, J. M., Franks, D. G., Valois, F. W. and Watson, S. W. (1985). A cyanobacterium capable of swimming motility. Science **230**, 7476.